Neutrophil human Fcg Receptor IIA and the b2 integrin Mac-1 cross-talk in autoimmune disease

Neutrophil human Fcγ Receptor IIA and the β2 integrin Mac-1 cross-talk in autoimmune disease

A dissertation presented

by

Florencia Rosetti Sciutto

to

The Division of Medical Sciences

in partial fulfillment of the requirements
for the degree of
Doctor of Philosophy
in the subject of
Immunology

Harvard University
Cambridge, Massachusetts

April 2014

Dissertation Advisor: Dr. Tanya N. Mayadas Florencia Rosetti Sciutto

Neutrophil human Fcγ Receptor IIA and the β2 integrin Mac-1 cross-talk in autoimmune disease

Abstract

Systemic lupus erythematosus (SLE) is a chronic multiorgan autoimmune disorder characterized by abundant immune complex (IC) deposition, with nephritis being a major cause of morbidity and mortality. Yet, IC deposition alone is not sufficient for disease development suggesting that additional factors dictate the propensity for developing target organ injury. Genome-wide association studies have identified polymorphisms in the leukocyte integrin Mac-1 (CD11b/CD18, *ITGAM*) that associate with lupus nephritis. Although Mac-1 promotes inflammation by triggering leukocyte recruitment and cytotoxic functions, there is emerging evidence that it may also serve protective roles under certain conditions. We demonstrate that Mac-1 deficiency in the context of the uniquely human FcγRIIA, a receptor that binds IgG-IC, promotes susceptibility to lupus nephritis in two independent animal models. Analysis of renal tissue and intravital microscopy revealed that Mac-1 modulates neutrophil recruitment by FcγRIIA. The SLE-associated variant of Mac-1 rs1143679 (R77H), results in reduced Mac-1 functions, but the underlying mechanism remains undefined. CD18 integrin mediated adhesion is a multistep process that begins with affinity changes for ligand via transmission of allosteric signals. Moreover, mechanical forces (e.g. shear flow) paradoxically increase the lifetime of integrin-ligand bonds, referred to as "catch-bonds". Here, we show that neutrophils expressing Mac-1 R77H, and blocking antibodies to the extracellular β-propeller domain in which it resides, have markedly impaired Mac-1 adhesion to ligand under shear flow. R77H-expressing cells exhibit a shift in equilibrium towards a bent conformation, a lower affinity and on- and off- rate for ligand, and an inability to form catch-bonds. Additional mutants and activating antibodies reveal that R77H prevents allosteric signal transmission to the αI-domain required for productive ligand binding.

Together, our data indicate that Mac-1 is a key regulator of neutrophil FcγRIIA-dependent responses triggered by ICs, which may be exploited therapeutically to limit tissue injury in the context of SLE. Our findings also demonstrate, for the first time, the physiological importance of integrin allostery and catch bonds, and provide a potential molecular mechanism by which R77H reduces Mac-1 functions and thus increases the risk for SLE.

To Jose Carlos and Julieta, my happiness

Acknowledgments

I have been extremely fortunate to have met and been helped by so many people during these years of graduate school. I would like to specially thank:

My thesis advisor, Dr. Tanya Mayadas for all the enthusiasm and hard work she invested in my projects and my formation as a scientist. She gave me a special place in her lab and always made me feel an important member of the group. I am forever grateful for all her commitment, attention, and advice. Thank you.

Colleagues and friends: Thomas, Xavi, Lars, Enrique, Hiroshi, Jan, and Ibrahim, for all their help, guidance, and thoughtful ideas and comments. Paul and Elizabeth, for their constant support and their technical assistance.

The members of my thesis advisory committee, Arlene Sharpe, Shiv Pillai, and Bruce Horwitz, because their help was instrumental in guiding the aims of my projects.

Jack L. Strominger for kindly opening the doors of his lab, and giving me the professional guidance that led me to pursue my PhD.

All of the collaborators on the projects presented here, for their contributions which truly facilitated the progress of these projects.

My grandparents Carlos and Nilda, for their unconditional love.

My mom and Carlos for never doubting me and supporting all my decisions, always pointing to the bright side. Marcos and Virgilio for their love and big smiles.

Jose Carlos for believing in me. I cannot thank you enough for your love, patience and the enormous help you always give me. On your side, I always feel happy and loved.

And Julieta, you have given the extra spark to my life, I love you.

Table of Contents

Chapter 1. Introduction

Systemic lupus erythematosus (SLE) is a chronic autoimmune disease that affects more than 250,000 Americans. It shows a strong predilection for women (in a 9:1 ratio) and usually develops during the childbearing age (1). It may target multiple organs including the kidneys, joints, skin, and the central nervous system. There is compelling evidence that genes contribute to the development of SLE. The importance of environmental factors is also well recognized (2).

Patients with SLE develop a chronic autoimmune response manifested by the presence of autoantibodies and activated T cells. The factors that enable the development and perpetuation of autoimmunity in SLE are poorly understood. Current paradigms suggest that the combination of multiple risk alleles allow the initiation and development of SLE when the immune system is triggered by environmental factors such as infections, hormones, and an increased burden of apoptotic cell debris (2). The pathways through which risk alleles contribute to disease are mostly unknown. However, several phenotypic alterations in cells from both the innate and adaptive immune systems have been documented in SLE patients (3). For example, T cells display an enhanced activation state manifested by aberrant cytokine production (e.g. increased IL-17 and decreased IL-2 secretion) and provide increased levels of help to B cells. Defects in the negative selection process of B cells have been proposed to explain an increased abundance of autoreactive B cells in the B cell repertoire of patients with SLE. This factor, along with increased T cell help probably underlies the production of a large array of autoantibodies against soluble and cellular components (mostly against intra nuclear antigens). Dendritic cells (DCs) and macrophages have also been shown to have an overstimulated phenotype and function that

contributes to the production of inflammatory cytokines (e.g. IFNα) that further amplify the autoimmune response (4).

A consequence of the chronic autoimmune response of patients with SLE is the production and tissue deposition of immune complexes (IC). Deposition of IC is thought to be the main trigger of glomerulonephritis and other SLE manifestations (5,6). In fact, IC and complement deposition is a widespread finding in the dermo-epidermal interphase (lupus band) in the skin (7) and in the mesangial space of the glomeruli of patients with SLE (8-10). However, IC deposition can be observed in healthy skin (7) of patients and in kidneys that lack any sign of inflammation (8-10), suggesting that their mere presence cannot fully account for the development of local inflammation. In this regard, it is increasingly recognized that chronic autoimmunity in patients with SLE does not suffice for target organ inflammation. For example, development of autoantibodies precedes by several years the initiation of clinically relevant disease in patients with SLE (11). Moreover, the clinical heterogeneity of the disease indicates that factors independent of those that control the autoimmune response govern target organ involvement because patients with similar autoantibody profiles can present with completely different disease manifestations (12).

ICs can induce inflammation by activating the classical pathway of complement and engaging Fcγ receptors (FcγRs) in effector cells. Some products of complement activation (i.e. the anaphylatoxins C3a, C4a, and C5a) promote cell recruitment and activation (13). Others decorate the ICs (C1q and iC3b) and facilitate their deposition and recognition by effector cells. Both neutrophils and macrophages are potently activated by ICs and are observed within inflammatory infiltrates in lesions from patients with SLE (14).

The overall aim of this project was to study the molecular mechanisms that regulate the inflammatory response to IC deposition focusing on the role of neutrophils, human FcγRs and the integrin Mac-1 (CD11b/CD18), a known complement receptor, in this process. The understanding of these mechanisms is relevant not only to SLE, but may also apply to other IC-dependent diseases such as postinfectious glomerulonephritis and cryoglobulinemia.

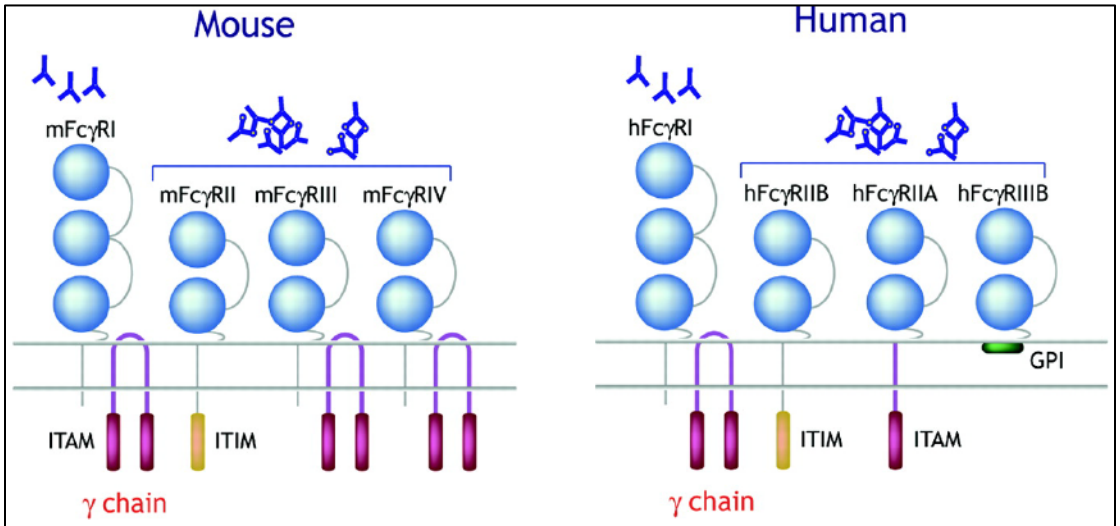

Figure 1. Structure of murine and human neutrophil FcγR. Murine neutrophils express three activating FcγR: FcγRI, FcγRIII, and FcγRIV, which require the γ-chain for their expression and signaling, and one inhibitory receptor: FcγRIIB, with an ITIM. Human neutrophils express: FcγRI, that associates with an ITAM-containing γ-chain; FcγRIIA, which has an ITAM motif on its α-chain; FcγRIIB, with an ITIM motif, and the GPI-anchored FcγRIIIB.

Neutrophils rapidly respond to inflammatory cues and efficiently eliminate pathogens through the production of reactive oxygen species (ROS) and the release of proteolytic enzymes. Neutrophil activation modulates the ensuing effector responses through the production of chemokines and cytokines. Neutrophils contribute to the inflammatory response in patients with SLE, likely in response to deposited ICs formed by IgG but there is no direct evidence for this. The role of FcγRs in diseases that are initiated by antibodies is supported by the fact that mice deficient in the γ chain ($\gamma^{-/-}$), which lack all the activating FcγRs, are protected in many IC-mediated models (e.g. models of lupus, arthritis, acute and progressive glomerulonephritis).

Because the repertoire of FcγRs is fundamentally different in human and mouse neutrophils (Figure 1), the role of the human neutrophil receptors cannot be adequately evaluated in murine models. Dr. Mayadas' lab has demonstrated that neutrophil-selective expression of the uniquely human FcγRIIA restores the susceptibility to IC-mediated inflammation (i.e. arthritis and glomerulonephritis) in $\gamma^{-/-}$ mice (15,16).

Mac-1 is a member of the integrin family of cell surface receptors, expressed only in leukocytes. It is a heterodimer formed by an α-chain (CD11b) coupled to a β-chain (CD18). Mac-1 has multiple ligands including the complement fragment C3 (iC3b), the intracellular adhesion molecule-1 (ICAM-1), and the platelet receptor GPIbα. Several proinflammatory functions have been attributed to Mac-1, mainly due to its capacity to promote adhesion-dependent functions (e.g. leukocyte recruitment to sites of inflammation, induction of phagocytosis of complement-opsonized particles, generation of ROS). However, Mac-1 has also been shown to have functions that oppose inflammation. For example, it regulates neutrophil apoptosis, it participates in the clearance of apoptotic cells and in the uptake of soluble ICs *in vitro* (17), and negatively regulates IFNα and TLR responses (18,19). In murine models of autoimmunity (e.g. lupus nephritis, asthma, and arthritis) disease severity worsens in the absence of Mac-1 (20-22). Additionally, a polymorphism in Mac-1 has been associated with SLE (23,24). This single nucleotide polymorphism (SNP) has been reported to decrease Mac-1 binding to its ligands (25), supporting the idea that engagement of Mac-1 results in immune-regulatory properties.

The general hypothesis of this project was that Mac-1 plays an immunomodulatory role by regulating neutrophil function in the context of an autoimmune disease. In support of this hypothesis, I have shown in two independent, novel mouse models of lupus that mice that

express human FcγRIIA selectively on neutrophils develop nephritis only when the mice lack Mac-1. In the first model, I demonstrate that passive transfer of serum from SLE patients induces nephritis in mice expressing the human FcγRIIA only when the mice additionally lack Mac-1. In the second model, a chronic autoimmune response results in the generation of lupus nephritis in the context of FcγRIIA, and the severity markedly increases in absence of Mac-1. In both models, Mac-1 deficiency results in FcγRIIA-dependent renal neutrophil accumulation. This potential immunomodulatory function of Mac-1 might be relevant for human disease, since the R77H variant of Mac-1 that strongly associates with SLE impairs Mac-1 functions. We provide a potential mechanism whereby the R77H reduces Mac-1 function: it impairs Mac-1 mediated adhesion to ligand under shear flow conditions, shifts the integrin equilibrium between the bent versus extended conformation, and prevents the formation of catch-bonds, a process that increases the life-time of the integrin-ligand bond when the leukocyte is exposed to mechanical forces such as shear flow.

Chapter 2. Human lupus serum induces neutrophil mediated organ damage in mice that is enabled by Mac-1 deficiency

Note: The contents of the sections I-IV have been published (26)

I. Introduction

SLE is a systemic autoimmune disease that affects multiple organs including the kidney, joints and skin, with development of nephritis being one of the most serious complications of this disorder. SLE is characterized by loss of tolerance to self-antigens and high titers of circulating autoantibodies (11). In mice, deletion of the common Fcγ-chain ($\gamma^{-/-}$) that results in the loss of activating FcγRs, protects lupus-prone New Zealand Black/New Zealand White mice from spontaneously developing lupus nephritis (27,28). Yet, there is little direct evidence that immune complexes (ICs) are causative as there are no reports that the passive transfer of SLE sera induces disease. Moreover, autoantibodies to classical lupus antigens such as dsDNA are not sufficient for development of nephritis in lupus-prone mouse strains and renal biopsies of SLE patients without clinically evident nephritis can exhibit IC deposition. Thus factors in addition to ICs likely dictate the propensity to develop target organ damage the identification of which remains a central question in the field (5,29,30).

Human genome-wide association studies have shown that small variations in a large number of genes are associated with lupus. The current paradigm assumes that these traits modulate, through different pathways, the expression of disease in lupus. Variations in one of these genes is the leukocyte integrin Mac-1 (*ITGAM*, CD11b/CD18) (4), a member of the leukocyte CD18 integrin family of adhesion molecules that are obligate heterodimers of unique CD11 subunits paired with a common CD18 chain. Mac-1 has multiple ligands including complement fragment

iC3b, and ICAM-1 on the endothelium (31), and the Mac-1 R77H polymorphism associated with lupus (24) leads to a reduction in its binding to both these ligands (25). The question remains as to whether Mac-1, which typically promotes inflammation and host defense (31) plays a role in the pathogenesis of lupus. The prevailing view is that Mac-1 on macrophages clears circulating ICs (24), although there is no direct evidence of this. Likewise, polymorphisms in human FcγRIIA and FcγRIIIB are associated with lupus through mechanisms that remain largely unclear (4). The physiological roles of the uniquely human neutrophil FcγRs, which structurally differ from their mouse counterparts (13,32), have been addressed in genetically engineered mice. Expression of the single polypeptide FcγRIIA, containing an ITAM, and the glycosyl-phosphatidyl-inositol (GPI)-anchored FcγRIIIB selectively on neutrophils of Fcγ-chain deficient mice (IIA$\gamma^{-/-}$, IIAIIIB$\gamma^{-/-}$), restored susceptibility of $\gamma^{-/-}$ animals to progressive anti-glomerular basement membrane (GBM) nephritis and K/BxN serum-induced arthritis (15,16). Although both human FcγRs promoted neutrophil accumulation, only FcγRIIA alone induced tissue injury likely through their known ability to promote neutrophil cytotoxic functions (15).

Difficulty in understanding the underlying mechanisms of SLE arises from the multifactorial influences on disease course including environmental, infectious and hormonal factors, the association of lupus with abnormalities at all levels of the immune system and the clinical heterogeneity of the disease (4). The disparate disease courses in SLE likely converge into a common route of end organ damage. Here, in a new model of lupus induced by the passive transfer of human SLE sera we provide direct evidence that SLE ICs are pathogenic, show a central role for neutrophils in target organ damage and demonstrate that two molecules, FcγRIIA and Mac-1, determine the capacity of ICs to cause tissue damage. In addition, these results coupled with the analysis of neutrophil behavior by intravital microscopy revealed a new

regulatory role for Mac-1 in FcγRIIA mediated neutrophil recruitment following deposition of circulating ICs.

II. Materials and Methods

Mice

Fcγ-chain deficient mice, human FcγRIIA and FcγRIIIB-expressing γ-chain deficient mice (IIAγ$^{-/-}$ or IIAIIIBγ$^{-/-}$), Mac-1-deficient mice (Mac-1$^{-/-}$) and CD18-deficient mice (CD18$^{-/-}$) have been described (15,33-35). Mac-1 deficient mice were bred with IIAγ$^{-/-}$ or IIAIIIBγ$^{-/-}$ mice to generate IIAγ$^{-/-}$Mac-1$^{-/-}$ and IIAIIIBγ$^{-/-}$Mac-1$^{-/-}$ animals or with wild type mice to generate IIAγ$^{+/+}$Mac-1$^{-/-}$ and IIAγ$^{+/+}$ mice. Mice were bred in a specific pathogen free facility. Age and gender matched mice 8–12 weeks old were used in all experiments. The Harvard Medical School Animal Care and Use Committee approved all procedures used in this study.

Passive transfer of human SLE sera or rabbit anti-GBM antibody

For the human SLE sera transfer model, mice were injected subcutaneously in both flanks with 2.5 μg of human IgG (Jackson ImmunoResearch Labs) in complete Freund's adjuvant (Thermo Scientific and Difco) on day -3. On days 0 and 2, 200μL of sterile serum was injected intravenously. For induction of nephrotoxic nephritis, mice were given rabbit IgG in CFA at day -3 in the footpad and rabbit αGBM antisera at day 0 as described (36) and urine and kidneys were collected at day 21.

Human sera samples

Human serum samples were obtained from the Lupus Clinic at the Beth Israel Deaconess Medical Center or Instituto Nacional de Ciencias Medicas y Nutricion Salvador Zubiran. Patients with SLE were diagnosed according to the classification criteria of the American College of Rheumatology (ACR). The inclusion criteria for SLE patients were patients who fulfilled ≥ 4 of

11 ACR criteria for SLE and that at the time of the first blood draw, had active disease (i.e. SLE disease activity index (SLEDAI) ≥6). Normal serum was obtained from healthy individuals matched for age, gender and ethnicity. At the time of serum collection, all individuals showed no signs or symptoms of infection. Informed consent was obtained from all patients and healthy donors under a BIDMC Institutional Review Board (IRB) approved protocol. Unless indicated, all experiments were performed using serum from SLE patient "A".

Disease evaluation

Functional assessment of renal damage: Spot urine samples were collected and urine albumin and creatinine were evaluated by ELISA (Bethyl Labs) and a chemical assay (Cayman Chemical Company) respectively (15) and expressed as a ratio of urine albumin to creatinine.

Clinical scoring of arthritis: Mice were evaluated every other day after induction of disease. Inflammation of each limb was scored as reported previously (37): 0, no evident inflammation; 1, redness or swelling of one toe; 2, redness or swelling of >1 toe; 3, ankle or tarsal-metatarsal involvement; 4, redness or swelling of the entire paw.

Histological assessment of tissue injury: Tissue sections were blindly evaluated. Histological score included endocapillary proliferation, leukocyte infiltration and crescents, as previously described (38). For joint lesions, histological scores reflected leukocyte infiltration, synovial thickening, and cartilage and bone erosion.

Histological studies

Kidneys were fixed in formalin and paraffin-embedded, or frozen in OCT medium and 5μM sections were prepared. Toe specimens were fixed in 4% paraformaldehyde and decalcified with

modified Kristensen's solution. After dehydration, the tissues were embedded in paraffin and 5 μm sections were made (39).

Immunohistochemistry: For kidneys, periodic acid-Schiff, H&E and dichloroacetate esterase (to identify neutrophils) on paraffin-embedded sections were performed as described (40). Neutrophils in 100 glomerular cross-sections were quantified and presented as neutrophils per glomerular cross-section. Immunohistochemistry on frozen sections was performed using a two-layer peroxidase method. Sections were immunostained with anti-F4/80 for macrophages (BioLegend), anti-CD3 (Serotech) for T cells, anti-C1q (Hycult Biotech) for C1q deposition and counterstained with Gill Hematoxylin No.2 (NewComerSupply Inc.). Tissue area occupied by macrophages or glomerular C1q deposition in four 20x consecutive fields was quantified using ImagePro. Sections of paraffin-embedded toes were stained with H&E and immunohistochemistry was performed with anti-NIMP-R14 (Abcam) for neutrophil quantification, anti-F4/80 (BioLegend) for macrophages, anti-CD3 (Serotech) for T cells or anti-human IgG (Invitrogen). The total number of neutrophils in a toe cross-section was counted and divided by the total tissue area in each section, using ImagePro.

Immunofluorescence: Human and mouse IgG deposition were evaluated on frozen sections using anti-human IgG or anti-mouse IgG (Invitrogen) Alexa fluor 488-conjugated antibodies, respectively. Deposition of C3 was evaluated using a FITC-conjugated anti-C3 antibody (ICN/CAPPEL). Images of at least 15 glomeruli per mouse were captured and glomerular fluorescence intensity was measured using the acquisition and analysis software Metamorph (Molecular Devices). To evaluate human IgG subclasses, immunofluorescence was performed using anti-human IgG1, IgG2, IgG3, and IgG4 antibodies (The Binding site) followed by an anti-sheep DyLight-488 conjugated antibody (Jackson ImmunoResearch Laboratories Inc.).

Electron microscopy: Kidney samples were taken 10 days after injection of SLE sera and processed using standard techniques.

Generation of a K562 stable cell line and analysis of binding to ICAM-1

The R77H mutation was introduced into human CD11b DNA by standard PCR techniques. K562 cells were transfected with WT or mutant (R77H) CD11b and CD18 plasmids by electroporation and confirmed by sequencing. Single cell sorting was used to select CD11b positive cells. Cells were cultured in RPMI 1640 media supplemented with 10% heat inactivated FBS, under constant selection using G418 (500μg/mL, Invivogen). CD11b expression was assessed by FACs analysis using anti-human CD11b-PE labeled antibody (BD Pharmingen). To evaluate K562 cell binding to ICAM-1Fc, cells were treated with 1mM $MnCl_2$ for 10min in HEPES buffer and drawn across a coverslip containing immobilized ICAM-1-Fc (15μg/mL, R&D) under 0.1dynes/cm^2 shear flow. The number of cells bound in 4 different fields was quantified every 2 minutes over a 10 min period.

IgG depletion and quantification of human IgG

SLE serum was incubated with Protein A/G coated agarose beads (Thermo Scientific) or control agarose beads. Depletion was determined by measuring human IgG by ELISA (Bethyl Labs). Human immune complexes were quantified in human and mouse serum using an ELISA kit with C1q as the capture element (ALPCO Immunoassays). Due to cross-reactivity with mouse IgG, an anti-human HRP antibody (Bethyl Labs) was used as the secondary antibody for the quantification of human ICs in murine serum samples.

Macrophage depletion using clodronate liposomes

Mice were given an intraperitoneal injection of 500μL of liposomes containing clodronate or PBS (41) on day -5 before the first SLE injection, followed by 200μL every 5 days. Tissue was harvested at day 10 or 14 after SLE sera injection. Macrophage depletion was confirmed by immunohistochemistry of kidneys and spleen using anti-F4/80 antibody.

Intravital microscopy evaluation of Reverse Passive Arthus reaction in the cremaster muscle

Rabbit IgG anti-bovine serum albumin (BSA) antibody (200μg/300μL; Sigma-Aldrich, St. Louis, MO) was injected intrascrotally, followed by an intravenous injection of BSA (300μg/100μL; Sigma-Aldrich, St. Louis, MO). After 3hrs, leukocyte recruitment in the cremaster of anesthetized mice was evaluated by intravital microscopy as previously described (15). Four venules per mouse were analyzed. Leukocyte rolling velocities were measured by tracking single leukocytes (10/venule) over several frames and calculating the distance moved per unit time (μm/s). Adherent leukocytes were defined as cells remaining stationary for 30 seconds and were expressed as the number of cells/mm^2 of venule.

MIP-2 was locally applied as previously described (42). Briefly, injections were done using a beveled glass pipette of 1mm outer diameter mounted on a manual micromanipulator (MM-33) (Warner Instruments, Hamden, CT). The tip was filled with 100 nmol/L of MIP-2 (US Biologicals). The pipette was placed and the number of rollers across a perpendicular line and adherent cells (Ab) in a 200 μm segment of the venule was recorded over a 1 minute period. Next, air pressure was applied to the pipette, to trigger the injection of MIP-2 (less than 1 μL). Successful injection was verified by the presence of swelling of the interstitial tissue surrounding

the pipette tip. The process of injection, and the following minute were recorded. The number of cells that were adherent after MIP-2 injection (Aa) was evaluated. The Δ adherent cells, which is the percent of rollers that adhered in response to MIP-2 injection, was calculated using the following equation: (Aa-Ab)/ #rollers X100.

Statistical analysis

Data are expressed as mean ± SEM. For proteinuria data, the line represents the median of the group. Differences were determined by Mann–Whitney test. For group analysis, one-way ANOVA was used for proteinuria data and two-way ANOVA was used for the cellular infiltration data. When significant differences were shown, data were subjected to Mann–Whitney test or Bonferroni test respectively for comparison between two mouse strains. P values <0.05 were considered significant.

III. Results

Human SLE serum induces nephritis in mice that express neutrophil human FcγRs and lack Mac-1

Human SLE serum was obtained from patients that had active disease (SLEDAI≥6) and no clinical evidence of infection. Gender and race matched healthy individuals served as controls. Mice preimmunized with human IgG/CFA received two intravenous injections of SLE sera at day 0 and day 2. Nephritis was monitored by analyzing albumin leakage in the urine over a 21 day period. SLE serum from patient "A" caused marked proteinuria in mice that expressed human FcγRs (hFcγRs) only when the mice additionally lacked Mac-1 (IIA$\gamma^{-/-}$Mac-1$^{-/-}$ and IIAIIIB$\gamma^{-/-}$Mac-1$^{-/-}$) (Fig. 2A). Proteinuria peaked at day 14 (Sup. Fig. 1A). Mac-1-deficient mice expressing FcγRIIA alone, without FcγRIIIB exhibited significant proteinuria suggesting that this hFcγR was sufficient for disease development (Fig. 2A). No proteinuria was observed in Mac-1-sufficient mice expressing hFcγRs (IIA$\gamma^{-/-}$ or IIAIIIB$\gamma^{-/-}$), Mac-1-deficient mice without hFcγRs ($\gamma^{+/+}$Mac-1$^{-/-}$) or wild-type animals (Fig. 2A). Surface expression of human FcγRs and the sister CD18 integrin, LFA-1 was similar in Mac-1 deficient and sufficient groups (Sup. Fig. 1B). Any effect of γ-chain deficiency superimposed on Mac-1 deficiency on disease susceptibility was ruled out as SLE serum induced nephritis in mice that expressed hFcγRIIA, lacked Mac-1, and were γ-chain sufficient (Fig. 2B).

Mouse anti-human IgG was detected in the serum (Sup. Fig. 1C) and in the kidney (Fig. 2C) after SLE sera transfer but this was minimal compared to that in wild-type mice subjected to anti-glomerular basement membrane (nephrotoxic) nephritis (Fig. 2C), a widely used model of immune-mediated disease induced by preimmunization with rabbit IgG/CFA followed by

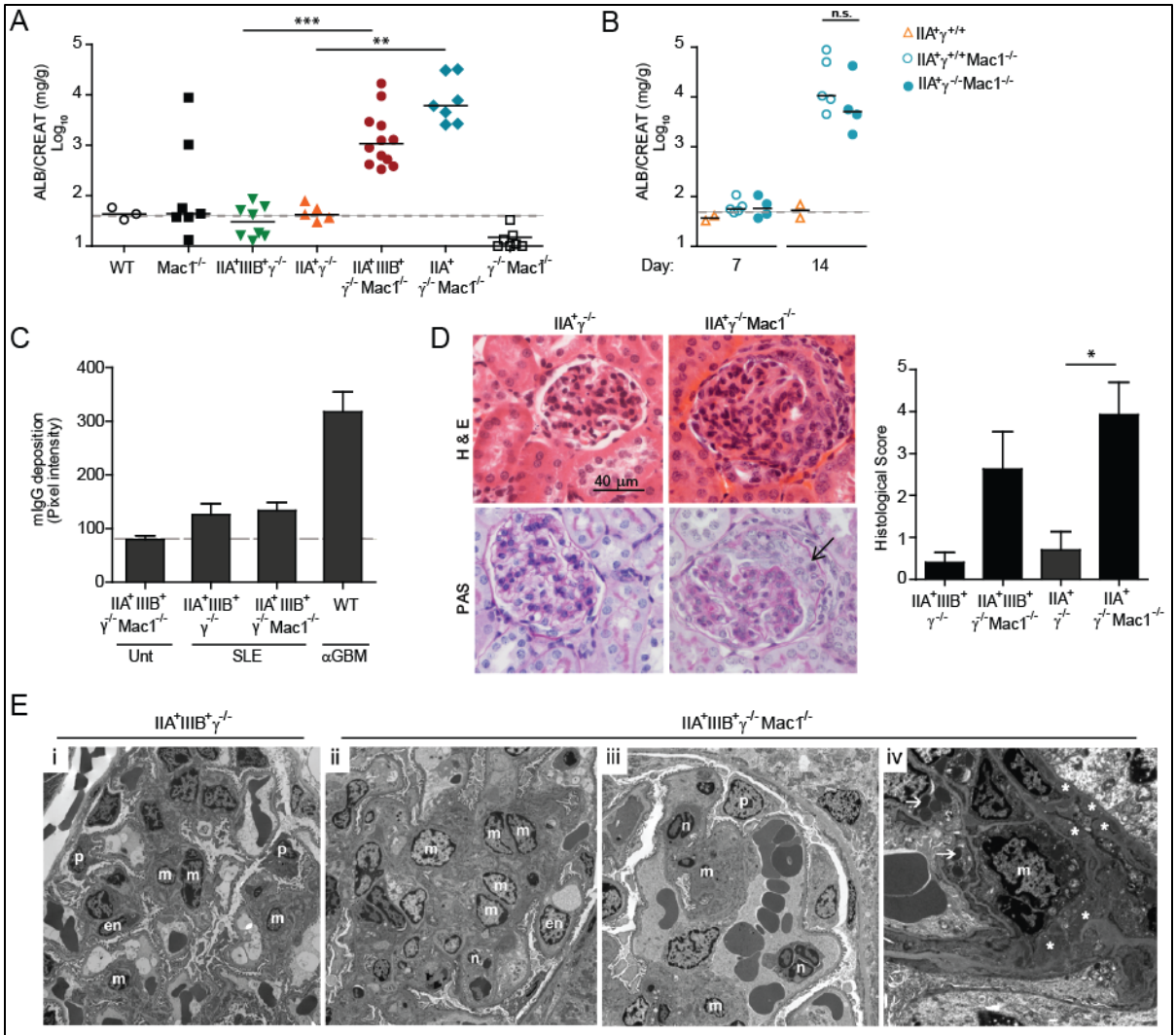

Figure 2. SLE sera induces nephritis in mice that express hFcγR and lack Mac-1. A) Mice received two intravenous injections of SLE sera "A" on day 0 and 2 and urine albumin (normalized to creatinine) at day 14 was evaluated. The dashed line indicates the mean of proteinuria in mice not given SLE sera. Each data point represents one mouse and the solid line is the median of the group. **B)** Mice expressing the FcγRIIA in the presence of the γ-chain (IIAγ$^{+/+}$), and the same that are additionally Mac-1 deficient (IIAγ$^{+/+}$Mac-1$^{-/-}$) were injected with SLE sera "A" and albuminuria was evaluated at day 7 and 14. Albuminuria in IIAγ$^{-/-}$Mac-1$^{-/-}$ mice given SLE sera was analyzed in parallel for comparison. Each dot represents one animal, and the line indicates the median of the group. ns= not significant. **C)** Murine anti-human IgG was quantified in renal tissue by immunofluorescence in indicated transgenic mice that were untreated (Unt) or 21 days following SLE sera "A" transfer (SLE). Wild-type mice given rabbit anti-GBM injection (WT αGBM) served as a positive control. Mean ±SEM are graphed. Dashed line is the average of pixel intensity in the "Unt" mice. **D)** Representative images of renal sections (day 21) stained with Hematoxilin and Eosin (H&E) or Periodic Acid Schiff (PAS). The arrow indicates a glomerular crescent which was observed in ~5% of the glomeruli. A histological score was given and Mean ±SEM was graphed (n≥5 mice per group). **E)** Electron microscopy of glomeruli of mice given SLE sera: (i) IIAIIIBγ$^{-/-}$ mice had normal glomerular architecture, (ii-iv) IIAIIIBγ$^{-/-}$Mac-1$^{-/-}$ mice exhibited mesangial expansion with increased cellularity (ii), neutrophils within capillary loops (iii) (x4730), mesangial electron-dense deposits (*) and lysosomal vacuoles containing protein reabsorption droplets (arrows) (iv) typically observed during proteinuria (x11100). en=endothelial, p=podocyte, m=mesangial cell, n=neutrophils. *p<0.05, **p<0.01 and ***p<0.001.

transfer of rabbit anti-glomerular basement membrane serum (43). Importantly, mouse anti-human IgG levels in both the serum and renal tissue were similar in disease susceptible and non-susceptible mice (Sup. Fig. 1C and Fig. 2C). Although a role for mouse anti-human IgG and/or ICs formed from human IgG reacting with antigens in the mouse serum cannot be formally ruled out it is unlikely to be critical for disease development for the following two reasons. First, SLE sera induced nephritis in the absence of preimmunization with CFA/human IgG (data not shown) albeit disease was more variable. Second, human FcγRs and thus by inference, human IgG is required for development of nephritis. In the anti-GBM murine model rabbit IgG triggers a robust murine anti-rabbit reaction, nonetheless, tissue injury is largely independent of the humoral response (44). We propose that as is known for other autoimmune models, activation of the innate immune response by CFA in our SLE model may be important independent of the adaptive immune response (45).

Histopathological and electron microscopy analyses of renal tissue from human SLE sera-treated mice were undertaken. Congruent with proteinuria, glomerular damage and inflammation were observed only in hFcγR^{+}γ$^{-/-}$Mac-1$^{-/-}$ animals (Fig. 2D, E) and were associated with mesangial deposits of ICs (Fig. 2E). Together these data suggest that Mac-1 deficiency enables SLE-induced kidney damage. This may have relevance to human disease since the R77H polymorphism in the *ITGAM* gene (that encodes the CD11b chain of Mac-1) associated with

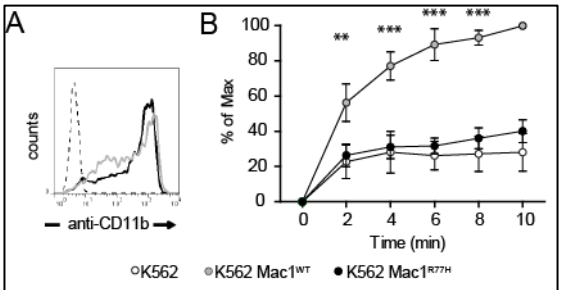

Figure 3. The SLE associated R77H mutation of Mac-1 abrogates its capacity to bind ICAM-1 under shear flow. A) Flow cytometry analysis of K562 cells stably expressing Mac-1 wild-type (WT) or Mac-1 R77H. Similar levels of Mac-1 were observed on the surface of Mac-1 WT and Mac-1 R77H transfected cells. **B)** Binding of K562 cells expressing WT or the R77H Mac-1 variant to plate-immobilized ICAM-1-Fc was evaluated under shear flow. Mac-1 R77H mutation prevented interaction with ICAM-1 compared to wild-type Mac-1. Mean ±SEM of 4 independent experiments is shown. **p<0.01, ***p<0.001.

SLE abrogates the capacity of Mac-1 expressed in a cell line (Fig. 3A), to bind its ligand ICAM-1 (Fig. 3B).

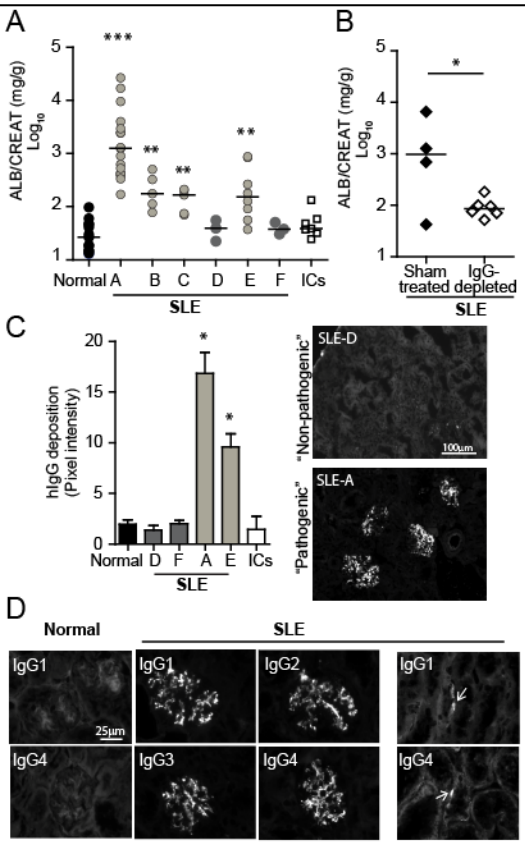

Figure 4. The pathogenicity of SLE serum correlates with the capacity of hIgG to deposit in the glomeruli. A) IIAIIBγ$^{-/-}$Mac-1$^{-/-}$ mice received sera from healthy donors (Normal, data is pooled from five donors), six SLE patients (denoted A-F), or heat aggregated human IgG (ICs). **p<0.01 and ***p<0.001 compared to mice that received normal sera. Each data point represents one mouse, and the line indicates the median. **B)** IIAIIIBγ$^{-/-}$Mac-1$^{-/-}$ mice were treated with SLE sera "A" subjected to sham or IgG depletion, and urine albumin was determined. **C)** Human IgG (hIgG) deposition in glomeruli was quantitated on day 21 in IIAIIIBγ$^{-/-}$Mac-1$^{-/-}$ mice injected with normal human sera, "non-pathogenic" (D, F) or "pathogenic" (A, E) SLE sera, or aggregated hIgG (ICs) (n≥3 mice per group). Mean ±SEM is given and representative pictures of selected samples are shown. *p<0.05. **D)** Glomerular deposition of human IgG isotypes (1-4) was evaluated by immunofluorescence in IIAIIIBγ$^{-/-}$Mac-1$^{-/-}$ given normal or SLE sera "A" (SLE). Focal tubular basement membrane deposition (arrows) was detected in some cases.

Pathogenicity of SLE serum depends on the IgG fraction and its capacity to deposit in glomeruli

Sera collected from different SLE patients were tested in susceptible IIAIIIBγ$^{-/-}$Mac-1$^{-/-}$ mice. Four out of six SLE sera induced nephritis, while sera from five healthy controls (normal serum), or heat aggregated human IgG (surrogate of ICs) failed to induce disease (Fig. 4A). Moreover, four out of five sera from SLE patients at an independent clinical center induced nephritis compared to normal controls (Sup. Fig.1D). Nephritis was observed with multiple SLE serum samples from the same patient when treatment and disease activity varied but circulating ICs remained elevated. IgG depletion of SLE serum "A" abrogated its nephritis-inducing capacity (Fig. 4B), which suggests that ICs in the sera are required for disease development (Fig. 2A). The sera that caused disease, henceforth referred to as "pathogenic sera" (e.g. SLE sera "A" and "E"), were associated with glomerular deposits of human IgG that exhibited a granular pattern characteristic of ICs (Fig. 4C). In contrast, no human IgG deposition was observed when "non-pathogenic" sera were injected; these included SLE sera "D" and "F" and sera from healthy controls (Fig. 4C). All four human IgG isotypes, IgG 1-4 were observed in the glomeruli, predominantly as deposits in the mesangium (Fig. 4D). Specificity of the antibodies was confirmed by analyzing their reactivity against purified human IgG1-4 in western blots (data not shown). In the case of serum "A", focal tubular basement membrane deposition of IgG was also detected (Fig. 4D), which is a pattern observed in human lupus nephritis. Sera pathogenicity (i.e. capacity of human ICs to deposit in glomeruli) did not correlate with the amount of ICs or IgG present in the sera (Sup. Table 1A), nor did it correlate with the patient type or lupus manifestations (Sup. Table 1B).

The susceptibility conferred by Mac-1 deficiency is not due to defects in IgG clearance

Levels of circulating (Fig. 5A) and deposited human IgG-ICs (Fig. 5B) as well as glomerular complement C1q and C3 deposition (Fig. 5B) were comparable between hFcγR expressing mice that were Mac-1 sufficient (IIAIIIBγ$^{-/-}$) or deficient (IIAIIIBγ$^{-/-}$Mac-1$^{-/-}$), as were peripheral blood neutrophil and leukocyte counts (Sup. Table 1C).

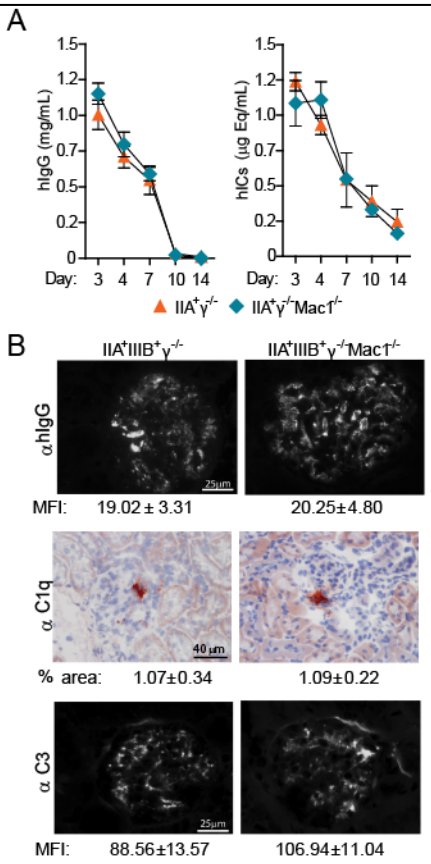

Figure 5. Immune complex clearance and deposition are similar in susceptible and non-susceptible mice. A) Serum was collected from animals at intervals up to day 14 after SLE sera "A" transfer. Circulating human IgG (hIgG) and human IgG-immune-complexes (hICs) were evaluated and the mean ±SEM were graphed. **B)** Kidneys were harvested at day 14 after SLE sera "A" transfer and renal sections were stained for hIgG, murine C1q, and complement C3. The mean fluorescence intensity (MFI, average pixel intensity, ±SEM) for glomerular hIgG and C3 and the percent of glomerular area positive for C1q (% Glm area ±SEM) were determined and found to be equivalent in both groups.

Passive transfer of human SLE serum induces arthritis in mice

Notably, two of the "pathogenic" SLE sera, "A" (Figure 6) and "E" (data not shown) caused arthritis in mice that affected primarily small joints, namely the distal interphalangeal and was evident at day 4. Patient "A" had clinical manifestations of arthritis, and Patient "E" did not have arthritis, but presented with Raynaud syndrome. There was no correlation between human symptoms and arthritis development as some sera from patients that clinically presented with nephritis and arthritis did not induce arthritis in mice (data not shown). Moreover, unlike nephritis, development of arthritis was more variable with different sera samples. As occurred with the nephritis, only hFcγR expressing mice lacking Mac-$1^{-/-}$ developed arthritis (Fig. 6A). Histopathological analyses revealed intense joint inflammation with cellular infiltration associated with bone and cartilage destruction (Fig. 6B). Significant deposition of human IgG-IC within synovial blood vessels was observed in both disease-susceptible and non-susceptible mice (Fig. 6C). Neutrophils were abundant in the lesions (Fig. 6D) while macrophages and T cells were not detected (data not shown).

Marked glomerular neutrophil infiltration is observed in susceptible mice while macrophages do not contribute to disease

Susceptible mice (hFcγ$R^{+}\gamma^{-/-}$Mac-$1^{-/-}$) exhibited abundant glomerular neutrophil infiltration at day 10 that significantly exceeded that in non-susceptible mice (Fig. 7A). In contrast, a mild interstitial macrophage and T cell infiltration was observed in both groups of mice (Fig. 7A). Thus Mac-1 deficiency appears to selectively enable neutrophil accumulation. To distinguish if the Mac-1-expressing cell responsible for resistance to nephritis corresponded to circulating (i.e. monocytes or neutrophils) or resident cells, we generated bone marrow chimeras. Bone marrow

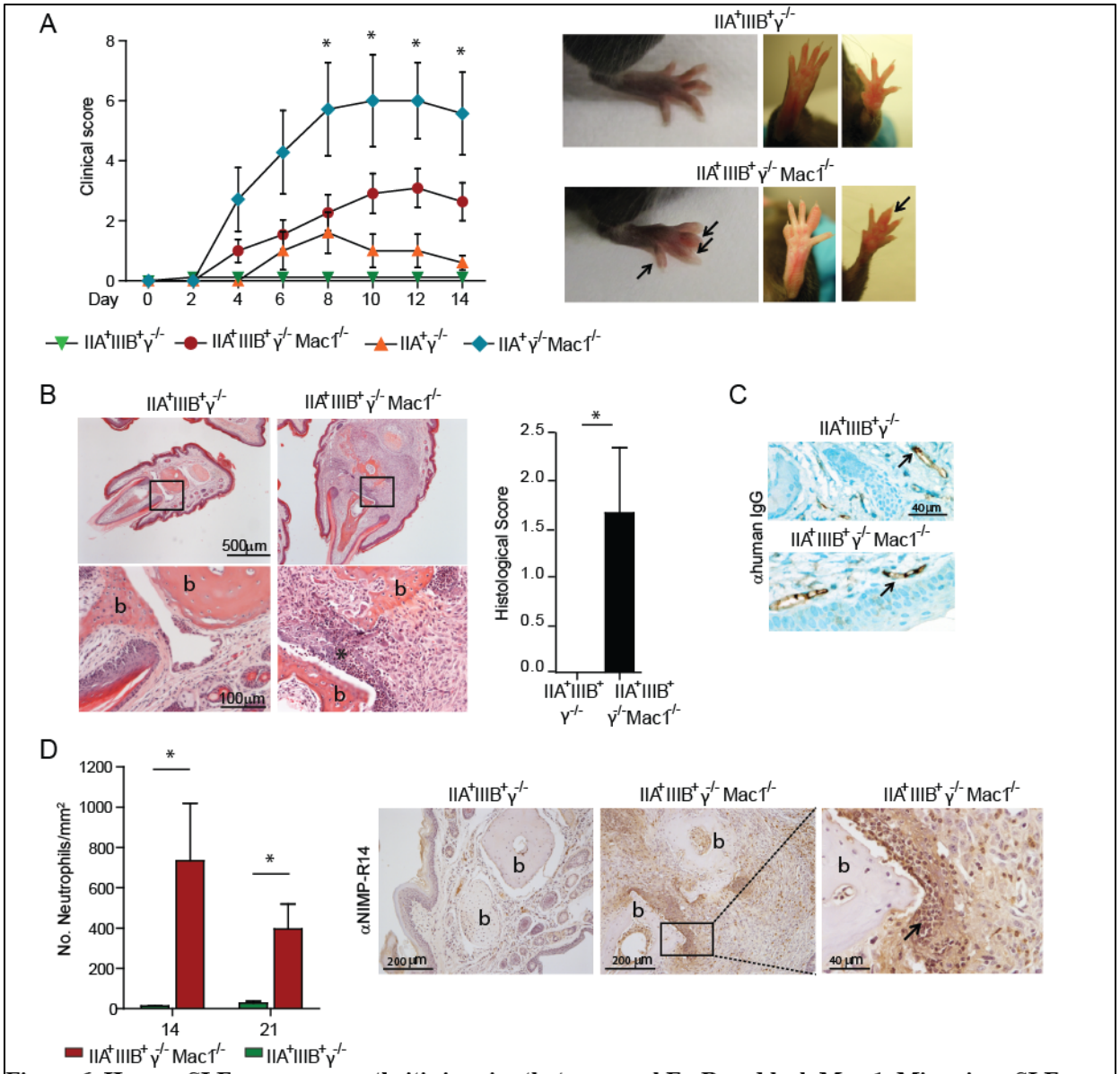

Figure 6. Human SLE sera cause arthritis in mice that express hFcγR and lack Mac-1. Mice given SLE sera "A" were evaluated for the development of arthritis. A) Inflammation of each limb was assessed and a clinical score was given as described in Methods. As shown in representative pictures, mostly small joint involvement (arrows) was observed. *p<0.05 compared to IIAIIIBγ$^{-/-}$ and IIAγ$^{-/-}$ given SLE sera. **B)** Representative images of histological sections stained with H&E (upper panels) with magnification of boxed area (lower panels) are shown for indicated mice. Bone (b) erosion and inflammatory cell infiltration (*) were apparent only in IIAIIIBγ$^{-/-}$Mac-1$^{-/-}$ mice. The histological score in affected limbs of IIAIIIBγ$^{-/-}$Mac-1$^{-/-}$ and similar digits in IIAIIIBγ$^{-/-}$ mice included leukocyte infiltration, synovial thickening, and cartilage and bone erosion. **C)** Tissue hIgG staining by immunohisto-chemistry showed intravascular IC deposition (arrows) in susceptible and non-susceptible mice treated with SLE sera. **D)** Neutrophils in joint sections harvested at indicated days after SLE serum injection were quantitated. Robust neutrophil accumulation was observed only in IIAIIIBγ$^{-/-}$Mac-1$^{-/-}$. Representative pictures of indicated mice are shown. Only IIAIIIBγ$^{-/-}$Mac-1$^{-/-}$ have neutrophil infiltrates (arrow) adjacent to damaged articular surfaces as well as periarticular soft tissue. All data are mean ±SEM. For B and D, *p<0.05.

from IIAγ$^{-/-}$ or IIAγ$^{-/-}$Mac-1$^{-/-}$ mice was transferred into lethally irradiated γ$^{-/-}$Mac-1$^{-/-}$ or γ$^{-/-}$ mice, respectively (i.e. IIAγ$^{-/-}$ → γ$^{-/-}$Mac-1$^{-/-}$ and IIAγ$^{-/-}$Mac-1$^{-/-}$ → γ$^{-/-}$), and 3 months later SLE serum was administered. IIAγ$^{-/-}$Mac-1$^{-/-}$ bone marrow provided susceptibility to nephritis when transferred into non-susceptible γ$^{-/-}$ mice suggesting that a lack of Mac-1 on hFcγRIIA expressing circulating cells allows the development of disease (Sup. Fig. 2A). Immunohistochemistry in tissue of γ$^{-/-}$Mac1$^{-/-}$ recipients of IIAγ$^{-/-}$ bone marrow revealed Mac-1 positive macrophages in the renal interstitium following human SLE serum transfer, suggesting that SLE serum induces renal infiltration of blood monocytes and their subsequent differentiation into macrophages (Sup. Fig. 2A). To determine if monocytes/macrophages contribute to renal injury, these populations were depleted prior to SLE serum transfer by administering clodronate liposomes, which are internalized by these cells and leads to their apoptosis (Sup. Fig. 2B). Macrophage-depleted IIAγ$^{-/-}$Mac-1$^{-/-}$ mice remained highly susceptible to nephritis (Fig. 7B) suggesting that macrophages do not significantly contribute to renal injury. Moreover, macrophage-depletion in disease non-susceptible (IIAγ$^{-/-}$) mice did not result in proteinuria (Fig. 7C) or glomerular neutrophil infiltration (data not shown) at day 10, suggesting that Mac-1 deficiency in monocytes/macrophages does not enable disease.

Mac-1 deficiency modifies the response of neutrophils towards tissue deposited immune complexes in vivo

Intravital microscopy experiments were performed by Kan Chen and Kevin Croce

To elucidate the mechanism(s) by which Mac-1 regulates FcγRIIA-mediated neutrophil accumulation, we conducted intravital microscopy of the cremaster muscle that allows the real time visualization of neutrophil behavior within the vessel wall. The Reverse Passive Arthus

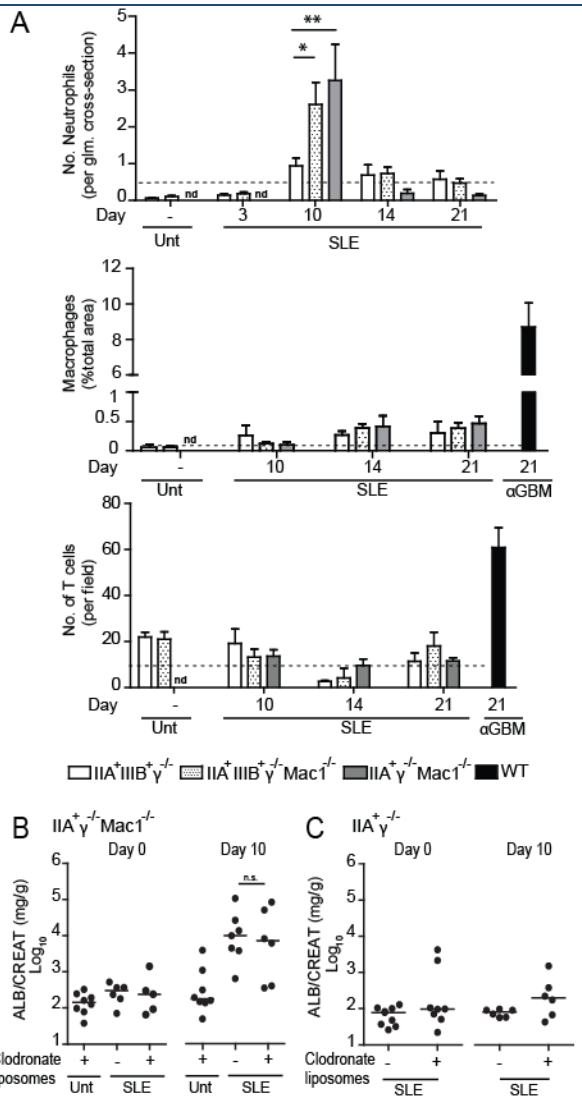

Figure 7. Disease in susceptible mice is associated with neutrophil accumulation; macrophages do not participate in disease development. A) Kidneys were harvested from mice at day 21 after injection of SLE serum "A". nd= not determined. Dotted line represents the mean value obtained in susceptible mice given normal human serum and harvested at day 10 (top panel) or day 14 (middle and bottom panels). Neutrophil, macrophage and T cell infiltration were quantified by immunohistochemistry. Mice treated with αGBM serum are included as a positive control for the indicated leukocyte infiltration. Mean ±SEM is shown. *p<0.05, **p<0.01 compared to IIAIIIBγ$^{-/-}$ injected with SLE sera. n=3-7 mice per group. Animals were treated with liposomes that contained clodronate (+) or PBS (-) and proteinuria was evaluated at indicated times in IIAγ$^{-/-}$Mac-1$^{-/-}$ **(B)** and IIAγ$^{-/-}$ **(C)** mice. *p<0.05. nd, not determined; ns, not significant.

(RPA) reaction, induced by the intravenous administration of soluble BSA and an intrascrotal injection of anti-BSA results in IC deposition within and outside the cremasteric vessels (15,46). The RPA induces neutrophil rolling that is P- and E-selectin dependent (46), while the slowing

of the rolling velocity and adhesion is dependent on murine FcγRs (47) and FcγRIIA (15). Following induction of the RPA, neutrophils in the venules of IIAγ$^{-/-}$Mac-1$^{-/-}$ mice rolled significantly slower than in IIAγ$^{-/-}$ mice (Fig. 8A). This was not a result of differences between the two groups in expression of LFA-1 on circulating neutrophils or neutrophils recruited to the cremaster (Sup. Fig. 2C). The slow rolling required FcγRIIA, as it was not observed in γ$^{-/-}$Mac-1$^{-/-}$, and γ$^{-/-}$ mice (Fig. 8B). The downmodulatory effect of Mac-1 was selective for ICs as the rolling velocity induced by an intrascrotal injection of TNFα was actually increased in IIAγ$^{-/-}$ Mac-1$^{-/-}$ mice compared to IIAγ$^{-/-}$ mice (data not shown) as previously described (48). In the RPA, the observed slower neutrophil rolling in IIAγ$^{-/-}$Mac-1$^{-/-}$ mice was not associated with an increase in the number of adherent cells compared to IIAγ$^{-/-}$ mice (Fig. 8C). E-selectin mediated activation of LFA-1 has been shown to slow neutrophil rolling velocity, and in turn lead to efficient firm adhesion only in response to a local chemoattractant stimulus, Macrophage Inflammatory Protein-2 (MIP-2) (42). Accordingly, the local microinjection of MIP-2 favored adhesion of neutrophils in IIAγ$^{-/-}$Mac-1$^{-/-}$ compared to IIAγ$^{-/-}$ animals subjected to the RPA (Fig. 8D). IC induced slow rolling and MIP-2 induced neutrophil adhesion is likely LFA-1 dependent as these steps were markedly diminished in CD18 deficient mice (Fig. 8E, F).

In summary, FcγRIIA-dependent slow rolling, which correlates with efficient leukocyte adhesion in response to MIP-2 is regulated by Mac-1, with a deficiency in this integrin resulting in a further decrease in rolling velocity and subsequent enhanced responsiveness of neutrophils to a local chemotactic stimulus.

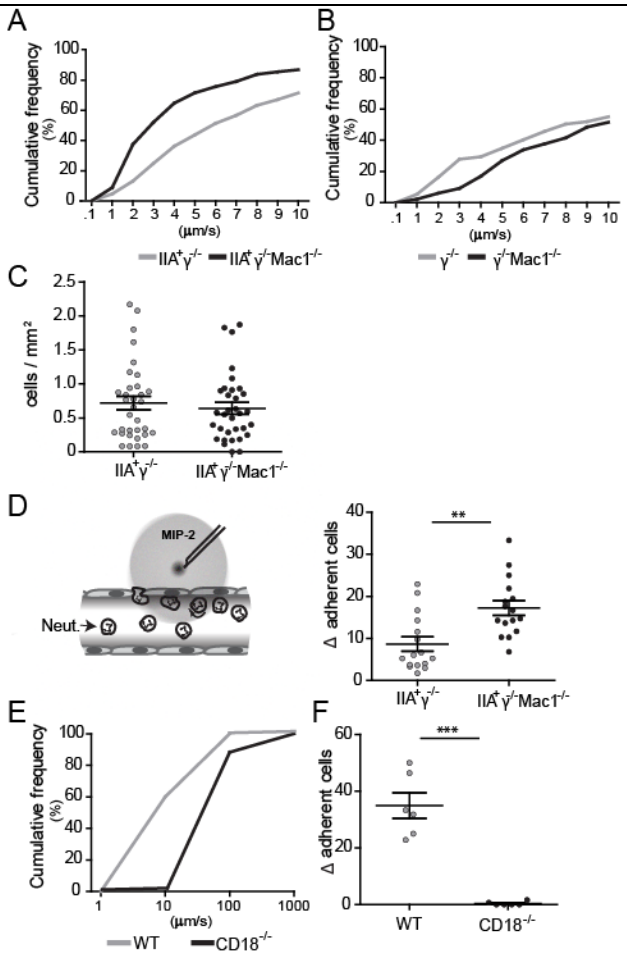

Figure 8. Mac-1 deficiency slows the rolling velocity, and increases the chemoattractant induced adhesion of neutrophils following the Reverse Passive Arthus reaction. The RPA was induced in the cremaster and 3hrs later, the mice were prepared for intravital microscopy and neutrophil rolling velocity was measured in hemodynamically similar venules of **A)** IIA$\gamma^{-/-}$Mac-1$^{-/-}$ and IIA$\gamma^{-/-}$ mice (n=33 venules in 6 mice per group), and **B)** $\gamma^{-/-}$Mac-1$^{-/-}$ and $\gamma^{-/-}$ mice (n=13 venules in 3 mice per group). Cumulative histograms of rolling velocities are shown. **C)** The number of adherent neutrophils in mice analyzed in panel A was determined. **D)** Mice were subjected to the RPA, the cremaster was prepared for intravital microscopy and a local injection of MIP-2 was given as depicted in the diagram. The increase in neutrophil adhesion after local MIP-2 injection (Δ of adherent cells) in IIA$\gamma^{-/-}$ and IIA$\gamma^{-/-}$Mac-1$^{-/-}$ mice was calculated (n=15-16 venules in 6-7 mice per group). **E)** Cumulative histogram of neutrophil rolling velocities of WT and CD18$^{-/-}$ mice subjected to the RPA, and **F)** Δ of adherent cells upon MIP-2 injection are shown (n=6 venules in 3 mice per group). For (C), (D) and (F), mean ±SEM are graphed. **p<0.01, ***p<0.001.

IV. Discussion

In this study, we show in a novel lupus model that IC deposition and organ damage are not inextricably linked but that additional genetic factors dictate the propensity for target organ damage. In particular, we demonstrate that the neutrophil response to deposited ICs and subsequent tissue injury, following human lupus sera transfer is modulated by a functional association between an integrin and an IgG receptor. The role of Mac-1 in attenuating FcγRIIA mediated neutrophil recruitment in the context of deposited ICs, is unanticipated from previous work that have established Mac-1 largely as a positive regulator of neutrophil influx and inflammation (31,49). Our data predict that the R77H Mac-1 variant, which leads to reduced binding to its ligands, may have functional consequences for SLE patients and offer a mechanism by which Mac-1 dysfunction may contribute to end organ injury in SLE.

Disease susceptibility permitted by the absence of Mac-1 was not related to alterations in IC handling presumably by macrophages. Moreover, Mac-1 on macrophages and indeed macrophages themselves did not influence disease susceptibility. Thus this cell type, abundant in SLE lesions (50) is not essential for target organ injury in our model at least in the time frame of our experiments. Instead Mac-1 deficiency likely predisposes to disease development due to unrestrained FcγRIIA mediated neutrophil accumulation in the kidney. The reported physical interaction of Mac-1 with human FcγRs on the cell surface (51), and the sharing of intracellular ITAM-based signaling cascades by these two receptors (52) led us to the intriguing possibility that Mac-1 on neutrophils, *in cis*, modulates neutrophil FcγRIIA activity and function.

FcγRIIA on neutrophils clearly has the capacity to induce tissue injury in vivo (15,16). However, in the context of ICs deposits in the kidney and joints, the regulation of FcγRIIA mediated

neutrophil recruitment appears to be a key step in conferring disease susceptibility. Recent work suggests that binding of FcγRIIA to ICs and function may be regulated. In vitro, the G-protein coupled receptor agonists C5a and fMLP enhances (16,53) while co-engagement of FcγRIIB inhibits (54) FcγRIIA function. How is FcγRIIA regulated by Mac-1? Clues were provided by intravital microscopy. Slowing of the velocity of rolling cells improves their efficiency of firm adhesion (48) and in the RPA, FcγRIIA plays an important role in mediating slow rolling and leukocyte arrest (15). Additionally, CD18 integrins are required as slow rolling and MIP-2 mediated adhesion in the RPA is abrogated in CD18 deficient mice. We postulate that FcγRIIA promotes the activation of LFA-1. A deficiency in Mac-1 heightens FcγR activity towards ICs and subsequent LFA-1 activation that in turn leads to further deceleration of the rolling velocity and increased responsiveness to MIP-2. Mac-1 may be responsible for mitigating FcγRIIA mediated signaling or limiting FcγRIIA mobility or clustering, the molecular details of which require further investigation. Human FcγRIIA appears to functionally interact with murine Mac-1 *in cis* suggesting that this interaction uses conserved features of human and mouse Mac-1.

The observed decrease in neutrophil accumulation in Mac-1 deficient mice in other models of IC mediated disease including acute anti-GBM, thrombotic glomerulonephritis, and bullous pemphigoid (40,55,56), suggest differential roles for Mac-1 in distinct models of IC-based diseases. Complex biological circuits predict dual and sometimes opposing roles for the same receptor that is cell type and context dependent. For example, incomplete phosphorylation of the ITAM following engagement of B or T cell receptors by low affinity/valency ligands favors inhibitory over activating signaling by these immune receptors (57). Moreover, non-sustained FcαRI clustering markedly inhibits whereas sustained FcαRI aggregation promotes cell activation through differential recruitment of the tyrosine kinase Syk versus an inhibitory protein

phosphatase SHP-1 (58,59). We posit that Mac-1 relays similar context dependent inhibitory and activating signals, a hypothesis that is supported by the finding that although the R77H Mac-1 polymorphism is a susceptibility factor for lupus (24) it does not predispose to rheumatoid arthritis (60). Interestingly, FcγRIIIB may also play context dependent roles in IC mediated inflammation. While low expression of FcγRIIIB is associated with SLE (61), high FcγRIIIB levels increase susceptibility to anti-neutrophil cytoplasmic antibody (ANCA)–associated systemic vasculitides, diseases associated with in situ rather than soluble ICs (62). This concept is recapitulated in our mouse models. Human SLE serum induced nephritis was reduced in mice expressing both human FcγRIIA and FcγRIIIB versus FcγRIIA alone, which contrasts with the greater proteinuria following anti-GBM nephritis in mice expressing both hFcγRs compared with mice expressing FcγRIIA alone (15).

Our studies suggest that neutrophils are the primary cellular link between IgG and target organ damage in our model. Neutrophils are present in renal SLE lesions (63,64), precede macrophage infiltration (63), and are appreciated as a sign of disease severity (65). Importantly, recent studies identified a subset of neutrophils in SLE patients that synthesize type I IFNs, induce endothelial cell damage (66), release neutrophil extracellular traps (NETs) that are potentially autoantigenic, and drive IFNα production by dendritic cells (67,68). SLE sera transfer results in the development of lesions that recapitulate several features of lupus nephritis. The mice obviously lack the imbalances in the adaptive immune response and therefore chronicity of the disease. However like SLE patients, where development of lupus nephritis is not associated with autoantibodies of singular IgG specificity (68), a spectrum of IgG1-4 subtypes were found deposited in the glomeruli, with the capacity of SLE sera to induce proteinuria being directly correlated with their ability to deposit. Histological features similar to human disease include

mesangial hypercellularity and mesangial deposits (mainly IgG), C3 deposition, endocapillary and extracapillary proliferation (crescents) and neutrophils. The lack of the interstitial component, thickening of the membrane, or podocyte effacement is likely because the immune deregulation in SLE patients is much more profound than in our model. Renal injury in our model is unlikely a consequence simply of an immune response against heterologous human IgG as normal human serum, some SLE patient serum and heat aggregated human IgG failed to induce nephritis and murine anti-human IgG antibody deposition in the glomeruli.

Indiscriminate immunosuppression remains the prevailing therapy in SLE with significant toxicity, and the expectations from therapeutic targeting of the aberrant immune system have remained unfulfilled (29). Our data in a humanized mouse model indicate that deposition of circulating autoantibodies is not sufficient for target organ damage. Rather, regulation of neutrophil FcγRIIA by Mac-1 fundamentally influences IC-mediated end organ damage. Moreover, our humanized passive SLE sera transfer model will aid in delineating additional mechanisms specifically driving lupus induced tissue injury and serve as a preclinical platform to test new therapeutics targeted at preventing lupus end organ damage.

Chapter 3. Evaluation of the role of Mac-1 in autoimmune organ damage

Evidence obtained in patients with SLE and their healthy relatives, as well as data from murine models of autoimmune disease, indicate that tolerance failure is not sufficient to generate end organ damage. This suggests that factors that regulate local inflammation and effector responses to products of the autoimmune response (i.e. deposited ICs) dictate susceptibility to end organ damage. Accordingly, we have shown that Mac-1 modulates the activation of neutrophils through FcγRIIA and only in its absence does ICs trigger a pathogenic response (26). To provide further evidence that Mac-1 exerts a protective role by limiting the activation of neutrophils in the context of autoimmune end organ damage, we tested the hypothesis that immune complex generation in a congenic *Sle1b* lupus prone mouse model characterized by high circulating ICs, will result in glomerulonephritis only when neutrophil FcγRIIA is expressed in the absence of Mac-1.

In the current view of SLE pathogenesis, each element of the immune system contributes to the disease in a specific manner. This has been studied by Wakeland's group in a spontaneous murine model of lupus (NZM2410 mice). Through genetic analyses, they have demonstrated that the development of autoimmune disease in NZM2410 mice is governed by three risk loci independent of the MHC (69). These loci (*Sle1*, *Sle2*, and *Sle3*) have been expressed independently in the C57BL/6 background and their contributions to disease have been studied. Mice carrying the *Sle1* locus develop high titers of IgG anti-nuclear autoantibodies. However, their frequency of nephritis is low (less than 20% of mice develop glomerulonephritis at the age of 12 months) and its severity is minimal. In contrast, the *Sle2* locus affects the behavior of B cells and induces elevated levels of polyreactive IgM. The *Sle3* locus causes high titers of IgM

and IgG and severe nephritis (70). Within the *Sle1* congenic interval, three sub-loci have been associated with loss of tolerance to chromatin: *Sle1a*, *Sle1b*, and *Sle1c*. The effects of the *Sle1b* sub-locus are dominant, as the serological and cellular characteristics closely resemble those of mice that carry the complete *Sle1* interval (71).

In order to evaluate the hypothesis that Mac-1 has a role in the protection against end organ damage, we used the *Sle1b* mice as a model were the tolerance breach has occurred, but the autoimmune response has not resulted in organ inflammation and clinical manifestations. For this purpose we introgressed *Sle1b* into the Mac-$1^{-/-}$ mice in the presence or absence of human FcγRIIA. Mice were followed for one year (Fig. 9A) and evaluation of the development of glomerulonephritis was assessed by the presence of albuminuria. Histologic signs of active involvement of the glomeruli by lupus nephritis manifested by leukocyte neutrophilic infiltration (0-3), cellular proliferation (0-3), wire loop (0-3), and crescents formation (0-3) were assessed as previously described (38). A combined score was generated and mild and severe lupus nephritis activity was considered based on 1-4 and ≥5 of total scores, respectively.

Significant levels of albuminuria were detected at 6 months of age in *Sle1b* mice that expressed FcγRIIA and lacked Mac-$1^{-/-}$ (Fig. 9B). The histological evaluation of the kidneys performed on samples from 12 month old mice, revealed that the presence of FcγRIIA in the *Sle1b* mice increased the susceptibility for development of glomerulonephritis (i.e. 20% of *Sle1b* mice developed mild glomerulonephritis whereas all *Sle1b*FcγRIIA mice succumbed to disease; 80% mild and 20% severe). Importantly, the absence of Mac-1 in *Sle1b*FcγRIIA mice markedly increased the severity of glomerulonephritis (i.e. all *Sle1b*FcγRIIA mice developed glomerulonephritis; 33% mild and 66% severe) (Fig. 9C). It is worth mentioning that two

specimens that expressed Mac-1 showed abundant ICs deposition (manifested by several wire loops), but no neutrophil infiltration.

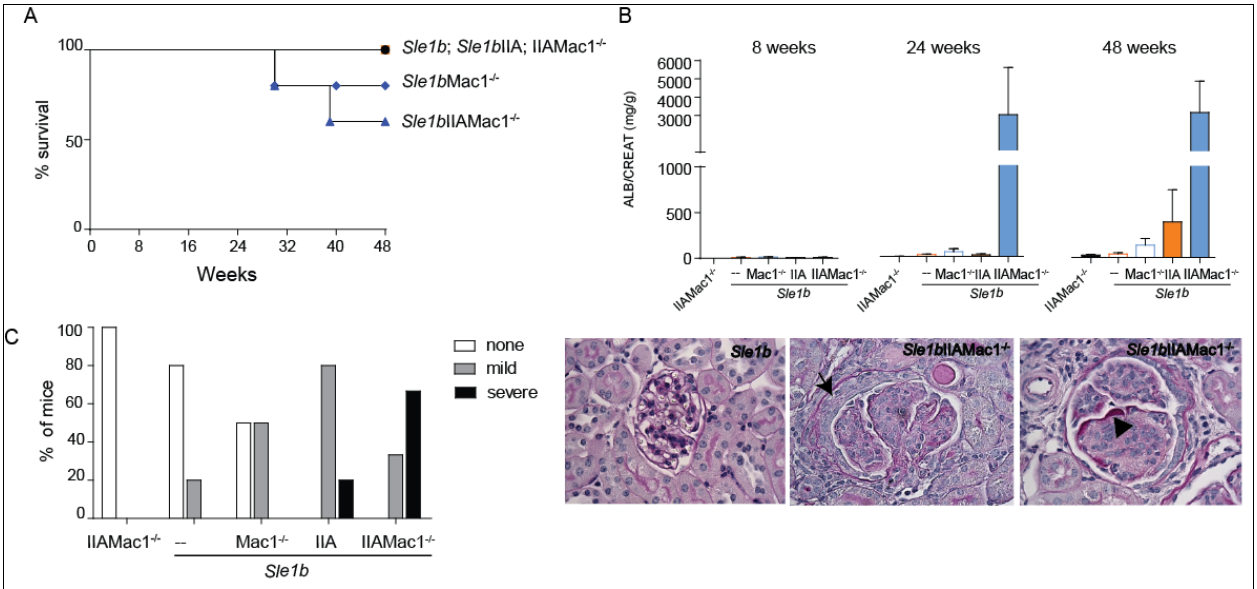

Figure 9. Evaluation of the effect of Mac-1 in progression of lupus nephritis. A) Survival curve for 48 weeks of indicated mice. **B)** Evaluation of albuminuria (normalized to creatinine) of indicated mice at 8, 24 and 48 weeks. **C)** Histological evaluation of kidney at 12 months of age. Percentage of mice that develop none, mild or severe glomerulonephritis is shown. Representative pictures of normal (*Sle1b*) or affected glomeruli (*Sle1b*IIAMac1$^{-/-}$) are shown (Periodic acid-Schiff stain, original magnification x600; arrow indicates a crescent, and arrow head indicates wire loop formation).

These results support a role for Mac-1 as a critical regulator of neutrophil responses to deposited ICs that leads to tissue damage. We proposed that the absence of Mac-1 on neutrophils bearing FcγRIIA lowers their threshold of activation leading to tissue injury. However, there are alternative explanations for our findings. For example, we cannot rule out the possibility that Mac-1 deficiency on other cell types, such as B-cells, macrophages or NK cells indirectly influences neutrophil FcγRIIA function. The finding that the presence of FcγRIIA alone increases the risk for glomerulonephritis is interesting, because it may reveal the potency of the human FcγRIIA *vs.* the mouse activating FcγRs in SLE-IC-induced tissue damage. However, we cannot rule out the possibility that it is due to an increase of the total FcγR pool (i.e. endogenous

murine FcγRs and FcγRIIA) and therefore potentially a greater neutrophil response to ICs. It is possible that the absence of Mac-1 promotes neutrophil accumulation indirectly. That is, kidney inflammation could further amplify the autoimmune response by increasing the availability of autoantigens, and their presentation in an inflammatory setting. Finally, it is possible that the human FcγRIIA in mice is more potent than the murine FcγRs because it does not engage the regulatory machinery that modulates murine FcγR activity. For example, human FcγRIIB downregulates FcγRIIA responses in macrophages, a process that may not happen with murine FcγRIIB. This is an unlikely explanation as neutrophils do not express FcγRIIB (72). Further analyses (described in the next chapter) will be pursued to better delineate the mechanisms through which Mac-1 negatively regulates FcγRIIA dependent neutrophil activation and organ damage.

Chapter 4. Engagement of Mac-1 on neutrophils generates intracellular signals that can potentially modulate the activity of FcγRIIA

I. Introduction

Neutrophils are abundant, terminally differentiated cells that are rapidly recruited to sites of inflammation, where they efficiently engulf and eliminate pathogens through the production of reactive oxygen species (ROS) and the release of proteolytic enzymes. Once activated, neutrophils also produce chemokines and cytokines that amplify the intensity and the duration of the immune response. These mechanisms contribute to the efficient clearance of pathogens and shape the landscape for the ensuing adaptive immune response. However, in the context of sterile inflammation, such as in autoimmune diseases, the products released by neutrophils can promote significant tissue injury (64).

In autoimmune conditions where high amounts of immune complexes exist (due to excessive production or deficient clearance), neutrophils are activated through surface receptors, such as Fcγ receptors (FcγR) and the complement receptor Mac-1. FcγRs are a heterogeneous group of molecules that bind the constant region of IgG. These molecules are expressed by many cell types including neutrophils, monocytes, natural killer cells, dendritic cells (DC), and basophils. Functionally, FcγR can be divided into activating and inhibitory receptors that transmit their signals via ITAM or ITIM, respectively. All murine activating FcγRs (FcγRI, FcγRII, FcγRIII, and FcγRIV) require the presence of the signaling γ-chain (which contains an ITAM) for their surface expression and signal transduction (73). Accordingly, mice deficient in γ-chain do not express any activating FcγR and are protected in several models of IC-mediated inflammation

(e.g. SLE-serum (26) and anti-GBM induced nephritis, RPA reaction (15), and KBxN arthritis (16)). Human cells express three families of FcγR: FcγRI, FcγRII (FcγRIIA, FcγRIIB, FcγRIIC), and FcγRIII (FcγRIIIA and FcγRIIIB). They all possess extracellular Ig-like domains, but differ in their transmembrane and intracytoplasmic regions. FcγRIIA is a single polypeptide chain containing an activating motif (ITAM) in its cytoplasmic domain. This molecule, which has no murine homologue, preferentially binds IgG forming ICs (73). Due to the differences between human and mouse neutrophil FcγR repertoire, murine models have been inadequate to evaluate the physiological functions of the human neutrophil FcγR and their contribution to disease. Moreover, the specific role of neutrophil FcγRs in disease pathogenesis has been limited in mouse models generated with global deletions of activating receptors. This has limited our capacity to understand the role of specific human FcγRs in neutrophils under physiological or pathological conditions. This issue has been addressed by the generation of transgenic mice that express FcγRIIA selectively on neutrophils. By crossing these mice with $\gamma^{-/-}$ mice (that lack all murine activating FcγR) the role of FcγRIIA has been examined. Transgenic mice expressing human FcγRIIA on neutrophils significantly regain susceptibility to IC-mediated diseases, suggesting that FcγRIIA on neutrophils may serve as a primary link between ICs and tissue injury (15,16).

Given its potent pro-inflammatory functions, FcγRIIA activity on neutrophils must be tightly regulated, yet the mechanisms for this remain largely undefined. The ITIM-bearing FcγRIIB has been described as a modulator of FcγR responses, through the action of the inositol polyphosphate 5-phosphatases SHIP-1, SHIP-2 and SHP1 (SH2-domain-containing protein tyrosine phosphatase-1). These molecules oppose the signaling pathways activated by FcγRIIA

by hydrolyzing phosphoinositide intermediates. In addition, SHIP activation (through phosphorylation) has been proposed to result from FcγRIIA activity, as a negative feedback mechanism (74). SHP-1 has also been found to associate with the ITAM of FcγRIIA and to dephosphorylate the p85 subunit of PI3K and Syk, downstream molecules activated by FcγRIIA (75). We have demonstrated that the β2 integrin Mac-1, inhibits FcγRIIA-induced slow rolling of neutrophils over ICs and protects against the development of FcγRIIA-dependent glomerulonephritis, suggesting that Mac-1 is a regulator of FcγRIIA activity. Physical interaction between Mac-1 and FcγRIIA by fluorescent resonance energy transfer (FRET) and by coimmunoprecipitation has been described. This interaction has been found to be via the I-domain (E^{252}-R^{261}) of Mac-1 (76) and has been mostly regarded as pro-inflammatory because it enhances Fc-dependent phagocytosis, antibody-dependent cell-mediated cytotoxicity, cytokine production (i.e. LTB4), and adhesion to ICs (76). However, it is becoming clear that Mac-1 can also exert negative functions over effector receptors (18,19,77).

The overall aim of this section was to study the mechanism through which the FcγRIIA signaling cascade is modified by Mac-1 engagement.

II. Material and Methods

Antibodies and Reagents

The following Abs were used for Western blot analysis: rabbit anti-p-PLCγ, rabbit anti-p-Akt, rabbit anti-p-Pyk2, rabbit anti-p-ERK1/2, rabbit anti-p-PKCδ, rabbit anti-p-p40(phox) (Cell Signaling Technology); mouse anti-β-actin (Sigma). Anti-Rabbit IgG HRP-conjugated antibody was purchased from Cell Signaling and anti-mouse IgG HRP-conjugated antibody from Jackson ImmunoResearch.

Goat anti-mouse IgG (Kirkegaard & Perry Laboratories) and mouse anti-FcgRIIA (StemCell, clone IV.3) antibodies were used to coat plates for crosslinking experiments. Immune complexes on a plate were formed using anti-BSA and BSA (Sigma). Anti-CD32 FITC (BD bioscience) and anti-CD11b APC conjugated antibodies were used for flow cytometry analyses. Lyn phosphorylation was inhibited by preincubating the neutrophils with PP1 (Sigma, 10nM), before activation through FcγRIIA.

Mice

C57BL/6J mice expressing the FcγRIIA in a γ-chain deficient background (IIA$\gamma^{-/-}$) (15) were breed with C57BL/6J PKC$\delta^{-/-}$ mice, to obtain mice that express FcγRIIA in γ-chain and PKCδ deficient background (IIA$\gamma^{-/-}$ PKC$\delta^{-/-}$). Mice that express FcγRIIA in γ-chain and Mac-1 deficient background (IIA$\gamma^{-/-}$ Mac-1$^{-/-}$) (26) were used as positive control. Lyn$^{-/-}$ and WT control bone marrow neutrophils were obtained from Dr. Lowell's laboratory (UCSF, CA). Mice were bred and maintained in a virus- and antibody-free facility. Experiments performed with these mice were approved by the Harvard Medical School Animal Care and Use Committee.

Cells isolation and crosslinking analyses

Bone marrow neutrophils were isolated from femurs and tibias by washing out the bone marrow with ice-cold RPMI 2% FCS. Using a percoll based gradient, neutrophils were collected from the section obtained in the 65 and 75% percoll. Cells were used immediately after isolation.

For crosslinking of FcγRIIA, plates were coated with a goat-anti-mouse antibody (5μg/mL) in carbonate-bicarbonate buffer overnight at 4°C. The wells were then coated with an anti-FcγRIIA antibody. Results were confirmed with coting of plates with BSA-antiBSA immune complexes as previously described (15). BMN were placed in the plates, and were centrifuged for 1 min at 500 rpm, to homogenize the starting point. The assays that followed were performed at 37°C.

Western blots

Bone marrow neutrophils were placed on a plate and incubated for the indicated times at 37°C. Cell were directly lysed in loading buffer containing 2β-mercapto-ethanol and boiled. Proteins were loaded in 4-20% SDS gels (BioRad) under reducing conditions and transferred to a nitrocellulose membrane. Protein containing membranes were probed with relevant primary antibodies, followed by HRP-conjugated antibodies, and were developed using ECL and femto (in particular when probed for phospho-PKCδ) (ThermoScientific).

Spreading assay

Cell crosslinking was induced over coated glass coverslips for 30min. Cells were washed 3 times, and fixed with 4% paraformaldehyde for 10 min. After saponin permeabilization (0.1%, for 2 mins) the cells were stained with phalloidin (Invitrogen) and the coverslips were placed on slides in mounting media with DAPI.

ROS production

Bone marrow neutrophils were incubated in plates pre-coated with crosslinking-antibodies, in HBSS medium containing homovanillic acid and peroxidase IV (Sigma). After 60min, ROS production was measured in a fluorescence plate reader (Molecular Devices). ROS production was inhibited by pretreatment of the cells with DPI (10μm; Sigma).

Induction of nephritis using SLE-serum and evaluation of albuminuria

Induction of nephritis was performed as previously reported (26). Briefly, mice were immunized with complete Freund's adjuvant with hIgG intradermically. Three days after, two intravenous injections of 200μL of serum were performed (on day 0 and 2). Urine was collected on day 0, 7 and 14 and analyzed for the presence of albumin by ELISA (Bethyl Labs).

HL-60 culture and transduction

HL-60 cells were cultured in RPMI 1640 supplemented with 10% of heat-inactivated FCS, 2mM of L-glutamine and penicillin/streptomycin (0.1 mg/ml). Cell differentiation was achieved by adding 1.25% DMSO to the culture media for 7 days. For virus preparation, 293T cells (clone 17, from ATCC) were transfected with the lentiviral construct containing the scrambled or hCD11b-specific shRNA sequence (MISSION shRNA lentivirus, Sigma-Aldrich) in addition to the packaging plasmids psPAX2 and pMD2.G (Addgene) using Lipofectamin (Invitrogen). 24hrs after transfection the cells were washed. Media was collected at 48 and 72hrs, and HL60 cells were infected using the supernatant of the transfected cells (previously clean by a 0.25μm filter). A stable cell line was generated by selection of shRNA expressing cells with puromycine (1 μg/mL).

III. Results

Clustering of FcγRIIA by immune complexes initiates a cascade of signaling events. Activation of the Src family of tyrosine kinases (e.g. Hck, and Lyn (78,79)) phosphorylates the FcγRIIA ITAM that in turn serves as a docking site for SH-2 domain containing cytosolic enzymes and adapters such as Syk and the p85 subunit of PI3K. Recruitment of Syk, via its SH2 domains, to the dual phosphorylated tyrosine residues in the ITAM motif, results in its activation. Activation of Syk leads to its association with, and phosphorylation of, many downstream substrates including the adaptor protein SLP76, the guanine exchange factors for Rac GTPases, Vav and PLCγ and p85 of PI3K. p85 brings PI3K in proximity to its substrates at the cell membrane, which results in the formation of phosphatydilinositol-3,4,5-triphosphate (PIP3). PIP3 creates a docking site for pleckstrin homology (PH)-domain containing enzymes such as Bruton's tyrosine kinase (BTK) and phospholipase Cγ (PLCγ) (80). Together, these receptor proximal complexes trigger an increase in downstream processes including an increase in calcium levels, PKC activation (73), and Pyk2 dependent cytoskeletal re-arrangements.

FcγRIIA crosslinking-induced phosphorylation of PKCδ and Pyk2 depends on Mac-1

Neutrophils from mice that transgenically express FcγRIIA, (without other murine activating FcγRs receptors; $\gamma^{-/-}$), in the absence or presence of Mac-1 were used to evaluate how the signaling cascade induced by FcγRIIA crosslinking on neutrophils was modified by Mac-1. Expression of FcγRIIA was comparable between these cells (Fig. 10A).

Neutrophil spreading over ICs has been shown to be dependent on Mac-1, suggesting that FcγRIIA crosslinking induces inside-out activation of Mac-1 (40) and signaling through Mac-1

(Fig. 10B). In order to engage Mac-1 during signaling of FcγRIIA, crosslinking was induced on a plate bound assay. Neutrophils were added to ICs, and lysates were collected at the indicated time points.

Phosphorylation of several known FcγRIIA- and Mac-1-induced proteins was evaluated. Interestingly, PKCδ, a novel PKC that has been shown to have negative regulatory properties towards ITAM-bearing receptors (i.e. FcεR on mast cells (81), GPVI on platelets (82), and the B cell antigen receptor (BCR) (83)) was shown not to be phosphorylated in the absence of Mac-1 (Fig 10C). Clustering of Mac-1 has been shown to induce PKCδ translocation to the membrane and its activation by phosphorylation by the Src kinases, Hck and Lyn (84). The negative regulatory effect of PKCδ has been proposed to be by activation of the 5-phosphatase SHIP-1 that interferes with effector signaling pathways by hydrolyzing PIP3 to PIP2. In the context of FcεR and GPVI, Lyn-dependent phosphorylation of PKCδ was shown to be necessary for its association with SHIP-1 (81,82).

Phosphorylation of the proline-rich tyrosine kinase 2 (Pyk2) was also induced upon FcγRIIA crosslinking in a Mac-1-dependent manner (Fig. 10C). It has previously been shown that Pyk2 activation requires engagement of the β2 integrins, LFA-1 and Mac-1 (49,85). Activation of Pyk2 by Src kinases leads to actin reorganization and activation of downstream MAPK. In macrophages, Pyk2 has been shown to negatively regulate TLR4- (18,86) and Dectin-1- (87) induced signaling and IL-10 production (18,86). The formation of the SHP-1-Pyk2-Src proteins complex was shown to be important for negative regulatory properties of Pyk2 (86). FcγRIIA-induced activation of PLCγ, AKT, p40phox, and Erk1/2 were not affected by the absence of Mac-1 (Fig. 10C).

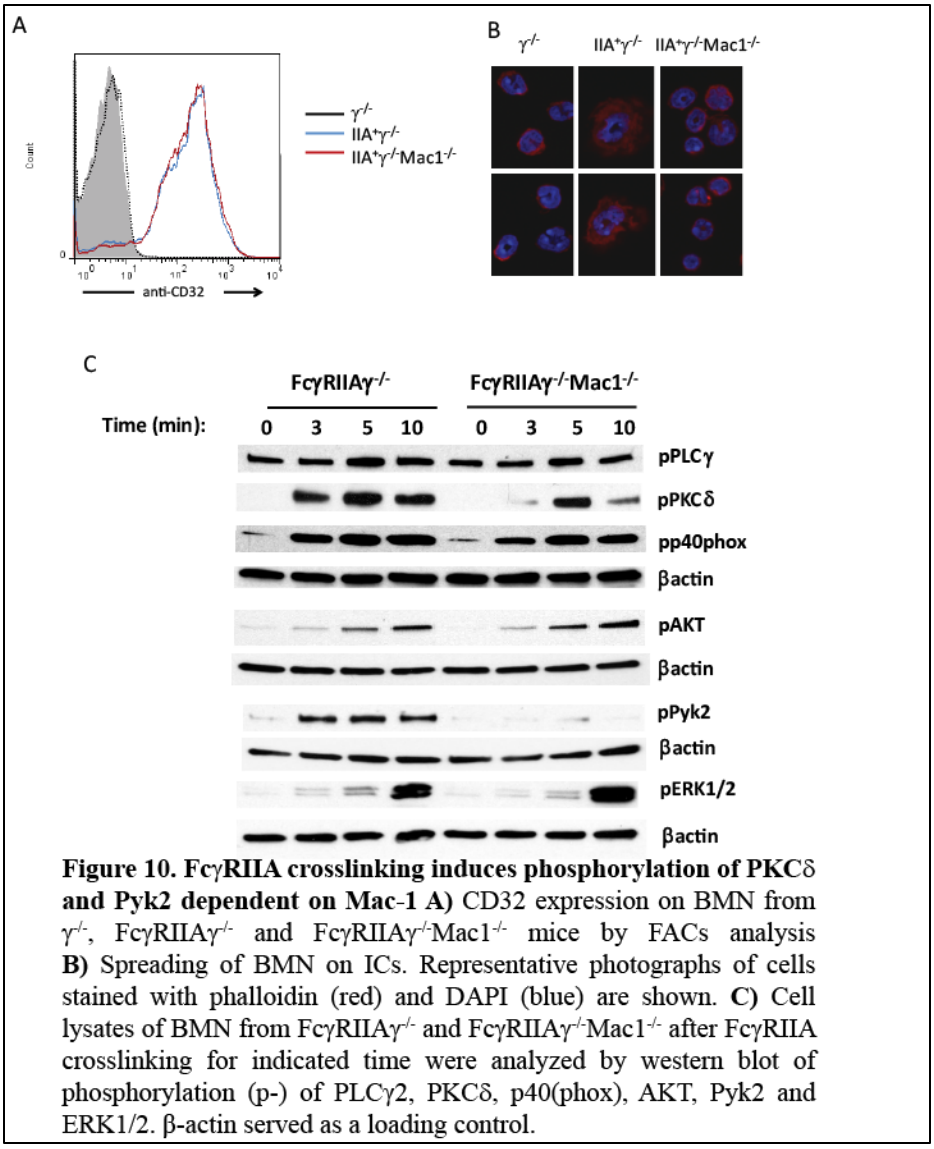

Figure 10. FcγRIIA crosslinking induces phosphorylation of PKCδ and Pyk2 dependent on Mac-1 A) CD32 expression on BMN from $\gamma^{-/-}$, FcγRIIA$\gamma^{-/-}$ and FcγRIIA$\gamma^{-/-}$Mac1$^{-/-}$ mice by FACs analysis **B)** Spreading of BMN on ICs. Representative photographs of cells stained with phalloidin (red) and DAPI (blue) are shown. **C)** Cell lysates of BMN from FcγRIIA$\gamma^{-/-}$ and FcγRIIA$\gamma^{-/-}$Mac1$^{-/-}$ after FcγRIIA crosslinking for indicated time were analyzed by western blot of phosphorylation (p-) of PLCγ2, PKCδ, p40(phox), AKT, Pyk2 and ERK1/2. β-actin served as a loading control.

Potential negative role for FcγR-mediated ROS generation in autocrine, down-regulation of FcγR signaling

Neutrophil adhesion enhances ROS production likely through integrin signaling (88). Using the plate bound FcγRIIA crosslinking assay, Mac-1-deficient cells showed a defect in cell spreading and accordingly, impaired ROS production (Fig. 11A). Similarly, PKCδ $^{-/-}$ neutrophils exhibited a reduction in FcγR generation of ROS in the plate bound crosslinking assay (Fig. 11B).

Although it is clear that excessive ROS production may be deleterious, it may also serve as a second messenger. For example, ROS has been shown to activate PKCδ (89). Furthermore, activation of SHIP by NADPH oxidase-stimulated Lyn has also been reported (90). Thus, we hypothesized that Mac-1/PKCδ-dependent ROS generation negatively regulates FcγR activity through activation of Lyn. In order to study the contribution of ROS in FcγRIIA signaling, a specific NADPH oxidase pharmacological inhibitor (DPI) was used. As expected, ROS production was completely inhibited, as well as cell spreading (91) (Fig. 11C). Interestingly, phosphorylation of PKCδ and Pyk2 were also inhibited (Fig. 11D). Phosphorylation of other molecules like p40phox, were not affected, recapitulating the phenotype induced by Mac-1 deficiency.

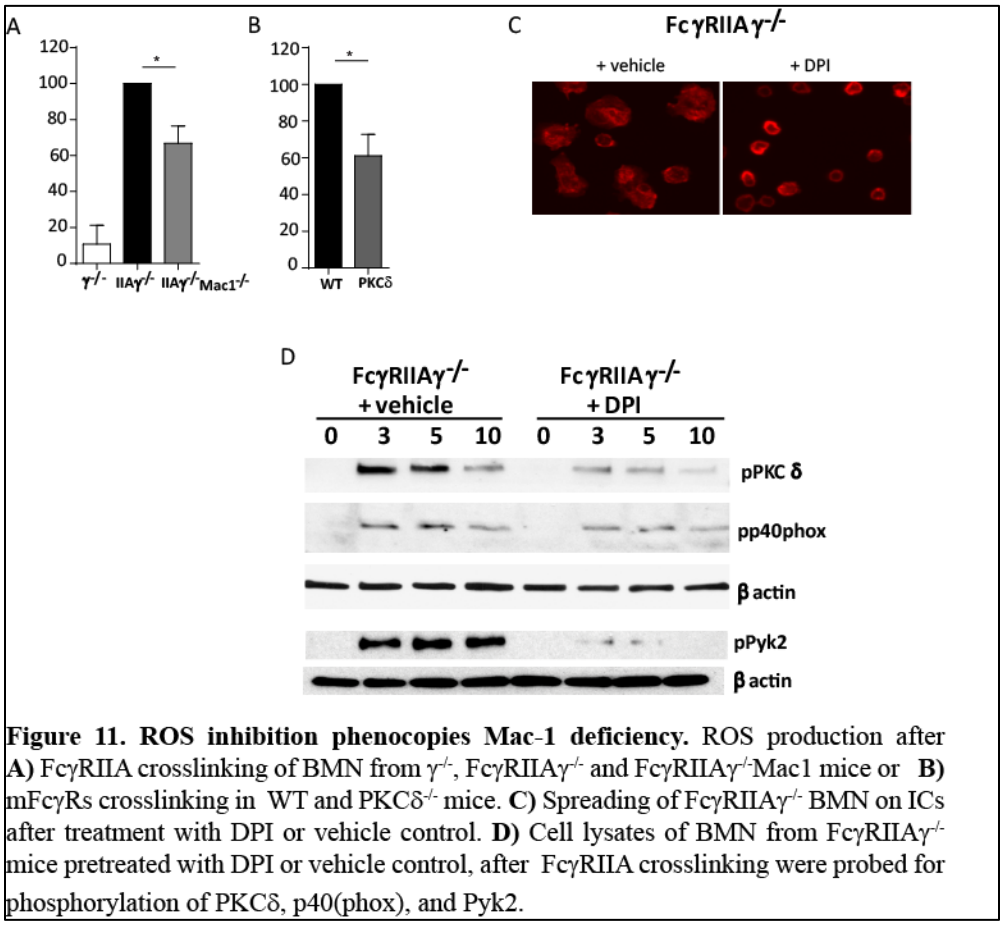

Figure 11. ROS inhibition phenocopies Mac-1 deficiency. ROS production after **A)** FcγRIIA crosslinking of BMN from $\gamma^{-/-}$, FcγRIIA$\gamma^{-/-}$ and FcγRIIA$\gamma^{-/-}$Mac1 mice or **B)** mFcγRs crosslinking in WT and PKCδ$^{-/-}$ mice. **C)** Spreading of FcγRIIA$\gamma^{-/-}$ BMN on ICs after treatment with DPI or vehicle control. **D)** Cell lysates of BMN from FcγRIIA$\gamma^{-/-}$ mice pretreated with DPI or vehicle control, after FcγRIIA crosslinking were probed for phosphorylation of PKCδ, p40(phox), and Pyk2.

Role of Lyn in Pyk2 and PKCδ activation in the context of FcγRIIA crosslinking

PKCδ and Pyk2 have been shown to be downstream of Lyn, and their activation depends on ROS after FcγRIIA crosslinking. Thus, we hypothesized that, upon FcγRIIA engagement, NADPH-stimulated Lyn will be necessary for PKCδ and Pyk2 phosphorylation. To test this hypothesis, bone marrow neutrophils from $Lyn^{-/-}$ mice were used. Murine FcγR were crosslinked in a plate using ICs, and cell lysates were evaluated by Western blot. Phosphorylation of PKCδ and Pyk2 was not only present, but enhanced in the absence of Lyn (Fig. 12A). To rule out the possibility that FcγRIIA was triggering different regulatory responses than its murine FcγR counterparts, a pharmacological inhibitor or Src kinases (PP1) was tested in neutrophils from $FcγRIIAγ^{-/-}$ mice. Again, of PKCδ and Pyk2 was enhanced when cells were treated with PP1 (Fig. 12B).

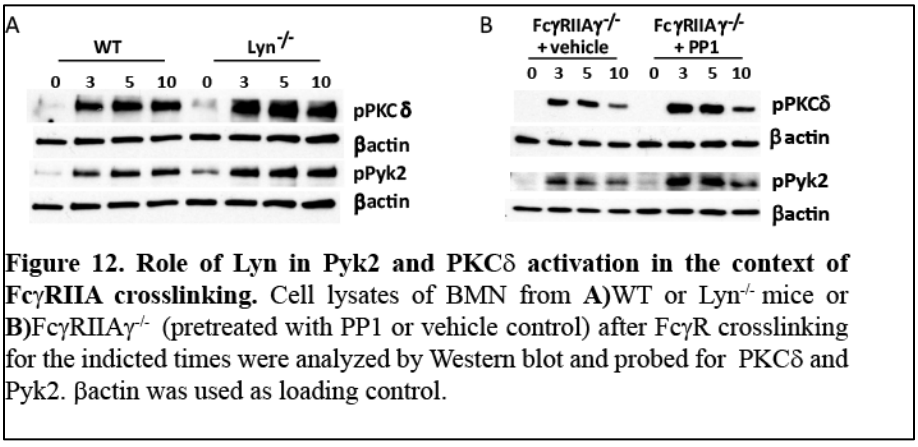

Figure 12. Role of Lyn in Pyk2 and PKCδ activation in the context of FcγRIIA crosslinking. Cell lysates of BMN from **A)**WT or $Lyn^{-/-}$ mice or **B)**$FcγRIIAγ^{-/-}$ (pretreated with PP1 or vehicle control) after FcγR crosslinking for the indicted times were analyzed by Western blot and probed for PKCδ and Pyk2. βactin was used as loading control.

$IIAγ^{-/-}PKCδ^{-/-}$ mice are not susceptible to SLE-serum induced nephritis

To test the hypothesis that the regulatory activity of Mac-1 on FcγRIIA requires PKCδ, we generated mice that express FcγRIIA (in the absence of other murine FcγR), and additionally lack PKCδ ($FcγRIIAγ^{-/-}PKCδ^{-/-}$), and injected them with pathogenic SLE patient serum (26).

Mice that express the FcγRIIA, with or without Mac-1 were used as negative and positive controls, respectively. Albumin in the urine was evaluated as a read-out of glomerular damage. FcγRIIAγ$^{-/-}$PKCδ$^{-/-}$ mice were resistant to developing nephritis by the SLE serum (Fig. 13). These results suggest that the regulatory properties that Mac-1 exerts over FcγRIIA activity, are not critically dependent on PKCδ.

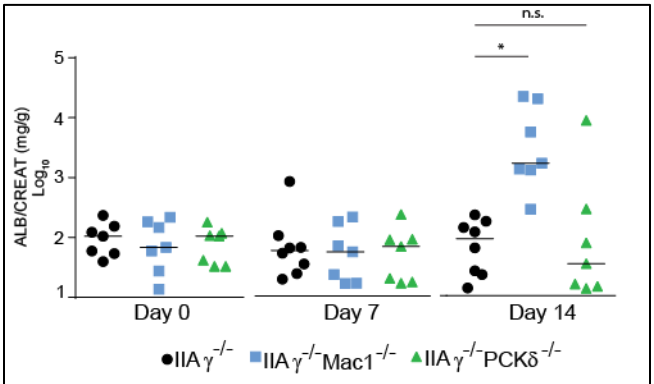

Figure 13. IIAγ$^{-/-}$PKCδ$^{-/-}$ mice are resistant to SLE-serum induced nephritis. Mice from the indicated groups received two intravenous injections of SLE-serum day 0 and 2 and urine albumin (normalized to creatinine) at day 0, 7 and 14 was evaluated. Each data point represents one mouse and the solid line is the median of the group.

Strategy for an unbiased evaluation of Mac-1 modulation of FcγRIIA signaling upon crosslinking.

In order to identify signaling molecules or pathways modified by Mac-1 that may be potentially important in regulating FcγRIIA activity, we are planning to perform an unbiased evaluation of FcγRIIA signaling by SILAC (stable isotope labeling with amino acids in cell culture). To perform this experiment, cells have to be propagated in culture for long periods of time to incorporate the labeled amino acids, Therefore, primary neutrophils are not suitable cells for this purpose. Thus, we turned to HL-60 cells, which are human promyelocytic leukemia cells that can be differentiated into a neutrophil-like cells using DMSO or DMEF in the medium culture. I

have generated two stable HL-60 cell lines, that express scrambled or hCD11b shRNAs (Fig. 14A). When the expression of Mac-1 was knocked-down, cells did not spread over ICs, as we described for Mac-$1^{-/-}$ murine neutrophils (Fig. 14B). These cells will serve as a great tool to study how Mac-1 may modify signaling downstream of FcγRIIA.

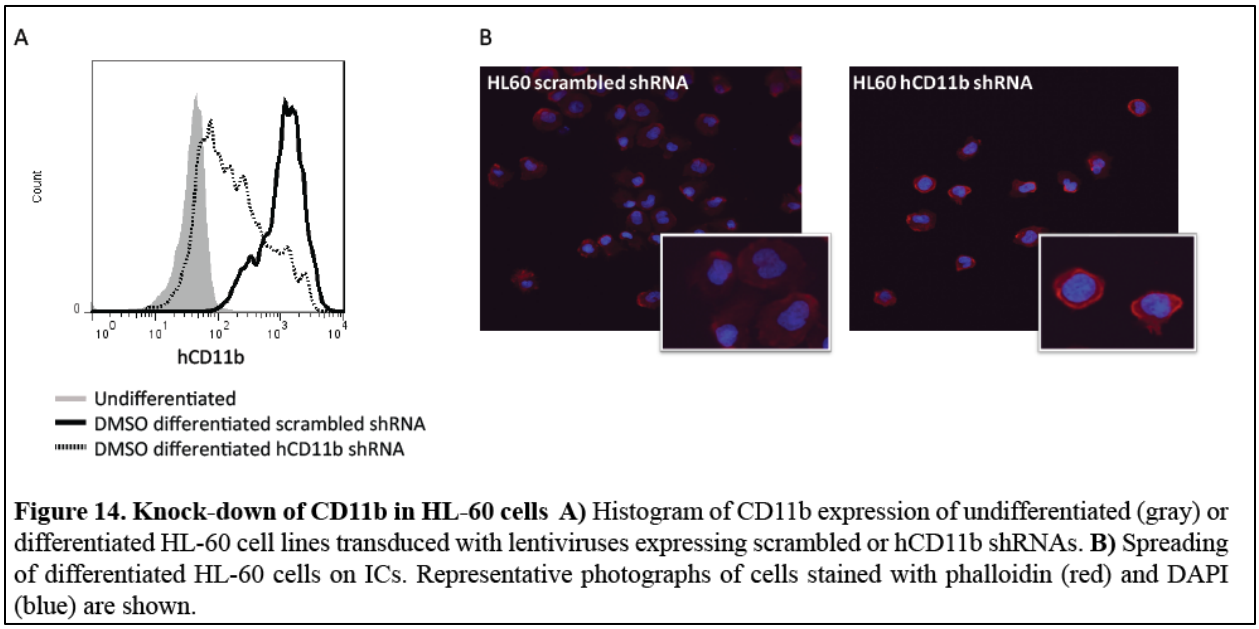

Figure 14. Knock-down of CD11b in HL-60 cells A) Histogram of CD11b expression of undifferentiated (gray) or differentiated HL-60 cell lines transduced with lentiviruses expressing scrambled or hCD11b shRNAs. **B)** Spreading of differentiated HL-60 cells on ICs. Representative photographs of cells stained with phalloidin (red) and DAPI (blue) are shown.

IV. Discussion

FcγRIIA crosslinking on a plate bound assay induces Mac-1-dependent spreading and signaling (phosphorylation of PKCδ and Pyk2), that results in enhanced ROS production. ROS may be part of a negative feedback loop that downregulates FcγRIIA signaling. Because Mac-1 enhances ROS, its activation could contribute to FcγRIIA inhibition by enhancing an ROS-dependent negative feedback loop. Accordingly, pharmacological inhibition of ROS phenocopies Mac-1 deficiency.

It is challenging to demonstrate this hypothesis, because we currently lack a functional read-out of Mac-1 dependent negative regulation of FcγRIIA. As discussed in the Introduction, Mac-1 can couple with FcγRs to enhance neutrophil functions *in vitro* and *in vivo* (40), while in vivo, we have a clear demonstration that Mac-1 can be inhibitory in a pathway that we propose is linked to FcγRIIA downregulation. The identification of a way to elicit Mac-1 inhibitory functions in vitro, by differential engagement of Mac-1 is being pursued to address this problem.

Interestingly, the downregulation of PKCδ by the absence of Mac-1 seemed to be specific for the context of FcγRIIA. When crosslinking of murine FcγR was performed, the absence of Mac-1 did not modify the PKCδ. We believe that it is possible that FcγRIIA induces different signals compared to murine FcγRs, and uniquely crosstalk with Mac-1. This serves as a further impetus to delineate the Mac-1 dependent inhibitory pathways regulating human FcγRIIA. The evaluation of how Mac-1 regulates FcγRIIA signaling in a large unbiased screen using the human cell line (i.e.HL-60 cells) will provide valuable data in this respect.

The observed resistance to the SLE-serum induced nephritis of the FcγRIIA mice lacking PKCδ$^{-/-}$ mice suggests either that PKCδ does not significantly contribute to the generation of negative signals affecting FcγRIIA function or that PKCδ deficiency on other cell types prevents the development of glomerulonephritis, independent of its direct role on FcγRs. The latter, can be evaluated using bone marrow chimeras of FcγRIIAγ$^{-/-}$PKCδ$^{-/-}$ cells, into not genetically modified host, to analyze their susceptibility to SLE-serum induced nephritis.

Chapter 5. A lupus-associated variant of Mac-1 exhibits defects in integrin allostery and force induced integrin interactions with ligand.

I. Introduction

Leukocytes rapidly adhere upon changes in the affinity and avidity of their integrins for ligands presented by activated endothelium, platelets and microbes. Adhesion via the leukocyte CD18 integrin, composed of a α (CD11) and β (CD18) subunit, promotes leukocyte recruitment and the elimination of microbes. Overall, the integrin is in equilibrium between low, intermediate and high affinity conformations with cell activation, ligand binding, and the cytoskeleton regulating the equilibrium between these states. (92). Mechanical forces also contribute to changes in integrin binding affinity probably by inducing conformational changes. Application of force prolongs the lifetime of the interaction between integrins such as α5β1 (93) and the β2 integrin LFA-1 (94) with their respective ligands (95,96) in a process referred to as "catch-bonds". Such tensile forces allow integrins on circulating leukocytes to rapidly develop adhesive interactions with the vessel wall (97,98). During an immune response, β2 integrins may also experience force upon binding microbes or forming an immunological synapse with antigen presenting cells (99). Although there is clear physiological evidence for the importance of CD18 integrins and associated signaling proteins in immune responses both in humans and mouse models, there is no evidence to date that alterations in integrin allostery or catch bonds have pathological consequences.

Genome wide association studies have identified a variant of the *ITGAM* gene, which encodes the α chain (CD11b) of the β2 integrin Mac-1 (macrophage-1 antigen complex; CD11b/CD18)

as a risk factor for systemic lupus erythematosus (SLE) (23,24), a multi-organ autoimmune disease (2). After the HLA, *ITGAM* is the second strongest locus associated with risk for SLE (24). The risk effect has been mapped to the single nucleotide polymorphism (SNP) rs1143679 that results in the substitution of an Arginine for a Histidine in the position 77 (R77H) of CD11b (23,24). The strong association of the rs1143679 SNP with SLE has been confirmed in several populations (i.e. African, European and Hispanic, but was not associated in Korean and Japanese populations) by a meta-analysis that includes independent data sets with an overall odds ratio of 1.83 (100). Studies assessing the effect of the R77H variant in many cell types have concluded that compromised R77H ligand binding capacity contributes to SLE pathogenesis (25,77,101-104). Yet, the molecular mechanism for how this variant may affect ligand binding is unclear, as it is not located in the ligand binding I domain.

Mac-1 is expressed on myeloid cells with particularly high levels on neutrophils, and on some lymphocyte subsets, including NK and B cells. It has several ligands including complement iC3b, ICAM-1 and fibrinogen and promotes leukocyte recruitment and phagocytic uptake and destruction of targets (31). However, negative regulatory functions for Mac-1 have also been described. It can inhibit signaling through the B cell receptor (BCR), toll-like receptors (TLR), and type I interferon receptor (18,19,77). Moreover, recent work by our group demonstrated that in a model of lupus, Mac-1 protects against the development of glomerulonephritis induced by IgG-immune complexes by potentially negatively regulating the human IgG receptor, FcγRIIA (26).

Structurally, the α and β subunits of integrins consist of N-terminal domains that form the integrin head, which connect to upper and lower legs, transmembrane domains, and short C-terminal cytoplasmic tails. Overall, the integrin is in dynamic equilibrium between three states: a

bent closed headpiece conformation that is low affinity, an extended-closed conformation also with low affinity, and an extended-open headpiece conformation (99). Stimulation of cells with chemokines or divalent cations places the integrin in an intermediate affinity, which is driven to high affinity by ligand binding. The main ligand binding I-domain (headpiece) is inserted in the α-subunit β-propeller domain near its interface with the β2 subunit βI domain (105,106). The αI and βI domains are structurally homologous and ligand binding depends on the presence of divalent cations (Mg^{2+} or Mn^{2+}) that bind to a Metal Ion-Dependent Adhesion Site (MIDAS) within both domains (107). The metal ion in the αI domain MIDAS coordinates an invariant Glu or Asp residue shared by all integrin ligands (108). Allostery is relayed by the interaction of the internal ligand formed by the α7 helix of the I-domain making contact with the MIDAS of the β subunit I-like domain. The pistoning of the α7 helix also contributes to the formation of catch bonds since an antagonistic molecule of the internal ligand site in the βI domain (XVA143) inhibits this process (94). Upon head piece opening, reshaping of the βI domain MIDAS, which is at the interface with the α subunit β-propeller domain is transmitted by the βI domain α7 helix downward shift to the interface with the hybrid domain causing the hybrid domain to swing out and full extension of the integrin. Bidirectional allosteric changes are required for productive ligand binding. In α I-less domain integrins (i.e. α3-α9 and αIIb), ligand binding occurs in the interphase between the α subunit β-propeller and the β subunit I-like domain (107). However, in α I-domain containing integrins it is unclear how the β-propeller domain, in which the SLE-associated variant R77H resides, influences affinity.

Here, we provide evidence that R77H substitution impairs the ligand binding capacity of Mac-1 under shear flow by changing the equilibrium between the bent-closed and extended-open state

of the integrin and identify a novel role for R77 and the β-propeller domain in which it resides, in establishing force-induced catch bonds. Results from mutants introduced into the R77H and activating antibodies indicate that R77H prevents the transmission of bidirectional allosteric signals to the αI domain required for affinity and catch bond formation.

II. Materials and Methods

Reagents and Antibodies

Human IgM (Jackson ImmunoResearch), Protein A (Pierce Thermo Scientific), Human ICAM-1Fc (R&D) and fMLP (Sigma-Aldrich) were purchased. Serum used as a source of iC3b was obtained from healthy volunteers. Blood was drawn and handled according to protocols for protection of human subjects approved by the Brigham and Women's Hospital Institutional Review Board, and all volunteer subjects gave written informed consent. CBRM1/29, CBRM1/32, CBRM1/20, CBRN1/6, CBRN 3/4, CBRLFA1/2 and CBRLFA1/7 were a gift from T. Springer (Harvard University, Boston MA) and were used as previously described (106,109). Anti-hCD11b activated (CBRM1/5), anti-hCD11b clone ICRF44, anti-hCD3, anti-hCD14, anti-hCD32, anti-hCD16, anti-hCD11a, anti-hCD62L and goat anti-mouse IgG conjugated antibodies were purchased from BioLegend, and the anti-hCD18 (monoclonal antibody 24, m24) antibody from Abcam. Leukadherin-1 was purchased from Calbiochem (EMD Millipore).

Lentiviral constructs

The R77H mutation was introduced into the human CD11b using standard PCR approaches. cDNA constructs for CD18 ^{L132A} and ^{V124A} were a gift from T. Springer. cDNAs of CD11b^{WT} and ^{R77H} , were cloned in the lentiviral plasmid pWPI (modified from the Addgene, plasmid #12254, from Didier Trono laboratory, by removing the EGFP cassette), whereas the cDNA for CD18$^{WT/L132A}$ and ^{V124A}, were cloned in the pWPI containing an EMCV IRES-EGFP cassette (Addgene plasmid #12254). GFFKR mutants (CD11b$^{WT/GFFKR}$ and CD11b$^{R77H/GFFKR}$) were generating by including a stop codon before the GFFKR sequence, by standard PCR. 293T cells (clone 17, from ATCC) were transfected with the lentiviral construct (pWPI) in addition to the

packaging plasmids psPAX2 and pMD2.G (Addgene, plasmids #12260 and #12259 from the laboratory of Didier Trono) using Lipofectamin (Invitrogen). 24hrs after transfection the cells were washed. Media was collected at 48 and 72hrs, and K562 cells were infected with the supernatant of the transfected cells that had been passed through a 0.25μm filter.

Cells

K562 cells, which lack endogenous CD11b and CD18 expression, were transduced with lentiviruses. Single cell sorting was performed for positive expressing cells. Multiple clones expressing similar surface levels of CD11b were used in functional assays. Clones were cultured in RPMI 1640 supplemented with 10% of heat-inactivated FCS, 2mM of L-glutamine and penicillin/streptomycin (0.1 mg/ml) (Lonza). Genotyped human blood samples used in these studies were provided by the Genotype and Phenotype Registry, a service of the Tissue Donation Program at The Feinstein Institute for Medical Research, Manhasset, New York, USA. Samples from non- or variant (R77H)-carrying donors contained similar numbers of peripheral blood neutrophils. To evaluate the role of the β-propeller using antibodies, blood from non-genotyped healthy volunteers was used following the Human Use Committee Board of Brigham and Women's Hospital guidelines. Neutrophil isolation from blood samples was performed as previously described (110).

Static and shear flow adhesion assays

Ligand coating of surfaces: iC3b coating was performed on 96 well opaque bottom plates (Costar) or glass coverslips. Human IgM (10μg/mL) diluted in carbonate-bicarbonate buffer (pH 9.4) was incubated overnight at 4^{o}C. Fresh serum was diluted 1:1 with PBS (Ca^{2+} and Mg^{2+}) and

incubated at 37°C for 2hrs (heat inactivated serum was used as control). Blocking of unspecific binding to the surface was achieved by incubating with 1% PVP (Sigma) for 1hr at 37°C. ICAM-1 coating on glass coverslips was as follows. Coverslips were incubate with Protein A (1μg/mL, used to orient the ICAM-1Fc molecules), for 1hr at 37°C, followed by ICAM-1 (10μg/mL) overnight at 4°C. Blocking of unspecific binding to the surface was achieved by incubating with 2% BSA (Sigma-Aldrich) and 0.5%PVP for 1hr at 37°C.

Integrin Activation: For integrin activation with Mg/EGTA, K652 cells were washed using Hanks balanced salt solution without Ca^{2+} and Mg^{2+} (HBSS-, Lonza) with 5mM EDTA, washed again using HBSS to remove EDTA and resuspended in HBSS containing Mg^{2+} and EGTA (2mM of each, Mg^{2+}/EGTA). For Mn^{2+} induced activation, K562 cells were washed in Hepes buffer (20mM Hepes, 150mM NaCl, and 2mg/mL Glu) containing 2mM EGTA and 0.5mM $MnCl_2$, and resuspended in Hepes buffer with 1mM $MnCl_2$. Human neutrophils were activated with 500nM fMLP in PBS plus 2mM Ca^{2+} and Mg^{2+}.

Static adhesion assays: Cells were labelled with CFSE (Molecular Probes, Invitrogen), as recommended by manufacturer, and 25,000 cells were placed on ligand-coated wells of 96 well plates in the presence of the activation stimulus. The initial fluorescence intensity was measured by a spectrophotometer (Molecular devices). Cells were incubated for 30min at 37°C, and washed 4 times with warm buffer. Fluorescence intensity of the remaining cells was measured and the percentage of adhered cells was calculated. Static adhesion assays were also performed over glass coverslips used in the flow shear experiments, to rule out that differences in results between the static and flow assays was due to the ligand coating surface (i.e. glass versus tissue culture plastic). For these experiments, manual count of adherent cells in 4 different high power fields was performed, and the percentage of cells that adhered relative to $CD11b^{WT}$ treated with

Mn^{2+} was graphed. For blocking experiments using the anti-β-propeller antibodies, the percent inhibition relative to CBRLFA1/7 (antibody control) was calculated.

Shear flow adhesion assay: Cells were perfused through a flow chamber at 1 dynes/cm^2 for a min. Shear flow was then decreased to 0.38 dynes/cm^2, and the number of cells accumulating in four different fields was counted every 2 minutes for the indicated time in minutes. Live-cell imaging of cell adhesion was recorded by a video camera coupled to a Nikon TE2000 inverted microscope equipped with a 20×0.75 NA phase contrast objective and VideoLab software (Mitov).

Biomembrane force probe assays

RBCs, platelets and beads preparation: Human red blood cells (RBCs) were isolated from whole blood of healthy volunteers by finger prick according to protocols approved by the Institutional Review Board of Georgia Institute of Technology. Freshly isolated human RBCs were firstly biotinylated by covalently linking with biotin-PEG3500-SGA (JenKem USA) for 30 minutes incubation at room temperature (94). Biotinylated RBCs were then incubated with nystatin (Sigma-Aldrich) in N2 buffer (265.2 mM KCl, 38.8 mM NaCl, 0.94 mM KH_2PO_4, 4.74 mM Na_2HPO_4, 27 mM sucrose; pH 7.2, 588 mOsm) for 30 minutes in 0^oC. Nystatin-loaded biotinylated RBCs were washed twice with the N2 buffer and re-suspended in the N2 buffer for the BFP experiments.

To obtain ICAM-1/streptavidin (SA) coated glass beads, borosilicate glass beads (Duke Scientific) were firstly covalently coupled with mercapto-propyl-trimethoxy silane (United Chemical Technologies). Meanwhile, ICAM-1 was covalently linked with NHS-PEG-MAL (JenKem USA) by incubation in carbonate/bicarbonate buffer (pH 8.5) for half an hour, and then

the complex together with streptavidin-maleimide (Sigma-Aldrich) was covalently linked to the glass beads in phosphate buffer (pH 6.8) for overnight incubation at room temperature and finally re-suspended in phosphate buffer plus 0.5% BSA.

Measurement of molecular densities on the surfaces of BFP beads: To measure the Mac-1 density, K562 cells were first incubated with a PE-conjugated anti-hCD11b antibody (ICRF44, BioLegend) at 10μg/ml in the D-PBS (0.493mM $MgCl_2$, 1.47mM KH_2PO_4, 137.9mM NaCl, 8.06mM $Na_2HPO_4 \cdot 7H_2O$, 0.884mM $CaCl_2$, 2.68mM KCl, pH 7.4) at room temperature for 30 minutes and then washed for 3 times in the D-PBS. To measure the surface ICAM-1 density, ICAM-1/streptavidin (SA) beads were first incubated with a PE-conjugated anti-ICAM-1 monoclonal antibody (HA58, eBioscience) at 10 μg/ml in the phosphate buffer at room temperature for 30 minutes and then washed for 3 times in the phosphate buffer. Then fluorescent intensities of K562 cells or beads were measured by a BD LSR flow cytometer (BD Biosciences). The intensity results were compared to standard calibration beads (BD Quantibrite PE Beads, BD) to determine site densities of Mac-1 or ICAM-1 on K562 cells and beads, respectively (by dividing total number of molecules per cell or bead to the cell or bead surface area. The cell or bead surface area was calculated from the radii measured with a customized LabView (National Instrument) program (averagely 7.28μm for a K562 cell and 1μm for a bead).

Biomembrane Force Probe (BFP) apparatus: The principles and technical details of BFP have been elaborated in previous papers (111,112). In brief, a streptavidinylated glass bead is glued to the apex of a biotinylated RBC, which is aspirated by a micropipette to form an ultra-sensitive force probe (Fig. 3A). The bead was coated with ICAM-1, which acts as the ligand for Mac-1 (Fig. 3B). A K562 cell that was transfected to express Mac-1 is aspirated by an opposing micropipette, which is driven by a piezoelectric translator (Physical Instrument) with sub-

nanometer precision via a capacitive sensor feedback control (Fig. 3A). The probe bead and the target cell are aligned in a cell chamber filled with the L15 chamber media (L15 with 1% BSA, 5mM HEPES, 2mM Mg^{2+} and 2mM EGTA) and observed under an inverted microscope (Nikon TiE, Nikon) through two cameras. One camera (Prosilica) captured real-time images (Fig. 3A) at a video rate (30 frames per second, fps), while the other (Prosilica) does at a higher speed (1,600 fps) when the images were limited to 100 pixel by 30 pixel rectangular region of interest across the contact interface between the bead and the RBC. A custom image analysis LabView (National Instrument) program tracked the bead position precisely in real-time (113). The binding kinetics measurements were described in following sections of lifetime assay, thermal fluctuation assay and adhesion frequency assay.

The BFP spring constant *k* was determined from the suction pressure inside the probe pipette that holds the probe bead and the radius of the probe pipette, the diameter of the spherical portion of the RBC that is outside of the probe pipette, and the contact area between the probe and the RBC (111,112). It was set as 0.3pN/nm in the force-clamping assay for 10pN and higher clamping forces, and 0.25pN/nm for clamping forces lower than 10pN.

Force-clamping assay: To measure bond lifetimes under a certain force, we used the force-clamping assay which has been described previously (114). Generally, in the force-clamping assay, the K562 cell was driven repeatedly to approach and contact the probe bead with a 20-pN impingement force for 2s to allow a receptor-ligand bond to form. The target pipette was then retracted at a speed of 3μm/s. In the case that a binding event survived the retraction phase, the target pipette would be held at a desired clamping force to wait for the bond to dissociate, and then returned to the original position to start the next cycle (Fig. 3C). Lifetime was determined as

the time length from the instant when the force reached the desired level to the instant of bond dissociation.

Thermal fluctuation assay: Thermal fluctuation assay is a BFP experimental mode that allows for lifetime measurements under zero-force (94,111). After touching the bead for a certain contact time, the K562 cell was retracted to the zero-force position and kept in contact with the bead via thermal motions without either compression or tension. Bond association/dissociation under zero-force was manifested as a sudden drop/increase in the thermal fluctuations of the bead, which is quantified by the average standard deviation of a sliding interval of 70 points of the bead's position over time, σ.

Adhesion frequency assay: Adhesion frequency assay uses a BFP experimental mode named force-rupture assay to measure the two-dimensional (2D) kinetics of the bonding between a receptor and a ligand by measuring the adhesion frequency. To detect an adhesion, the K562 cell was driven to approach and contact the probe bead at a given contact duration (t_c) and retract, and an adhesion was signified by a tensile force signal caused by the retraction. This approach-contact-retraction cycle was repeated 50 times for at least 3 cell-bead pairs at each t_c (0.1, 0.2, 0.5, 1, 2, 5 seconds). The probability of bond formation is summarized as an adhesion frequency, P_a, under each t_c. 2D effective affinity (AcKa) and off-rate (koff) were derived by fitting the following Equation to P_a data at various t_c (115),

$$P_a = 1 - \exp\{-m_r m_l A_c K_a [1 - exp(-k_{off} t_c)]\} \quad (1)$$

where m_r and m_l are the respective surface densities of Mac-1 and ICAM-1 measured by flow cytometry. The effective on-rate ($A_c k_{on}$) was then calculated as $A_c k_{on} = A_c K_a \cdot k_{off}$.

Lifetime analysis: We chose six forces, 5pN, 10pN, 15pN, 25pN, 30pN, 35pN to conduct force clamping experiments. According to the chosen clamping force, lifetimes were categorized into bins that cover successive force ranges, each of which has an approximate width of 5pN. The average lifetime in each bin was collected to plot the lifetime curve as a function of clamping force.

Spring constant analysis: The spring constant of the integrin-ligand complex was analyzed based on the results of BFP force-rupture assay and force-clamping assay (116,117). During the retraction phase in each cycle, the slope of the force versus displacement curve reflected the spring constant of the system, including the cell and the molecular complex that were serially linked, while the stiffness of the bead and micropipettes are large enough to be neglected in contributing to the spring constant of the system. Thus, the reciprocal of the system spring constant, $1/k_{sys}$, equals the sum of the reciprocals of the cellular and molecular spring constants, $1/k_{cell} + 1/k_{mol}$. A reasonable assumption supported by previous calibrations (116) is that the molecular complex can resist tension but not compression, while the cell spring constant is the same regardless of tension or compression. Thus k_{cell} and k_{sys} were estimated from the respective slopes of the red and purple dashed lines, which are linear fits to the compression and tension segments, respectively, of the retraction phase in the force versus displacement curve (Fig. 3A). The molecular spring constant of the integrin-ligand complex was calculated by $k_{mol} = 1/(1/k_{sys}- 1/k_{cell})$.

The distribution of the spring constant values under each experimental condition is then fitted by a two-summit Gaussian distribution:

$$p=A_1*\exp\{-0.5*[(k_x- k_{mol1})/D_1]^2\}+A_2*\exp\{-0.5*[(k_x- k_{mol2})/D_2]^2\} \qquad (2)$$

in which A_1 and A_2 are the amplitudes, and D_1 and D_2 are the standard deviations of the two sub-distributions, which should also meet the normalization condition:

$$A_1 * D_1 + A_2 * D_2 = \frac{1}{\sqrt{2\pi}} \quad (3)$$

k_{mol1} and k_{mol2} are the two mean spring constants of the integrin-ligand complex which correspond respectively to the bent and extended conformation of the integrin.

Statistical analysis

All data are presented as mean ± SEM. Differences were determined by *t*-test. For group analysis, two-way ANOVA was used, when significant differences were shown, data was subjected to Turkey test for multiple comparison. *P* values <0.05 were considered significant.

III. Results

The R77H variant of *ITGAM*, maps to the β-propeller domain and has no effect on Mac-1 surface expression or activation.

Since Mac-1 has not been crystalized, the recently reported crystal structure of the active form of another closely related integrin CD11c/CD18 (60% homology in the α subunit, (118)) was used to model Mac-1 and map the R77 region in its ternary structure (Fig 15A). The R77H resides in the β-propeller. The location of binding sites of activation reporter antibodies, functional blocking antibodies and controls used in our study are also indicated on the schematic (Fig. 15A).

K562 cell lines stably expressing the common ($CD11b^{WT}$) and the risk-associated variant ($CD11b^{R77H}$) were generated in order to study the functional repercussions of the R77H in CD11b-dependent assays. Cells expressing comparable levels of surface CD11b were used (Sup. Fig. 3A) and K562 cells that did not express CD11b served as negative controls to confirm CD11b specificity. Mn^{2+} induced activation of CD11b, examined with a CD11b-specific reporter antibody (CBRM1/5) that recognizes the I-domain and CD18-specific reporter antibodies (Kim127 and MoAb24), was comparable in $CD11b^{WT}$- and $CD11b^{R77H}$-expressing cells (Sup. Fig. 3B). Similar assays were performed in human neutrophils obtained from healthy genotyped donors homozygous for the *ITGAM* (CD11b) common or risk variant (R77H; rs1143679). Surface expression of Mac-1 was comparable between the groups (Sup. Fig. 3C), as was fMLP-induced exposure of the reporter antibody CBRM1/5 (Sup. Fig. 3D), and rosetting and subsequent phagocytosis of complement iC3b-coated RBCs. fMLP-induced expression of neutrophil activation markers (i.e. L-selectin shedding and CD16), as well as other surface

molecules (i.e. CD11a and CD32) were also normal (Sup. Fig. 3E). Kim127 binding indicates integrin extension (119) and internal ligand binding (120), m24 measures headpiece opening (121), and iC3b-RBC rosetting requires integrin extension, an open headpiece, hybrid-domain swing out (121) and internal ligand binding (120). Thus, together our data suggest that $CD11b^{R77H}$ can adopt an extended conformation with open headpiece following direct activation with divalent cation (Mn^{2+} and Mg^{2+}/EGTA) or agonists that induce inside-out signaling (i.e. fMLP) and has no effect on overall neutrophil activation.

R77H impairs ligand binding under shear flow.

To assess the effect of R77H on the ligand binding capacity of Mac-1, adhesion assays were performed under static conditions. Equivalent binding of $CD11b^{WT}$ and $CD11b^{R77H}$ K562 cells to an iC3b coated surface was observed when cells were treated with Mn^{2+} (Fig 15B). However, when activated with Mg^{2+}/EGTA, $CD11b^{R77H}$ cells showed a significant defect in their capacity to bind.

In contrast, $CD11b^{R77H}$-bearing cells were significantly impaired in their capacity to bind iC3b or ICAM-1 under shear flow, in the presence of either divalent cation Mn^{2+} or Mg^{2+} (Fig. 15C). Under Mn^{2+} conditions, all βI-domain metal sites (MIDAS, ADMIDAS and LIMBS) are occupied with Mn^{2+} and the βI-domain moves to the active state. The open/active βI-domain increases the internal ligand flickering and moves the αI-domain to the open/high affinity state. Under static conditions, the high ligand density coupled with the active αI-domain maximizes the on-rate (but not the off-rate) thus bypassing the requirement for R77. Adhesion under shear flow is a result of on- and off-rate and has a more stringent requirement for optimal integrin-ligand interactions. Under these conditions, R77/β-propeller mediated integrin allosteric signals

is essential for productive adhesion. Following Mg/EGTA, which results in metal coordination only at the MIDAS site, the βI-domain also moves to the active state. However, under this condition, the R77H mutation prevents the internal ligand from being stably immobilized to the αI-βI domain interface. This results in a lower internal ligand on-rate and defective iC3b binding under static condition, compared to the $CD11b^{WT}$ Mac-1, which populates its αI-domain into the active state and achieves high affinity on-rate and adhesion.

Blockade of the β-propeller region reduces ligand binding under flow

Functional blocking antibodies that map to the β-propeller domain and control antibodies (109) (Fig. 15A and Sup. Fig. 4) were used to evaluate the contribution of the β-propeller domain to integrin mediated adhesion under static and shear flow conditions. Blockade of the β-propeller by CBRN1/6 and CBRN3/4 abrogated ligand binding under shear flow, but only partially affected adhesion under static conditions, thus recapitulating the effect of the R77H variant (Fig. 15D, E and Sup.Table 2). Binding of a control antibody, CBR LFA1/7, had no blocking effect. The CBRM 1/32 had the highest blocking ability (Sup. Table 2). As the epitope for this antibody is at the interphase between the β-propeller and βI subunit, (Fig 15C) it may have its effects by disrupting the interaction between these two domains.

Primary human neutrophils expressing the R77H variant exhibit impaired ligand binding only under shear flow

Human neutrophils from healthy genotyped donors homozygous for the *ITGAM* (CD11b) common or risk variants and non-variant carriers were evaluated in adhesion assays. Neutrophils carrying the R77H risk variant had no detectable defects in their capacity to bind iC3b in a static adhesion assay upon activation with fMLP (Fig. 15F). However, they showed a significant

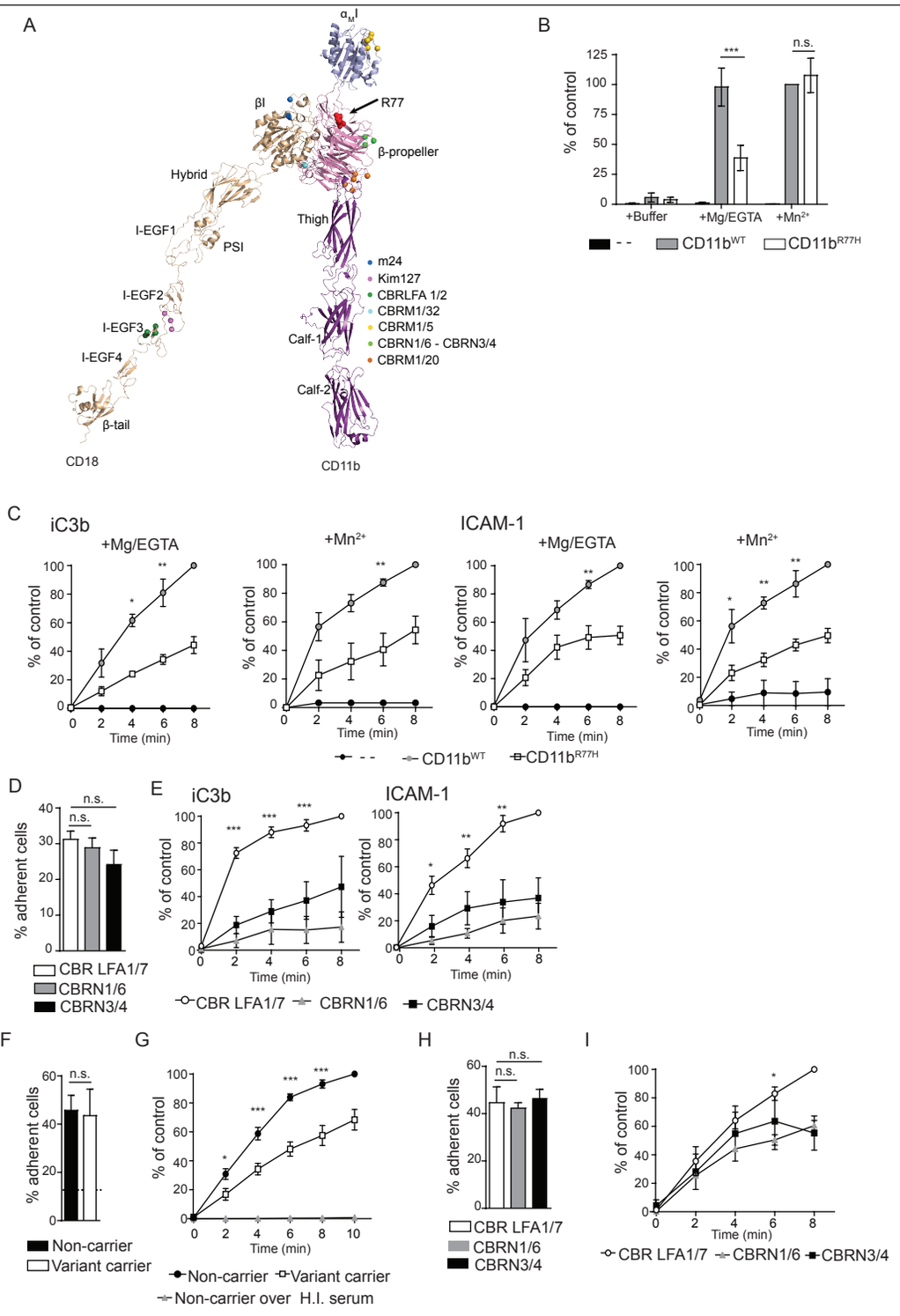

Figure 15. Analysis of the functional effects conferred by the R77H variant of the human ITGAM gene A) Model of CD11b/CD18, using the CD11c/CD18 crystal structure. R77 region is shown by the arrow and epitopes for the mentioned antibodies are also indicated. **B)** Adhesion of K562 cells lacking CD11b (- -), or stably expressing the common ($CD11b^{WT}$) or risk-associated ($CD11b^{R77H}$) variants on a complement coated surface. CD11b activation was induced with Mg^{2+}/EGTA or Mn^{2+}. Results are presented as percentage of adhered cells relative to cells expressing $CD11b^{WT}$ in the presence of Mn^{2+}. Cumulative data from 6 independent experiments is shown. **C)** Adhesion to complement and ICAM-1 of Mg^{2+}/EGTA or Mn^{2+} activated cells under shear flow (0.38 dynes/cm^2) was evaluated at the indicated time points. Results are presented as percentage of adhered cells relative to cells expressing $CD11b^{WT}$ at 8 min. Cumulative data from 4 (iC3b) and 3 (ICAM-1) independent experiments is shown. **D)** K562 cells expressing $CD11b^{WT}$ were activated with Mn^{2+}. Binding to ligand-coated surfaces was assessed in **(D)** static conditions or **(E)** under shear flow (0.38dynes/cm^2). CBRN1/6 and CBRN 3/4 antibodies were used to block different the β-propeller, and CBRLFA1/7 antibody was used as an antibody control. **F)** Adhesion of fMLP-activated neutrophils over complement (iC3b) was evaluated under static conditions. Dotted line represents background binding of cells to a blocked non-coated surface (heat inactivated serum). Cumulative data from 4 independent experiments is shown. **G)** Adhesion of fMLP-activated neutrophils to iC3b under shear flow (0.38dynes/cm^2), evaluated at the indicated time points. Results are presented as percentage of adhered neutrophils relative to the adhesion of neutrophils from the non-carrier control donor at 10 min. Cumulative data from 15 samples is shown. Asterisks indicate the difference in adhesion between cells or neutrophils expressing $CD11b^{WT}$ and $hCD11b^{R77H}$ or from non-carriers and carriers (*p<0.05, **p<0.01, ***p<0.001).

decrease in ligand binding under shear flow (Fig. 15G), concordant with the results using integrin expressing K562 cells stimulated with Mn^{2+}. The variant neutrophils exhibited a tendency to reduced velocity, albeit this was not significant but had normal spreading over a iC3b coated surface (Sup. Fig. 5A and B) when compared to neutrophils bearing the common variant, suggesting the possibility that integrin mediated migration, which requires optimal integrin on- and off-rates may be compromised by R77H. Antibodies for the β-propeller domain were also evaluated in human neutrophils (Sup. Fig. 4B). As in the K562 cell line, the CBRN1/6 and CBRN 3/4 significantly inhibited ligand binding under shear flow, but were less effective in blocking cell adhesion in the static binding assay (Fig. 15H, I and Sup. Table 2). Ninety percent of the samples homozygous for the R77H (rs1143679) variant were also homozygous for the other two SLE-associated SNPs (r1143678 and rs1143683); the remaining 10% of the samples were heterozygous for these SNPs. However, given the similarity in phenotype of $CD11b^{R77H}$ K562 cells and variant carrier human neutrophils we anticipate that R77H is principally responsible for the defect in adhesion under flow.

These results suggest that the β-propeller plays a previously undefined role in ligand adhesion under shear flow. The β-propeller domain may facilitate the correct orientation of the coordinating residues on the βI domain that are required for its interaction with the α7-helix from the α subunit I-domain.

Separation of α and β subunit tails and integrin extension rescues the R77H binding defect

To gain insight into how the R77H variant affects ligand binding, $CD11b^{R77H}$ additionally containing activating mutations of the β subunit (L132A or V124A) (Sup. Fig. 6A) were tested in adhesion assays. These mutations were recently described to stabilize CD11c/CD18 in an open

headpiece ("cocked") and extended state with increased affinity for the internal ligand (120). We evaluated whether these mutations restored the capacity to bind to iC3b under shear flow. Wild-type integrins ($CD11b^{WT}/CD18^{V124A}$, $CD11b^{WT}/CD18^{L132A}$) exhibited increased binding to complement under flow as predicted from the published report. Cells bearing the $CD11b^{R77H}$ and $CD18^{L132A}$ or ^{V124A} ($CD11b^{WT}/CD18^{V124A}$, $CD11b^{WT}/CD18^{L132A}$) remained significantly impaired in their ability to bind ligand under shear flow (Fig 16A). As an alternative mechanism to induce activation of Mac-1 I-domain, the small molecule Leukadherin-1 (LA-1), which binds to SILEN, a coordination residue in the α I domain (122,123) was used. This molecule is reported to promote ligand binding, without inducing global conformational changes (122,123). Pretreatment with this molecule (104) did not rescue the capacity of $CD11b^{R77H}$ bearing cells to bind iC3b under shear flow (Fig. 16B) but enhanced leukocyte adhesion of $CD11b^{WT}$ was induced, as previously described (124).

These results together with the normal Mn^{2+} induced binding of reporter antibodies and adhesion under static conditions, suggests that the R77H variant does not affect the exposure of the αI-domain, but rather the transmission of allosteric signals required for the βI-domain to reach full activation. In order to test this hypothesis, we evaluated the ability of the CBR LFA1/2 antibody

(Fig. 15A) that induces the full extension of the integrin and the separation of the α and β subunit cytoplasmic tails thus resulting in full integrin activation to rescue the adhesion defect in $CD11b^{R77H}$ cells. CBR LFA1/2 rescued the ligand binding defect in $CD11b^{R77H}$ cells (Fig. 16C). A genetic approach was undertaken to validate this conclusion. GFFKR is a regulatory sequence in the CD11b cytoplasmic tail that stabilizes the integrin in an inactive conformation with mutation of this sequence resulting in a constitutively active integrin (125), and the separation of

the cytoplasmic tails (97) (Sup. Fig. 6B). Deletion of GFFKR in CD11b^{R77H} rescued the ability of cells to bind ligand under shear flow (Fig. 16D). Therefore, the R77H adhesion defect could be overcome by forcing the separation of the cytoplasmic tails using both immunological and genetic approaches.

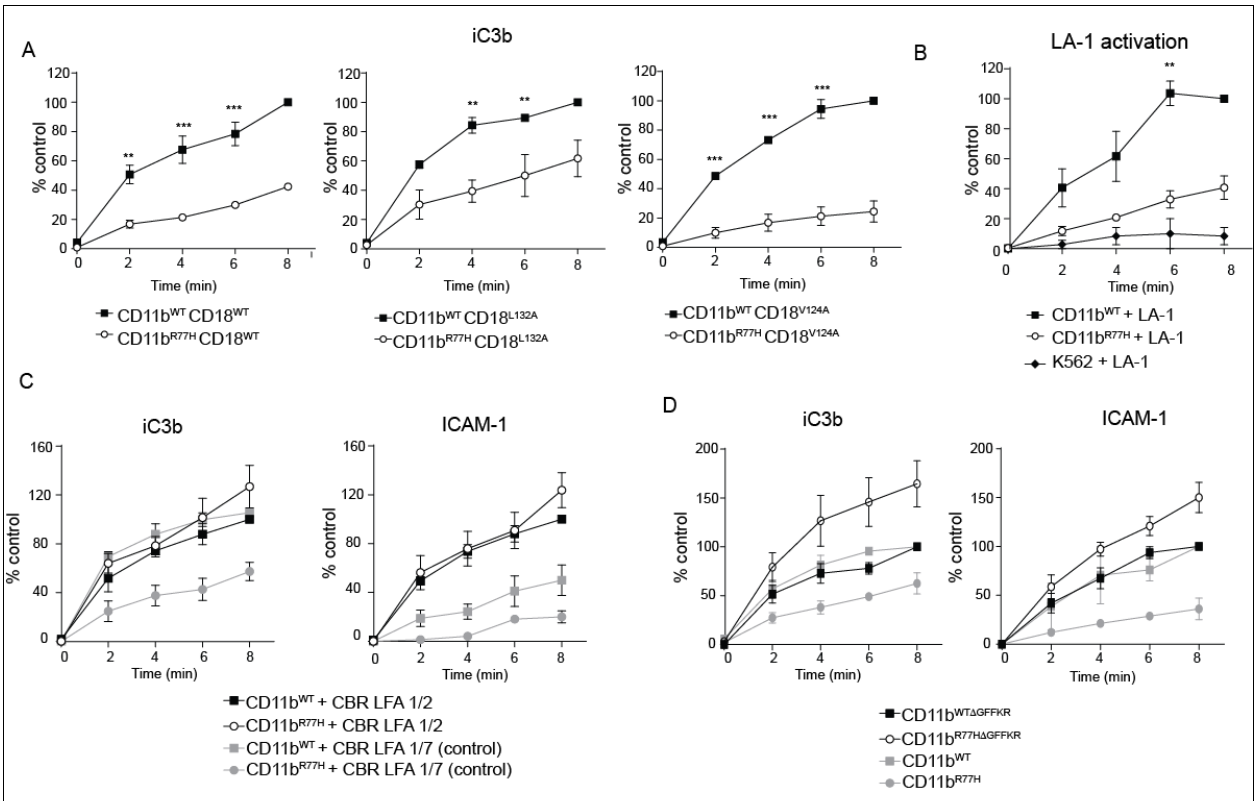

Figure 16. Cytoplasmic tail separation rescues the R77H ligand binding defect. (A) Adhesion of K562 cells stably expressing the CD11b^{WT} or CD11b^{R77H} associated with CD18^{WT}, CD18^{V124A} or CD18^{L132A} β2 chain variants to iC3b was evaluated under shear flow (0.38dynes/cm^2). **(B)** Adhesion of K562 cells expressing CD11b^{WT} or CD11b^{R77H} to a complement coated surface was evaluated after pretreatment with leukoadherin-1 (15μM; LA-1) or vehicle control (DMSO). Cumulative data of three independent experiments is shown. **(C)** Activation of CD11b^{WT} or CD11b^{R77H} K562 expressing cells was induced with the CBR LFA1/2 antibody (20μg/mL), and adhesion to iC3 or ICAM-1 under shear flow was assessed (in the presence of Mn^{2+} or Mg^{2+}/EGTA, respectively). CBRLFA1/7 antibody was used as a control antibody. **(D)** Effect of GFFKR region deletion on CD11b^{WT} or CD11b^{R77H} adhesion to iC3b and ICAM-1 (in the presence of Mn^{2+} or Mg^{2+}/EGTA, respectively) under shear flow was evaluated. (**p<0.01, ***p<0.001).

The R77H mutation disrupts the ability to generate catch bonds, which is fully rescued by CBR LFA1/2 Biomembrane force probe experiments and analyses were performed by Yunfeng Chen from Dr. Cheng Zhu's Laboratory

Cell expressing $CD11b^{R77H}$ did not have a defect under static conditions when the on-rate was optimized with Mn^{2+} while under shear flow, $CD11b^{R77H}$ cells exhibited a significant defect, which is a measure of the integrin on and off rate. This suggested the possibility that R77H affected the integrin off-rate under conditions where mechanical forces were applied. To address the potential role of R77 and the β-propeller region in the mechanical reinforcement of integrin interactions with ligand we exploited a biomembrane force probe (BFP) (Fig. 17A and B), which allows the measurement of single bond interactions. The lifetime of the interaction between K562 cells expressing Mac-1 ($CD11b^{WT}$ or $CD11b^{R77H}$) and immobilized recombinant human ICAM-1 was measured under the application of different external forces (Fig. 17C).

BFP experiments were performed in the presence of Mg/EGTA to keep the cells in a moderately activating environment. An adhesion frequency assay between $CD11b^{WT}$ bearing K562 cells and ICAM-1 beads was firstly performed with and without CBRM1/29, an inhibitory antibody to the αI-domain which blocks the specific binding between Mac-1 and ICAM-1. After CBRM1/29 was added to the experimental buffer, the adhesion became progressively less frequent, which confirmed that the binding to ICAM-1 was largely specific for Mac-1 (Fig. 17D).

Mechanical regulation of Mac-1-ICAM-1 dissociation was then quantified using the K562 cell lines and ICAM-1 beads. The mean lifetimes are plotted against the corresponding forces to render the lifetime curves, in which the zero-force lifetimes were derived via the thermal fluctuation assay and force-involving lifetimes via the force-clamping assay respectively (Fig.

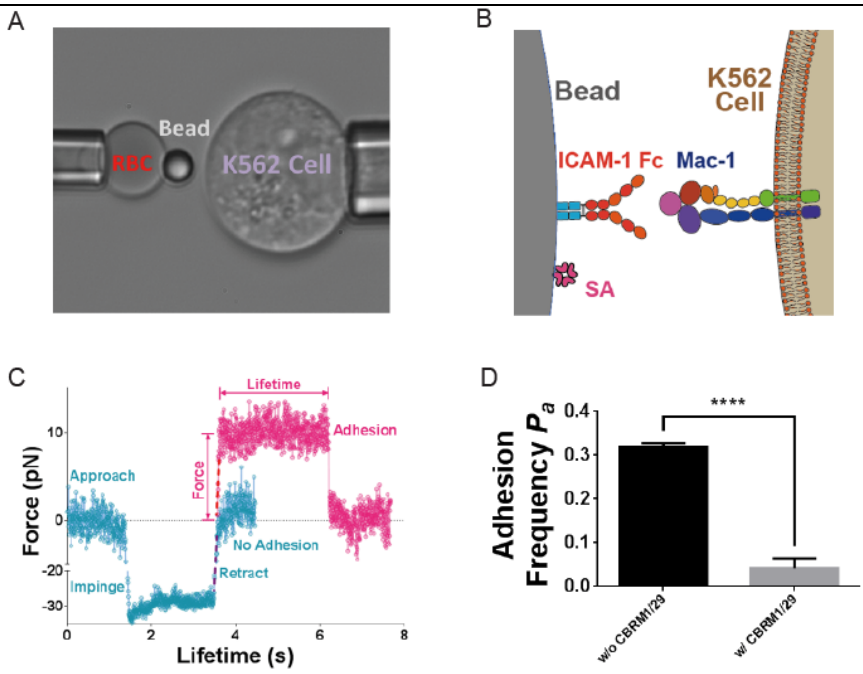

Figure 17 Biomembrane Force Probe (BFP) experiment. (A) BFP micrograph. A micropipette-aspirated RBC with a ICAM-1 probe bead attached to the apex (left) via biotin-streptavidin interaction was aligned against a target K562 cell held by an apposing micropipette (right). **(B)** Sketch of receptor-ligand system. The probe bead is double covalently coated with recombinant ICAM-1 and streptavidin. The K562 cell expresses Mac-1. **(C)** Superposition of force-traces of two BFP contact cycles without and with an adhesion. The cell holding micropipette is driven by a piezo to repeatedly contact with the probe, hold for a specific contact time, and retract to detect adhesion. The position of the bead was tracked by a high-speed camera to monitor the concurrent force. The cyan trace illustrated a contact cycle without binding where the retraction curve returned to zero force upon target cell retraction. The magenta trace illustrated a contact cycle with binding which was held at 10pN to render a lifetime until dissociation. Parameters of the lifetime event including force and lifetime are indicated on the figure. Two dashed lines (dark blue and red) represent the corresponding slopes of the force *vs* lifetime curve in the negative- and positive-force parts of the retraction phase, respectively. **(D)** Mac-1-ICAM-1 interaction test showed binding specificity between K562 cells and beads. Binding frequency of $CD11b^{WT}$-ICAM-1 without (Black Bar) and with (Gray Bar) blocking Ab CBRM1/29 are shown for comparison.

18). For $CD11b^{WT}$, as force increased, the lifetime first increased along and reached the maximum at ~13pN, then decreased, exhibiting a biphasic transition from catch to slip bond (Fig. 18A, cyan curve).

In comparison, the catch-slip trend of $CD11b^{R77H}$ was weakened: the sharp summit in $CD11b^{WT}$ transformed into a relatively flat plateau, which not only had the amplitude dropping one-fold lower, but also shifted leftwards and resulted in a severe shrinking of the catch regime to 0-5pN

only (Fig. 18A, magenta curve). Retained at a similar level in the lower force range, the lifetime in the higher force range shifted aggressively downwards from $CD11b^{WT}$, then finally converged with the $CD11b^{WT}$ curve at the highest forces where both lifetime curves approach zero. Especially, at ~13pN where $CD11b^{WT}$ reached the highest lifetime of 4s, the sustainability of $CD11b^{R77H}$ to associate with ICAM-1 was 3-fold lower (~1s). However, at zero-force $CD11b^{WT}$ and $CD11b^{R77H}$ had similar lifetimes, the difference between which was statistically insignificant. These results suggested that the R77H mutation disrupts the ability of Mac-1 to generate catch bonds. The decline of the catch bond impairs the ability of Mac-1 to sustain its associations with ICAM-1 under a higher external force, but is ineffective to the lower-force and force-free conditions, which is in strong agreement with the results from the adhesion assays above that R77H primarily impairs ligand binding under shear flow.

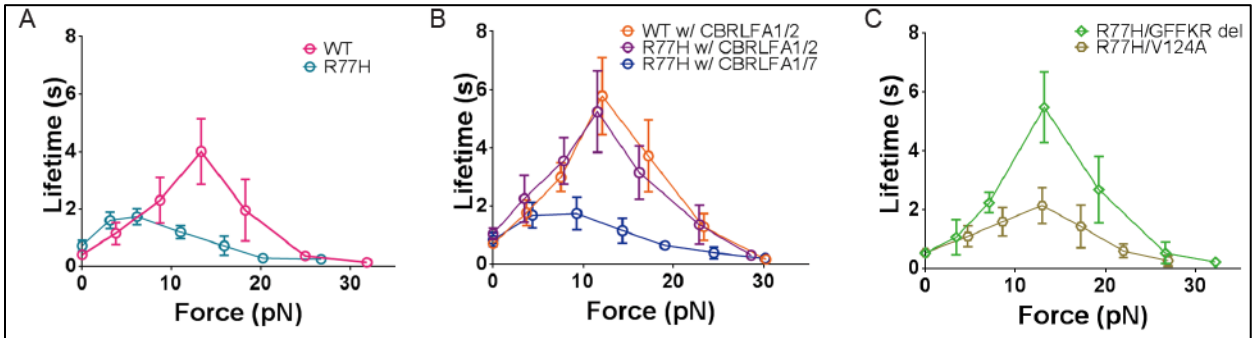

Figure 18. Lifetimes of Mac-1 binding to ICAM-1. (A) Plots of lifetime *vs* force of $CD11b^{WT}$ (magenta) and $CD11b^{R77H}$ (cyan) Mac-1 bearing K562 cells dissociating from the ICAM-1 bead. **(B)** Plots of lifetime *vs* force of $CD11b^{WT}$ and $CD11b^{R77H}$ Mac-1 bearing K562 cells preincubated with CBR LFA1/2 with pre-incubation of CBRLFA1/2 (orange for $CD11b^{WT}$ and purple for $CD11b^{R77H}$) and CBR LFA1/7 antibody control (blue, for $CD11b^{R77H}$) dissociating from the ICAM-1 bead **(C)** Plots of lifetime *vs* force of $CD11b^{R77H/GFFKR}$ (green) and $CD18^{V124A}CD11b^{R77H}$ Mac-1 (brown) bearing K562 cells dissociating from the ICAM-1 bead.

The addition of the CBR LFA1/2 antibody, rendered a robust catch-slip trend of the lifetime *vs* force for both $CD11b^{WT}$ and $CD11b^{R77H}$ (Fig. 18B). The lifetime of $CD11b^{WT}$ was moderately enhanced in all force ranges and realized a maximum amplitude of 6s, which is 0.5-fold higher than without the antibody (Fig. 18B, orange curve). This enhancement indicated that a

substantial fraction of the $CD11b^{WT}$ was still in the inactive (low-affinity) state. For $CD11b^{R77H}$, the increase of lifetime is mainly reflected at the forces higher than 5pN, which remarkably rescued the sharp catch-slip biphasic trend (Fig. 18B, purple curve). To be noted, the two lifetime curves nicely overlapped with each other in the whole force range, which indicated the impact of the mutation on off-rate was completely overcome by the antibody. As control, CBR LFA1/7 antibody, which is known to have no effect on the activity of the integrin, made no difference to the lifetime of $CD11b^{R77H}$, confirming the activating function of CBR LFA1/2 antibody (Fig. 18B, dark blue curve).

Plotting of the survival frequency *vs* lifetime curve clearly showed that binding between Mac-1 and ICAM-1 adopted two states in the presence of external forces, one with a larger off-rate (inactive) and the other with a smaller off-rate (active), which was indicated by the sudden slope change in the middle of each line (Sup. Fig. 7A, B). This existence of two binding states was not altered by the R77H mutation or the addition of the activating antibody, CBR LFA1/2 (Sup. Fig. 7C-H). However, the slope of the active state was steeper in the presence of R77H under all forces, indicating an increase in the off-rates, which provided an explanation for the catch-bond elimination (Sup. Fig. 7C, D). Indeed, the addition of CBR LFA1/2 antibody, which rescued the catch-bond in cell expressing $CD11b^{R77H}$, also reversed the slope change of its active state (Sup. Fig. 7G, H).

Integrin leg separation fully rescued the catch bond, while forced activation of βI domain had a partial effect

Deletion of the regulatory region GFFKR of the α subunit, induces the separation of the integrin transmembrane and cytoplasmic domains, which is reported to result in integrin activation via

inside-out signaling. The addition of GFFKR deletion to $CD11b^{R77H}$ fully rescued its impaired catch-slip trend (Fig. 18C). In fact, the resulting lifetime curve overlapped well with those of cells where Mac-1 was activated with the CBR LFA1/2 (Fig. 18C). This suggests a central role for leg separation in transmitting allosteric signals within the α-subunit that promotes internal ligand binding, a step that is essential for catch bond formation (94).

In comparison, the addition of another mutation, $CD18^{V124A}$, which stabilizes the βI domain in an active state and strengthens the internal ligand binding, did not increase the peak lifetime of $CD11b^{R77H}$ (Fig. 18C). However, the force regime of the "catch" phase was broadened to be similar to $CD11b^{WT}$, which indicated a partial rescue of the catch bond (Fig. 18C).

The bent/extended conformation correlates with integrin binding

Based on the results that tail separation and integrin extension induced by the activating antibody CBR LFA1/2 both enhanced $CD11b^{WT}$ binding and rescued the $CD11b^{R77H}$ binding defect, we assessed whether the overall integrin conformational change played a role in regulating the bond lifetime. Spring constants of the Mac-1-ICAM-1 complexes were collected from BFP data and summarized as an average for each condition (Fig. 19A). It is reasonable to hypothesize that the spring constant of the integrin was mainly determined by the bent/extended conformation, and that an integrin adopting the bent conformation is more flexible than extended, which has a smaller spring constant. This hypothesis has been proven true in another integrin, LFA-1, which has a closely structural resemblance to Mac-1 (114). Based on this hypothesis, a lower spring constant would suggest a larger portion of the individual integrins adopt a bent conformation. In fact, on average, $CD11b^{R77H}$ possessed a significantly lower spring constant than that of $CD11b^{WT}$. The addition of CBR LFA1/2 increased the spring constants of both $CD11b^{WT}$ and

$CD11b^{R77H}$, which is consistent with its function in triggering integrin extension. Moreover, similar to the lifetime difference, the difference between $CD11b^{WT}$ and $CD11b^{WT}$ Mac-1 spring constant was also eliminated by the activation with the CBR LFA1/2 antibody (Fig. 19A).

To quantitatively investigate how the ratio of integrin in bent and extended conformation is affected by the R77H mutation and activating antibody, the spring constant distributions were fit by a two-summit Gaussian distribution, assuming that the spring constant in bent or extended conformers each follows a Gaussian distribution. The means for bent (k_{bent}) and extended ($k_{extended}$) spring constant were pre-set to be identical for all four sets of conditions. According to the fitting result, about half (54.04%) of $CD11b^{WT}$ adopted an extended conformation, while only a small fraction (19.21%) of $CD11b^{R77H}$ was extended (Fig. 19B). Nonetheless, CBR LFA1/2 promoted both $CD11b^{WT}$ and $CD11b^{WT}$ into a much higher level of extension, which again eliminated the difference in their extension probability (Fig. 19B).

The fact that a higher percentile of integrin extension corresponded to generally higher amplitude of the lifetime curve makes it reasonable to hypothesize that the extension of the integrin has a strong positive correlation with the longevity of the lifetime. To test this hypothesis we randomly picked up lifetime events from the above four experiments and collected the lifetime and the spring constant of the integrin in each. A linear relationship was used for fitting, which rendered a positive correlation, with the slope tested to be significantly non-zero (Fig. 19C).

All the results above suggested that the full extension of the integrin strongly correlates with prolonged bond lifetime.

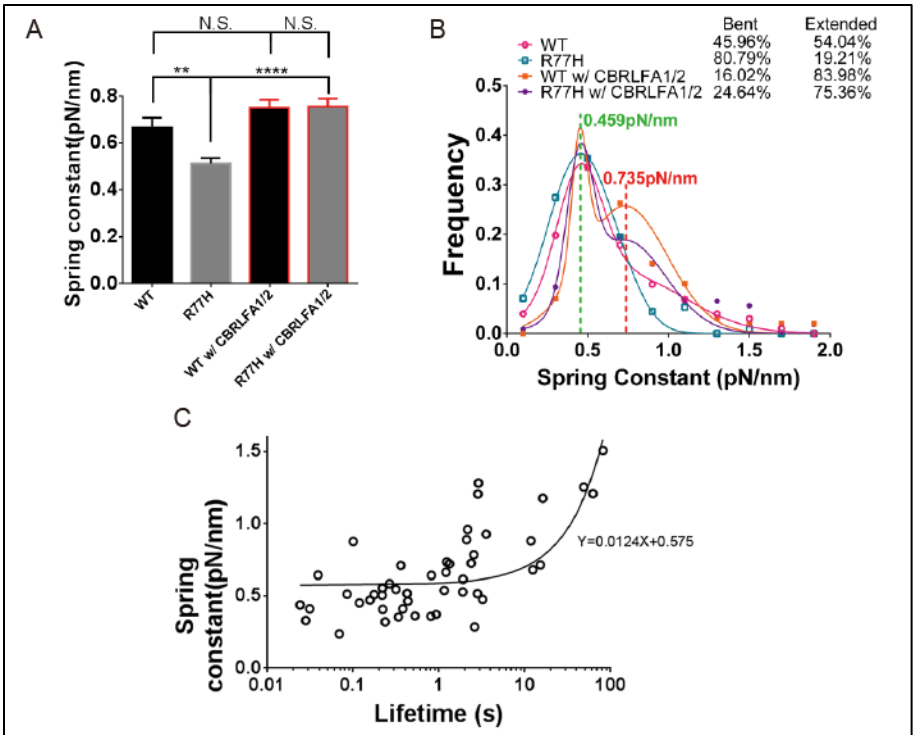

Figure 19. Molecular spring constants of Mac-1-ICAM-1 complex. (A) Average molecular spring constant of $CD11b^{WT}$ Mac-1 , $CD11b^{R77H}$ Mac-1, $CD11b^{WT}$ Mac-1 pre-incubated with CBR LFA1/2 and $CD11b^{R77H}$ Mac-1 pre-incubated with CBR LFA1/2 . **(B)** Spring constant distributions of each set of experiment in panel A. Each distribution was fitted with a two-peak Gaussian distribution with shared means. According to the fitting results, mean spring constant for the bent integrin is 0.459pN/nm (indicated with a green dashed line), and for the extended integrin is 0.735pN/nm (indicated with a red dashed line). The percentile of bent and extended integrins in each condition was also indicated. **(C)** Scatter plot of lifetime events against the spring constant of the same integrin. All lifetime events were randomly selected from all above experiment sets. The data was fit linearly. Non-zero test on the linear fitting slope was significant.

The R77H mutation reduced the binding affinity of Mac-1 at zero-force by decreasing its on-rate.

Adhesion frequency assays were performed to characterize Mac-1 binding to ICAM-1 in the force-free condition in the presence of Mg/EGTA (Fig. 20A). By fitting the curve to the two-dimensional adhesion model, effective affinity and off-rate were calculated (Fig. 20B, C) (115). The introduction of R77H to Mac-1 significantly reduced its binding affinity, but did not contribute much to the off-rate (Fig. 20B, C). Remembering that affinity is the ratio of on-rate to

off-rate, this indicated that R77H reduced the binding affinity via reducing its on-rate. The addition of CBR LFA1/2 increased the affinity of both $CD11b^{WT}$ and $CD11b^{R77H}$, although this increase in $CD11b^{WT}$ samples was not statistically significant; meanwhile, it also reduced their off-rates to a similar level (Fig. 20B, C). Deletion of GFFKR did not rescue, but further lowered the affinity deficiency caused by R77H, while V124A not only rescued the deficiency, but increased the affinity to about 1.5-fold that of $CD11b^{WT}$ (Fig. 20B, C). Considering that the addition of V124A had minor effects on the off-rate compared to the $CD11b^{R77H}$ single mutation and $CD11b^{WT}$, the affinity increase caused by it again resulted merely from the change in on-rate.

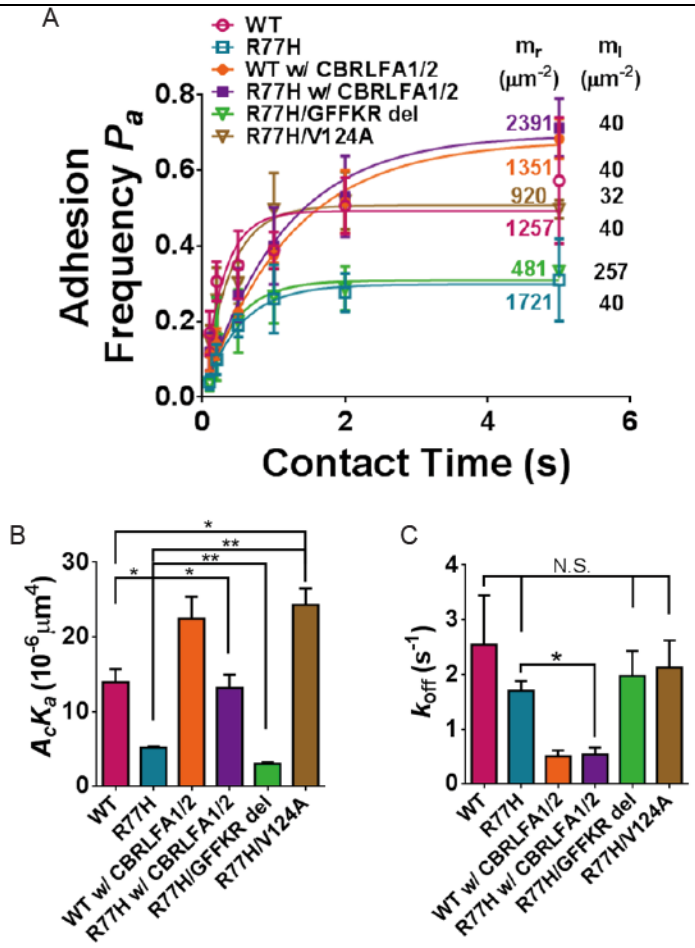

Figure 20. Adhesion Frequency Assay of Mac-1 and ICAM-1. (A) Adhesion frequency curves of K562 expressing $CD11b^{WT}$, $CD11b^{R77H}$, $CD11b^{WT}$ and $CD11b^{R77H}$ pretreated with CBR LFA 1/2 antibody, $CD11b^{R77H/GFFKR}$ and $CD18^{V124A}CD11b^{R77H}$. Site densities of Mac-1 (mr) and ICAM-1 (ml) were marked along each curve. **(B)** Effective affinity (AcKa) of each pair of Mac-1/ICAM-1 binding calculated from the fitting of the two-dimensional adhesion model. **(C)** Off-rate (koff) of each pair of Mac-1-ICAM-1 binding calculated from the fitting of the two-dimensional adhesion model.

IV. Discussion

We demonstrate that the SLE-associated variant R77H and the β-propeller region in which it resides may contribute to the adoption of a high affinity conformation of the βI-domain and in turn the establishment of force-induced catch bonds necessary for promoting adhesion between Mac-1 and its ligands under mechanical force. Previous work has suggest that the α-subunit is critical for ligand-binding specificity while the β-subunit was the most important for transmitting the conformational changes that activate ligand binding and connect to the cytoskeleton. The importance of R77H and the β-propeller domain in allosteric signaling provides new roles for the α-subunit in allostery transmission and provide a potential mechanism for the reported reduction in ligand binding in R77H expressing cells. Force induced regulation of adhesion between integrins and their ligands may be provided by shear flow within the vessel wall, by traction forces exerted by the actin cytoskeleton and actomyosin contraction in migrating cells and potentially by microbes captured by integrins at the cell surface. Our previous work suggests that Mac-1 regulates FcγRIIA dependent neutrophil adhesion in the context of immune complex deposition as assessed by intravital microscopy and in a model of human SLE sera induced lupus nephritis (26). We propose that R77H prevents Mac-1 engagement of its ligand and thus alleviates Mac-1 mediated inhibition of FcγRIIA dependent neutrophil recruitment to sites of IC deposition.

Where is the R77H lesion? The equilibrium between integrin states is likely regulated by inside-out signaling induced by chemokines and ligand binding, which induces incompletely understood cellular events that stabilize the open headpiece conformation, promotes full extension of the integrin and propagates outside-in signals that link to signal transduction and

anchorage to the actin cytoskeleton (Fig. 21). Affinity regulation of ligand binding of integrins is a complex process. Proper activation of the I-domain has been proposed to require the interaction of an invariant Glutamate residue of the α7 helix from the C-terminal region of the I-domain with the MIDAS of the βI-like domain, serving as an internal ligand. This interaction exerts a downward pull of the α7 helix, required for placing the βI and subsequently the αI in a high affinity state. Based on normal exposure of activation reporter epitopes (CBRM1/5, Kim127 and MoAb24), and the failure to rescue the ligand binding defect by the βI activating mutants, that increase the affinity of the βI-domain for the internal ligand (L132A and V124A) or LA-1 (an αI-domain agonist) suggests that the interaction of the αI- and βI-domains is compromised. This could be due to changes in rigidity of the β-propeller structure that consequently affects the flexibility of the αI-domain and therefore the flickering of the α-7 helix into the internal ligand binding pocket in the βI-domain. Cytoplasmic tail separation, well accepted to promote full integrin extension with open head piece and actin anchorage (108,126), may rescue R77H by allowing force induced allosteric changes.

R77H results in a reduction in integrin, on-rate and force-free off-rate. This is associated with an increase in the integrin fraction in the bent conformation, which is more flexible (lower stiffness) at the expenses of the fraction in the extended conformation, which is less flexibility. R77H also alters the force-regulated bond dissociation between Mac-1 and ICAM-1 by suppressing their catch bond. Both the catch bond force range and the extent of bond lifetime prolongation are reduced, resulting in a left- and down-shifted bond lifetime *vs* force curve. This resembles the change in the lifetime *vs* force curve of LFA-1 bond with ICAM-1 in the presence of XVA143 (94). XVA143 is a small molecule antagonist that binds the βI-domain binding site for the internal ligand at the α7-helix of the αI-domain. This resemblance suggests that R77H mutation

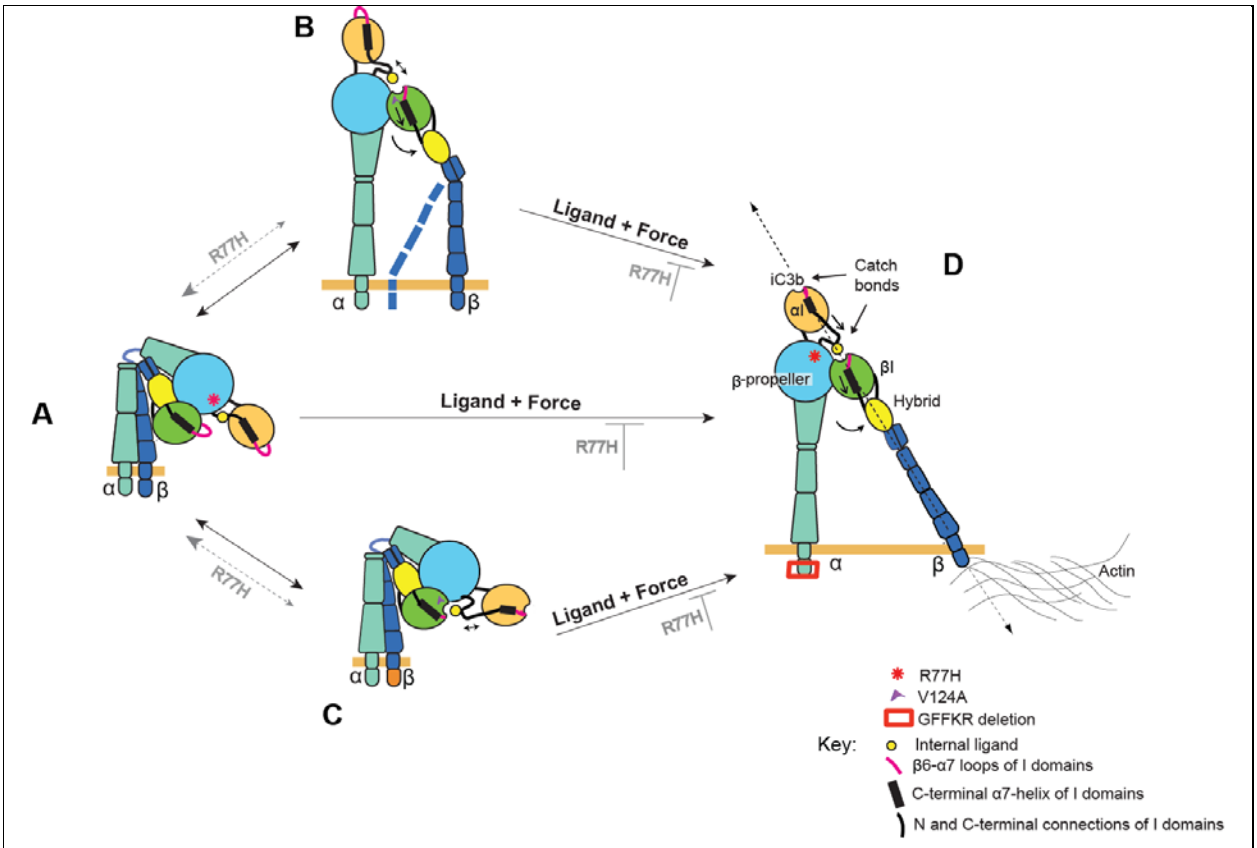

Figure 21. Model on how R77H affects ligand binding and catch bond formation by Mac-1. (A) Inactive, bent Mac-1 with a closed head piece. The αI domain is in the inactive conformation with the α7-helix in the up position and the MIDAS in the closed conformation. This state is favored by the R77H mutation(*). **(B)** and **(C)** depict Mac-1 conformations induced by inside-out signaling and metal ions. When force is applied by ligand (e.g. iC3b, ICAM-1) it is transmitted from the αI domain MIDAS to the α7-helix to induce the catch bond between the internal ligand and the βI domain, that in turn promotes the downward pull of the α7-helix to generate intermediate- and long-lived interactions resulting in Mac-1-ligand catch bonds **(D)**. This process is abrogated by the R77H mutation . The V124A mutation (➧) moves the βI domain into the active state and increases its affinity for the internal ligand, which partially rescues the R77H catch bond defect. Forced extension of Mac-1 using CBR LFA1/2 antibody bypasses the requierement for the R77 region and compeletely rescues the R77H phenotype. Deletion of the regulatory region GFFKR of the α subunit, frees the intracellular tails and decreases the threshold requirements for αI and βI domain interactions.

results in a defect in the αI-βI inter domain interaction that also exhibits catch bond behavior (94). The βI-domain activating mutation V124A, which places the βI domain in a constitutively active state (120), rescues affinity, on-rate, force-free off-rate, and the catch bond force range but not the extent of bond lifetime prolongation. While wild-type Mac-1 with a GFFKR deletion exhibits an open headpiece with high affinity state as reported, R77H with a GFFKR deletion adopts a closed headpiece conformation that remains in a bent low affinity state, which suggests an interference of allosteric relay between the αI and βI domain. The GFFKR deletion in the context of R77H increases the fraction of bent integrin, as revealed by molecular stiffness

analysis, thereby reducing the affinity by reducing on-rate, but not force-free off-rate. Under tensile force, however, the GFFKR deletion over rescues, the catch bond defect of the R77H mutation. The CBRLFA1/2 antibody increases the affinity by decreasing the force-free off-rate of the WT integrin, and rescues the affinity of R77H by decreasing the force-free off-rate. CBRLFA1/2 also produces the indistinguishable bond lifetime *vs* force curves for both $CD11b^{WT}$ and $CD11b^{R77H}$ with an enhanced catch bond that has the same force range but greater extent of lifetime prolongation. Together, these data suggest that a conformational change in multiple integrin domains is required for mechanically regulated binding of the integrin-ligand complex that is modulated in part by R77 dependent allosteric transmission to the αI-domain.

The R77H variant is a fairly common allele in the healthy population (~10% of the population). In non-autoimmune conditions, the influence of this variant may be minor, due to the existence of many regulatory checkpoints. However, in the context of SLE, where dysfunction of several aspects of the immune response occurs simultaneously, the R77H variant of CD11b might play an important modulatory role. Since CD11b is expressed on many leukocyte subsets, it can participate in several aspects of the disease. CD11b has been suggested to be a negative regulator of BCR activity (77), suggesting that when dysfunctional, it may lower the activation threshold of B cells. This could have repercussions in the maintenance of tolerance and in the amplification of self-reactive responses. Mac-1 can also inhibit the signaling of pro-inflammatory receptors (e.g. TLR, IFNαR) (18,19,101,104). However, the precise mechanisms through which Mac-1 exerts its inhibitory signal are not fully understood. Difficulty comes from a lack of information regarding inhibitory signaling events triggered by Mac-1 engagement. Spatial separation of the cytoplasmic domain has been suggested as a mechanism by which integrins transduce information across the cell membrane (97,98), therefore the proper engagement and transmission

of allosteric signals from Mac-1 ligand binding domains to the cytoplasmic tails are necessary to establish its potential regulatory roles.

Chapter 6. General Conclusions

There is emerging evidence that mechanisms that regulate effector responses to ICs probably determine the type of organ damage and its severity in patients with SLE. Our work suggests that Mac-1 may protect from tissue injury induced by ICs by modulating FcγRIIA-dependent neutrophil recruitment. This is supported by data obtained in two murine models of glomerulonephritis induced by circulating IgG immune complexes to lupus antigens. The relevance of the protective role of Mac-1 in SLE is further supported by several publications that a genetic variant of Mac-1 (R77H), shown to impair its function, confers a risk for SLE (24,25). Here we have provided a mechanism through which R77H could alter optimal interaction of Mac-1 with its ligands and thus contribute to the pathogenesis of SLE.

As exemplified in our SLE serum-induced nephritis model, and as previously reported in patients with SLE, the mere presence of ICs is not sufficient to induce disease. This observation suggests that regulatory mechanisms actively control neutrophil responses to deposited ICs. Our data suggests that Mac-1 is involved in this regulation. Whether the inhibition that Mac-1 is conferring represents a constant tonic inhibitory signal or is rather initiated upon neutrophil activation through FcγRIIA, is still undetermined. The biology of Mac-1 is complex as it can generate responses that may be context dependent and seemingly contradictory. It possesses a potent pro-inflammatory potential and the capacity to enhance murine FcγR responses and renal damage in an acute model of anti-GBM glomerulonephritis (127,128). Although the reasons for the differences in the role of Mac-1 needs further investigation, it is important to note that anti-GBM nephritis is induced by in situ antibody deposition in the glomerulus and is an acute response while renal damage in our lupus models requires a longer time period and is promoted

primarily by soluble immune complexes that deposit in the glomerulus. Moreover, the negative regulatory role of Mac-1 appears to be apparent primarily in the context of human FcγRIIA and not the murine FcγRs (26). There are other examples where opposing roles for the same receptor exist. The affinity/avidity of FcαR (129) and FcγRIII (72,130) for their ligands (i.e. monomeric vs. Ig forming ICs), determines the magnitude of the response and whether the outcome is activating or inhibitory (e.g. complete phosphorylation of Syk vs. the activation of inhibitory phosphatases and/or partial phosphorylation of Syk). The signaling cascade is also modified by the presence of other triggers, for example cytokines, which can differentially promote or inhibit responses (e.g. the presence of IFN-γ abrogates the induction of IL-10 by Mac-1 on macrophages (18)).

The role of β2 integrins in neutrophil recruitment was initially appreciated in patients with leukocyte adhesion deficiency type I (LAD I), where genetic defects on CD18 impair its expression, and therefore its association with the α subunits (i.e. CD11b, CD11a and CD11c). Neutrophils from these patients show a significant defect in recruitment to the sites of inflammation and chemotaxis. Moreover, a loss of function mutation in Kindlin-3, a cytoplasmic adaptor protein required for integrin activation (LAD III), phenocopies many of the defects in LAD I patients (131,132). Extensive work to dissect the contributions of each of these integrins in the recruitment cascade has been done. Mac-1 contributes to the establishment of firm adhesion and crawling on the endothelium. However, the study of knock-out mice have revealed that LFA-1 has a dominant role during the recruitment cascade. The interference of its function (i.e. by blocking antibodies or $CD11a^{-/-}$ mice) strikingly impedes neutrophil recruitment (133) and associated tissue injury (i.e. arthritis and nephritis in the MRL/lpr mice) (20,21). In contrast, CD11b deficiency does not consistently result in defects in neutrophil recruitment but in

combination with LFA-1 deletion can lead to a further reduction in neutrophil accumulation compared to LFA-1 deficiency alone (48,134). On the other hand, neutrophil migration was shown to be enhanced in CD11b$^{-/-}$ mice in some cases (133), which can explain the worsening of the disease intensity in certain contexts (20,21).

More recently, Mac-1 activation was shown to decrease inflammation in murine models (124). The use of the small molecule LA-1, reduced leukocyte migration, tissue accumulation, and injury *in vivo* (123,124). This was confirmed by *in vitro* studies that showed that LPS and PMA-induced migration over a Mac-1 ligand was significantly reduced by the activation of Mac-1 (123). A possible explanation is that partial Mac-1 activation results in the sequestration of the neutrophils at the vessel wall by increasing their adhesion to the inflamed endothelium and thus reducing leukocyte infiltration into tissues and associated injury.

We propose that Mac-1 limits immune complex mediated neutrophil recruitment by regulating human FcγRIIA activation in particular. This is based on the observation that in contrast to FcγRIIA-expressing mice, Mac-1$^{-/-}$ mice that express murine activating receptors are not susceptible to developing SLE serum-induced nephritis despite the equivalent ability of human and mouse FcγRs to bind human IgG (15). This suggests that the human single polypeptide FcγRIIA containing ITAM may be differentially regulated than the murine FcγR which associates with the ITAM–containing γ-chain. There may be differences in the downstream pathways engaged by the murine versus the human receptors, a possibility that is supported by the much more potent injury observed with human FcγRIIA versus murine FcγRs in a model of nephrotoxic nephritis despite similar expression levels of the human and murine receptors (15). Macrophages, DC, and B cells are cell types that significantly contribute to the loss of tolerance

and to the amplification and perpetuation of the autoimmune response in SLE. FcγRs and Mac-1 are also expressed on these cell types, so it is possible that the inhibitory functions of Mac-1 can also modify the behavior of these cells. The contribution of Mac-1 on each of these cell types could be addressed by the use of Mac-1 conditional knock-outs, which are currently not available.

We consider that the model we have generated represents an excellent tool to study the local factors that contribute to the development of end organ damage triggered by IC deposition. The contribution of molecules expressed on the endothelium and other resident renal cells that might be important in the amplification, perpetuation or mitigation of the inflammatory responses, can be addressed by generating bone marrow chimeras using bone marrow from mice that express FcγRIIA and lack Mac-1, into recipient mice that lack or overexpress a molecule of interest. Furthermore, the passive human lupus serum induced nephritis model, which leads to renal injury within 14 days could serve as a pre-clinical platform to test potential therapeutics that target the effector response in SLE. Our model would be more amenable for screening of compounds than the lupus prone strains of mice that develop disease over a 6-9 month period that is not synchronized because disease is induced by dysregulation of the adaptive immune response.

GWAS have significantly contributed to the identification of genes that confer risk for complex diseases. Over 40 loci have been found to be associated with SLE. The next step is to clarify how each of these genes affects the immune response in order to determine how the genetic variant contributes to disease. In contrast to most of the SNPs associated with SLE in the GWAS, the the rs1143679 variant of Mac-1 causes a non-synonymous mutation (R77H). Therefore, the

functional link between the SNP and the presence of SLE must be explained by a functional effect of Mac-1.

Understanding the mechanisms that contribute to SLE will facilitate the diagnosis and treatment of patients. In particular, the identification of the mechanisms that favor or oppose the development of renal injury in particular is of great interest since lupus nephritis is a major cause of morbidity and mortality in patients with SLE. It is estimated that over 60% of patients will develop nephritis during the course of their disease. Even though ICs and complement deposition are considered to trigger the effector responses associated with the development of disease, to date, most of the attention has been on elucidating the role of T cells and DC in disease pathogenesis. The role of neutrophils in lupus nephritis has not been completely established, despite reports of neutrophil infiltration during lupus nephritis. Our work suggests that modulating neutrophil responses might be a key to controlling the damage to target organs and that modulation of human FcγRIIA activity by Mac-1 may serve as a rheostat of neutrophil recruitment and cytotoxicity in the context of SLE.

Publications

The following are my publications as a graduate student

Review

1. Mayadas TN, **Rosetti F**, Ernandez T, Sethi S. Neutrophils: game changers in glomerulonephritis? *Trends Mol Med*. 2010 Aug;16(8):368-78.

Original articles

1. Niewczas MA, Gohda T, Skupien J, Smiles AM, Walker WH, **Rosetti F**, Cullere X, Eckfeldt JH, Doria A, Mayadas TN, Warram JH, Krolewski AS. Circulating TNF receptors 1 and 2 predict ESRD in type 2 diabetes. *J Am Soc Nephrol*. 2012 Mar;23(3):507-15.

2. Gohda T, Niewczas MA, Ficociello LH, Walker WH, Skupien J, **Rosetti F**, Cullere X, Johnson AC, Crabtree G, Smiles AM, Mayadas TN, Warram JH, Krolewski AS.Circulating TNF receptors 1 and 2 predict stage 3 CKD in type 1 diabetes. *J Am Soc Nephrol*. 2012 Mar;23(3):516-24

3. Crispín JC, Apostolidis SA, **Rosetti F**, Keszei M, Wang N, Terhorst C, Mayadas TN, Tsokos GC. Cutting edge: protein phosphatase 2A confers susceptibility to autoimmune disease through an IL-17-dependent mechanism. *J Immunol*. 2012 Apr 15;188(8):3567-71.

4. **Rosetti F**, Tsuboi N, Chen K, Nishi H, Ernandez T, Sethi S, Croce K, Stavrakis G, Alcocer-Varela J, Gómez-Martin D, van Rooijen N, Kyttaris VC, Lichtman AH, Tsokos GC, Mayadas TN. Human lupus serum induces neutrophil-mediated organ damage in mice that is enabled by Mac-1 deficiency. *J Immunol*. 2012 Oct 1;189(7):3714-23

5. Venkatesh D, Ernandez T, **Rosetti F**, Batal I, Cullere X, Luscinskas FW, Zhang Y, Stavrakis G, García-Cardeña G, Horwitz BH, Mayadas TN. Endothelial TNF receptor 2 induces IRF1 transcription factor-dependent interferon-β autocrine signaling to promote monocyte recruitment. *Immunity*. 2013 May 23;38(5):1025-37.

6. **Rosetti F**, Chen Y, Sen M, Thayer E, Azcutia V, Herter J, Luscinskas W, Cullere X, Zhu C, Mayadas TN. A lupus-associated variant of Mac-1 exhibits defects in integrin allostery and force induced integrin interactions with ligands. *Manuscript in preparation.*

Bibliography

1. Rahman, A., and D. A. Isenberg. 2008. Systemic lupus erythematosus. *N. Engl. J. Med.* 358: 929-939.

2. Tsokos, G. C. 2011. Systemic lupus erythematosus. *N. Engl. J. Med.* 365: 2110-2121.

3. Crispin, J. C., C. M. Hedrich, and G. C. Tsokos. 2013. Gene-function studies in systemic lupus erythematosus. *Nat. Rev. Rheumatol.* 9: 476-484.

4. Crispin, J. C., S. N. Liossis, K. Kis-Toth, L. A. Lieberman, V. C. Kyttaris, Y. T. Juang, and G. C. Tsokos. 2010. Pathogenesis of human systemic lupus erythematosus: recent advances. *Trends Mol. Med.* 16: 47-57.

5. Bagavant, H., and S. M. Fu. 2005. New insights from murine lupus: disassociation of autoimmunity and end organ damage and the role of T cells. *Curr. Opin. Rheumatol.* 17: 523-528.

6. Bagavant, H., U. S. Deshmukh, F. Gaskin, and S. M. Fu. 2004. Lupus glomerulonephritis revisited 2004: autoimmunity and end-organ damage. *Scand. J. Immunol.* 60: 52-63.

7. CORMANE, R. H. 1964. "BOUND" GLOBULIN IN THE SKIN OF PATIENTS WITH CHRONIC DISCOID LUPUS ERYTHEMATOSUS AND SYSTEMIC LUPUS ERYTHEMATOSUS. *Lancet* 1: 534-535.

8. Bagavant, H., and S. M. Fu. 2009. Pathogenesis of kidney disease in systemic lupus erythematosus. *Curr. Opin. Rheumatol.* 21: 489-494.

9. Gonzalez-Crespo, M. R., J. I. Lopez-Fernandez, G. Usera, M. J. Poveda, and J. J. Gomez-Reino. 1996. Outcome of silent lupus nephritis. *Semin. Arthritis Rheum.* 26: 468-476.

10. Valente de Almeida, R., J. G. Rocha de Carvalho, V. F. de Azevedo, R. A. Mulinari, S. O. Ioshhi, S. da Rosa Utiyama, and R. Nisihara. 1999. Microalbuminuria and renal morphology in the evaluation of subclinical lupus nephritis. *Clin. Nephrol.* 52: 218-229.

11. Arbuckle, M. R., M. T. McClain, M. V. Rubertone, R. H. Scofield, G. J. Dennis, J. A. James, and J. B. Harley. 2003. Development of autoantibodies before the clinical onset of systemic lupus erythematosus. *N. Engl. J. Med.* 349: 1526-1533.

12. Hinojosa-Asaola, A., J. Sanchez-Guerrero, and . 2013. Overview and Clinical presentation. In *Dubois' Lupus Erythematosus and Related Syndromes*, 8th ed. D. J. Wallace and B. H. Hahn, eds. Elsevier, Philadelphia. 304-310.

13. Mayadas, T. N., G. C. Tsokos, and N. Tsuboi. 2009. Mechanisms of immune complex-mediated neutrophil recruitment and tissue injury. *Circulation* 120: 2012-2024.

14. Davidson, A., C. Berthier, and M. Kretzler. 2013. Pathogenetic Mechanisms in Lupus Nephritis. In *Dubois' Lupus Erythematosus and Related Syndromes*, 8th ed. D. J. Wallace and B. H. Hahn, eds. Elsevier, Philadelphia. 237-255.

15. Tsuboi, N., K. Asano, M. Lauterbach, and T. N. Mayadas. 2008. Human neutrophil Fcgamma receptors initiate and play specialized nonredundant roles in antibody-mediated inflammatory diseases. *Immunity.* 28: 833-846.

16. Tsuboi, N., T. Ernandez, X. Li, H. Nishi, X. Cullere, D. Mekala, M. Hazen, J. Kohl, D. M. Lee, and T. N. Mayadas. 2011. Regulation of human neutrophil Fcgamma receptor IIa by C5a receptor promotes inflammatory arthritis in mice. *Arthritis Rheum.* 63: 467-478.

17. Mevorach, D., J. O. Mascarenhas, D. Gershov, and K. B. Elkon. 1998. Complement-dependent clearance of apoptotic cells by human macrophages. *J. Exp. Med.* 188: 2313-2320.

18. Wang, L., R. A. Gordon, L. Huynh, X. Su, K. H. Park Min, J. Han, J. S. Arthur, G. D. Kalliolias, and L. B. Ivashkiv. 2010. Indirect inhibition of Toll-like receptor and type I interferon responses by ITAM-coupled receptors and integrins. *Immunity.* 32: 518-530.

19. Han, C., J. Jin, S. Xu, H. Liu, N. Li, and X. Cao. 2010. Integrin CD11b negatively regulates TLR-triggered inflammatory responses by activating Syk and promoting degradation of MyD88 and TRIF via Cbl-b. *Nat. Immunol.* 11: 734-742.

20. Watts, G. M., F. J. Beurskens, I. Martin-Padura, C. M. Ballantyne, L. B. Klickstein, M. B. Brenner, and D. M. Lee. 2005. Manifestations of inflammatory arthritis are critically dependent on LFA-1. *J. Immunol.* 174: 3668-3675.

21. Kevil, C. G., M. J. Hicks, X. He, J. Zhang, C. M. Ballantyne, C. Raman, T. R. Schoeb, and D. C. Bullard. 2004. Loss of LFA-1, but not Mac-1, protects MRL/MpJ-Fas(lpr) mice from autoimmune disease. *Am. J. Pathol.* 165: 609-616.

22. Kanwar, S., C. W. Smith, F. R. Shardonofsky, and A. R. Burns. 2001. The role of Mac-1 (CD11b/CD18) in antigen-induced airway eosinophilia in mice. *Am. J. Respir. Cell Mol. Biol.* 25: 170-177.

23. Hom, G., R. R. Graham, B. Modrek, K. E. Taylor, W. Ortmann, S. Garnier, A. T. Lee, S. A. Chung, R. C. Ferreira, P. V. Pant, D. G. Ballinger, R. Kosoy, F. Y. Demirci, M. I. Kamboh, A. H. Kao, C. Tian, I. Gunnarsson, A. A. Bengtsson, S. Rantapaa-Dahlqvist, M. Petri, S. Manzi, M. F. Seldin, L. Ronnblom, A. C. Syvanen, L. A. Criswell, P. K. Gregersen, and T. W. Behrens. 2008. Association of systemic lupus erythematosus with C8orf13-BLK and ITGAM-ITGAX. *N. Engl. J. Med.* 358: 900-909.

24. Nath, S. K., S. Han, X. Kim-Howard, J. A. Kelly, P. Viswanathan, G. S. Gilkeson, W. Chen, C. Zhu, R. P. McEver, R. P. Kimberly, M. E. Alarcon-Riquelme, T. J. Vyse, Q. Z. Li, E. K. Wakeland, J. T. Merrill, J. A. James, K. M. Kaufman, J. M. Guthridge, and J. B. Harley. 2008. A nonsynonymous functional variant in integrin-alpha(M) (encoded by ITGAM) is associated with systemic lupus erythematosus. *Nat. Genet.* 40: 152-154.

25. MacPherson, M., H. S. Lek, A. Prescott, and S. C. Fagerholm. 2011. A systemic lupus erythematosus-associated R77H substitution in the CD11b chain of the Mac-1 integrin compromises leukocyte adhesion and phagocytosis. *J. Biol. Chem.* 286: 17303-17310.

26. Rosetti, F., N. Tsuboi, K. Chen, H. Nishi, T. Ernandez, S. Sethi, K. Croce, G. Stavrakis, J. Alcocer-Varela, D. Gomez-Martin, R. N. van, V. C. Kyttaris, A. H. Lichtman, G. C. Tsokos, and T. N. Mayadas. 2012. Human lupus serum induces neutrophil-mediated organ damage in mice that is enabled by Mac-1 deficiency. *J. Immunol.* 189: 3714-3723.

27. Schmidt, R. E., and J. E. Gessner. 2005. Fc receptors and their interaction with complement in autoimmunity. *Immunol. Lett.* 100: 56-67.

28. Ravetch, J. V., and S. Bolland. 2001. IgG Fc receptors. *Annu. Rev. Immunol.* 19: 275-290.

29. Wu, T., and C. Mohan. 2007. Three pathogenic determinants in immune nephritis--anti-glomerular antibody specificity, innate triggers and host genetics. *Front Biosci.* 12: 2207-2211.

30. Nguyen, C., N. Limaye, and E. K. Wakeland. 2002. Susceptibility genes in the pathogenesis of murine lupus. *Arthritis Res.* 4 Suppl 3: S255-S263.

31. Ehlers, M. R. 2000. CR3: a general purpose adhesion-recognition receptor essential for innate immunity. *Microbes. Infect.* 2: 289-294.

32. Hogarth, P. M. 2002. Fc receptors are major mediators of antibody based inflammation in autoimmunity. *Curr. Opin. Immunol.* 14: 798-802.

33. Scharffetter-Kochanek, K., H. Lu, K. Norman, N. N. van, F. Munoz, S. Grabbe, M. McArthur, I. Lorenzo, S. Kaplan, K. Ley, C. W. Smith, C. A. Montgomery, S. Rich, and A. L. Beaudet. 1998. Spontaneous skin ulceration and defective T cell function in CD18 null mice. *J. Exp. Med.* 188: 119-131.

34. Coxon, A., P. Rieu, F. J. Barkalow, S. Askari, A. H. Sharpe, U. H. von Andrian, M. A. Arnaout, and T. N. Mayadas. 1996. A novel role for the beta 2 integrin CD11b/CD18 in neutrophil apoptosis: a homeostatic mechanism in inflammation. *Immunity.* 5: 653-666.

35. Takai, T., M. Li, D. Sylvestre, R. Clynes, and J. V. Ravetch. 1994. FcR gamma chain deletion results in pleiotrophic effector cell defects. *Cell* 76: 519-529.

36. Rosenkranz, A. R., D. L. Mendrick, R. S. Cotran, and T. N. Mayadas. 1999. P-selectin deficiency exacerbates experimental glomerulonephritis: a protective role for endothelial P-selectin in inflammation. *J. Clin. Invest* 103: 649-659.

37. Baharav, E., S. Bar-Yehuda, L. Madi, D. Silberman, L. Rath-Wolfson, M. Halpren, A. Ochaion, A. Weinberger, and P. Fishman. 2005. Antiinflammatory effect of A3 adenosine receptor agonists in murine autoimmune arthritis models. *J. Rheumatol.* 32: 469-476.

38. Duffau, P., J. Seneschal, C. Nicco, C. Richez, E. Lazaro, I. Douchet, C. Bordes, J. F. Viallard, C. Goulvestre, J. L. Pellegrin, B. Weil, J. F. Moreau, F. Batteux, and P. Blanco. 2010. Platelet CD154

potentiates interferon-alpha secretion by plasmacytoid dendritic cells in systemic lupus erythematosus. *Sci. Transl. Med.* 2: 47ra63.

39. Chen, M., E. Boilard, P. A. Nigrovic, P. Clark, D. Xu, G. A. Fitzgerald, L. P. Audoly, and D. M. Lee. 2008. Predominance of cyclooxygenase 1 over cyclooxygenase 2 in the generation of proinflammatory prostaglandins in autoantibody-driven K/BxN serum-transfer arthritis. *Arthritis Rheum.* 58: 1354-1365.

40. Tang, T., A. Rosenkranz, K. J. Assmann, M. J. Goodman, J. C. Gutierrez-Ramos, M. C. Carroll, R. S. Cotran, and T. N. Mayadas. 1997. A role for Mac-1 (CDIIb/CD18) in immune complex-stimulated neutrophil function in vivo: Mac-1 deficiency abrogates sustained Fcgamma receptor-dependent neutrophil adhesion and complement-dependent proteinuria in acute glomerulonephritis. *J. Exp. Med.* 186: 1853-1863.

41. van, R. N., and A. Sanders. 1994. Liposome mediated depletion of macrophages: mechanism of action, preparation of liposomes and applications. *J. Immunol. Methods* 174: 83-93.

42. Ley, K., M. Allietta, D. C. Bullard, and S. Morgan. 1998. Importance of E-selectin for firm leukocyte adhesion in vivo. *Circ. Res.* 83: 287-294.

43. Fu, Y., Y. Du, and C. Mohan. 2007. Experimental anti-GBM disease as a tool for studying spontaneous lupus nephritis. *Clin. Immunol.* 124: 109-118.

44. Rosenkranz, A. R., S. Knight, S. Sethi, S. I. Alexander, R. S. Cotran, and T. N. Mayadas. 2000. Regulatory interactions of alphabeta and gammadelta T cells in glomerulonephritis. *Kidney Int.* 58: 1055-1066.

45. Billiau, A., and P. Matthys. 2001. Modes of action of Freund's adjuvants in experimental models of autoimmune diseases. *J. Leukoc. Biol.* 70: 849-860.

46. Norman, M. U., N. C. Van De Velde, J. R. Timoshanko, A. Issekutz, and M. J. Hickey. 2003. Overlapping roles of endothelial selectins and vascular cell adhesion molecule-1 in immune complex-induced leukocyte recruitment in the cremasteric microvasculature. *Am. J. Pathol.* 163: 1491-1503.

47. Stokol, T., P. O'Donnell, L. Xiao, S. Knight, G. Stavrakis, M. Botto, U. H. von Andrian, and T. N. Mayadas. 2004. C1q governs deposition of circulating immune complexes and leukocyte Fcgamma receptors mediate subsequent neutrophil recruitment. *J. Exp. Med.* 200: 835-846.

48. Dunne, J. L., C. M. Ballantyne, A. L. Beaudet, and K. Ley. 2002. Control of leukocyte rolling velocity in TNF-alpha-induced inflammation by LFA-1 and Mac-1. *Blood* 99: 336-341.

49. Li, X., A. Utomo, X. Cullere, M. M. Choi, D. A. Milner, Jr., D. Venkatesh, S. H. Yun, and T. N. Mayadas. 2011. The beta-glucan receptor Dectin-1 activates the integrin Mac-1 in neutrophils via Vav protein signaling to promote Candida albicans clearance. *Cell Host. Microbe* 10: 603-615.

50. Li, Y., P. Y. Lee, and W. H. Reeves. 2010. Monocyte and macrophage abnormalities in systemic lupus erythematosus. *Arch. Immunol. Ther. Exp. (Warsz.)* 58: 355-364.

51. Petty, H. R., R. G. Worth, and R. F. Todd, III. 2002. Interactions of integrins with their partner proteins in leukocyte membranes. *Immunol. Res.* 25: 75-95.

52. Mocsai, A., C. L. Abram, Z. Jakus, Y. Hu, L. L. Lanier, and C. A. Lowell. 2006. Integrin signaling in neutrophils and macrophages uses adaptors containing immunoreceptor tyrosine-based activation motifs. *Nat. Immunol.* 7: 1326-1333.

53. Nagarajan, S., K. Venkiteswaran, M. Anderson, U. Sayed, C. Zhu, and P. Selvaraj. 2000. Cell-specific, activation-dependent regulation of neutrophil CD32A ligand-binding function. *Blood* 95: 1069-1077.

54. Syam, S., P. Mero, T. Pham, C. A. McIntosh, P. Bruhns, and J. W. Booth. 2010. Differential recruitment of activating and inhibitory Fc gamma RII during phagocytosis. *J. Immunol.* 184: 2966-2973.

55. Liu, Z., M. Zhao, N. Li, L. A. Diaz, and T. N. Mayadas. 2006. Differential roles for beta2 integrins in experimental autoimmune bullous pemphigoid. *Blood* 107: 1063-1069.

56. Hirahashi, J., K. Hishikawa, S. Kaname, N. Tsuboi, Y. Wang, D. I. Simon, G. Stavrakis, T. Shimosawa, L. Xiao, Y. Nagahama, K. Suzuki, T. Fujita, and T. N. Mayadas. 2009. Mac-1 (CD11b/CD18) links inflammation and thrombosis after glomerular injury. *Circulation* 120: 1255-1265.

57. Waterman, P. M., and J. C. Cambier. 2010. The conundrum of inhibitory signaling by ITAM-containing immunoreceptors: potential molecular mechanisms. *FEBS Lett.* 584: 4878-4882.

58. Pasquier, B., P. Launay, Y. Kanamaru, I. C. Moura, S. Pfirsch, C. Ruffie, D. Henin, M. Benhamou, M. Pretolani, U. Blank, and R. C. Monteiro. 2005. Identification of FcalphaRI as an inhibitory receptor that controls inflammation: dual role of FcRgamma ITAM. *Immunity.* 22: 31-42.

59. Kanamaru, Y., S. Pfirsch, M. Aloulou, F. Vrtovsnik, M. Essig, C. Loirat, G. Deschenes, C. Guerin-Marchand, U. Blank, and R. C. Monteiro. 2008. Inhibitory ITAM signaling by Fc alpha RI-FcR gamma chain controls multiple activating responses and prevents renal inflammation. *J. Immunol.* 180: 2669-2678.

60. Phipps-Green, A. J., R. K. Topless, M. E. Merriman, N. Dalbeth, P. J. Gow, A. A. Harrison, J. Highton, P. B. Jones, L. K. Stamp, P. Harrison, B. P. Wordsworth, and T. R. Merriman. 2009. No evidence for association of the systemic lupus erythematosus-associated ITGAM variant, R77H, with rheumatoid arthritis in the Caucasian population. *Rheumatology. (Oxford)* 48: 1614-1615.

61. Niederer, H. A., M. R. Clatworthy, L. C. Willcocks, and K. G. Smith. 2010. FcgammaRIIB, FcgammaRIIIB, and systemic lupus erythematosus. *Ann. N. Y. Acad. Sci.* 1183: 69-88.

62. Aitman, T. J., R. Dong, T. J. Vyse, P. J. Norsworthy, M. D. Johnson, J. Smith, J. Mangion, C. Roberton-Lowe, A. J. Marshall, E. Petretto, M. D. Hodges, G. Bhangal, S. G. Patel, K. Sheehan-Rooney, M. Duda, P. R. Cook, D. J. Evans, J. Domin, J. Flint, J. J. Boyle, C. D. Pusey, and H. T. Cook. 2006. Copy number polymorphism in Fcgr3 predisposes to glomerulonephritis in rats and humans. *Nature* 439: 851-855.

63. Segerer, S., A. Henger, H. Schmid, M. Kretzler, D. Draganovici, U. Brandt, E. Noessner, P. J. Nelson, D. Kerjaschki, D. Schlondorff, and H. Regele. 2006. Expression of the chemokine receptor CXCR1 in human glomerular diseases. *Kidney Int.* 69: 1765-1773.

64. Mayadas, T. N., F. Rosetti, T. Ernandez, and S. Sethi. 2010. Neutrophils: game changers in glomerulonephritis? *Trends Mol. Med.* 16: 368-378.

65. Molad, Y., and B. N. Cronstein. 2007. Neutrophils (polymorphonuclear leukocytes) in systemic lupus erythematosus. In *Systemic Lupus Erythematosus: A Companion to Rheumatology*. G. C. Tsokos and J. S. Smolen, eds. Mosby, Philadelphia, PA. 281-286.

66. Denny, M. F., S. Yalavarthi, W. Zhao, S. G. Thacker, M. Anderson, A. R. Sandy, W. J. McCune, and M. J. Kaplan. 2010. A distinct subset of proinflammatory neutrophils isolated from patients with systemic lupus erythematosus induces vascular damage and synthesizes type I IFNs. *J. Immunol.* 184: 3284-3297.

67. Garcia-Romo, G. S., S. Caielli, B. Vega, J. Connolly, F. Allantaz, Z. Xu, M. Punaro, J. Baisch, C. Guiducci, R. L. Coffman, F. J. Barrat, J. Banchereau, and V. Pascual. 2011. Netting neutrophils are major inducers of type I IFN production in pediatric systemic lupus erythematosus. *Sci. Transl. Med.* 3: 73ra20.

68. Lande, R., D. Ganguly, V. Facchinetti, L. Frasca, C. Conrad, J. Gregorio, S. Meller, G. Chamilos, R. Sebasigari, V. Riccieri, R. Bassett, H. Amuro, S. Fukuhara, T. Ito, Y. J. Liu, and M. Gilliet. 2011. Neutrophils activate plasmacytoid dendritic cells by releasing self-DNA-peptide complexes in systemic lupus erythematosus. *Sci. Transl. Med.* 3: 73ra19.

69. Morel, L., U. H. Rudofsky, J. A. Longmate, J. Schiffenbauer, and E. K. Wakeland. 1994. Polygenic control of susceptibility to murine systemic lupus erythematosus. *Immunity.* 1: 219-229.

70. Morel, L., C. Mohan, Y. Yu, B. P. Croker, N. Tian, A. Deng, and E. K. Wakeland. 1997. Functional dissection of systemic lupus erythematosus using congenic mouse strains. *J. Immunol.* 158: 6019-6028.

71. Morel, L., K. R. Blenman, B. P. Croker, and E. K. Wakeland. 2001. The major murine systemic lupus erythematosus susceptibility locus, Sle1, is a cluster of functionally related genes. *Proc. Natl. Acad. Sci. U. S. A* 98: 1787-1792.

72. Jang, J. E., A. Hidalgo, and P. S. Frenette. 2012. Intravenous immunoglobulins modulate neutrophil activation and vascular injury through FcgammaRIII and SHP-1. *Circ. Res.* 110: 1057-1066.

73. Nimmerjahn, F., and J. V. Ravetch. 2008. Fcgamma receptors as regulators of immune responses. *Nat. Rev. Immunol.* 8: 34-47.

74. Tridandapani, S., Y. Wang, C. B. Marsh, and C. L. Anderson. 2002. Src homology 2 domain-containing inositol polyphosphate phosphatase regulates NF-kappa B-mediated gene transcription by phagocytic Fc gamma Rs in human myeloid cells. *J. Immunol.* 169: 4370-4378.

75. Ganesan, L. P., H. Fang, C. B. Marsh, and S. Tridandapani. 2003. The protein-tyrosine phosphatase SHP-1 associates with the phosphorylated immunoreceptor tyrosine-based activation motif of Fc gamma RIIa to modulate signaling events in myeloid cells. *J. Biol. Chem.* 278: 35710-35717.

76. Xiong, Y., C. Cao, A. Makarova, B. Hyman, and L. Zhang. 2006. Mac-1 promotes FcgammaRIIA-dependent cell spreading and migration on immune complexes. *Biochemistry* 45: 8721-8731.

77. Ding, C., Y. Ma, X. Chen, M. Liu, Y. Cai, X. Hu, D. Xiang, S. Nath, H. G. Zhang, H. Ye, D. Powell, and J. Yan. 2013. Integrin CD11b negatively regulates BCR signalling to maintain autoreactive B cell tolerance. *Nat. Commun.* 4: 2813.

78. Ghazizadeh, S., J. B. Bolen, and H. B. Fleit. 1994. Physical and functional association of Src-related protein tyrosine kinases with Fc gamma RII in monocytic THP-1 cells. *J. Biol. Chem.* 269: 8878-8884.

79. Kwiatkowska, K., J. Frey, and A. Sobota. 2003. Phosphorylation of FcgammaRIIA is required for the receptor-induced actin rearrangement and capping: the role of membrane rafts. *J. Cell Sci.* 116: 537-550.

80. Berton, G., A. Mocsai, and C. A. Lowell. 2005. Src and Syk kinases: key regulators of phagocytic cell activation. *Trends Immunol.* 26: 208-214.

81. Leitges, M., K. Gimborn, W. Elis, J. Kalesnikoff, M. R. Hughes, G. Krystal, and M. Huber. 2002. Protein kinase C-delta is a negative regulator of antigen-induced mast cell degranulation. *Mol. Cell Biol.* 22: 3970-3980.

82. Chari, R., S. Kim, S. Murugappan, A. Sanjay, J. L. Daniel, and S. P. Kunapuli. 2009. Lyn, PKC-delta, SHIP-1 interactions regulate GPVI-mediated platelet-dense granule secretion. *Blood* 114: 3056-3063.

83. Pracht, C., S. Minguet, M. Leitges, M. Reth, and M. Huber. 2007. Association of protein kinase C-delta with the B cell antigen receptor complex. *Cell Signal.* 19: 715-722.

84. Xue, Z. H., C. Q. Zhao, G. L. Chua, S. W. Tan, X. Y. Tang, S. C. Wong, and S. M. Tan. 2010. Integrin alphaMbeta2 clustering triggers phosphorylation and activation of protein kinase C delta that regulates transcription factor Foxp1 expression in monocytes. *J. Immunol.* 184: 3697-3709.

85. Rodriguez-Fernandez, J. L., L. Sanchez-Martin, C. A. de Frutos, D. Sancho, M. Robinson, F. Sanchez-Madrid, and C. Cabanas. 2002. LFA-1 integrin and the microtubular cytoskeleton are involved in the Ca(2)(+)-mediated regulation of the activity of the tyrosine kinase PYK2 in T cells. *J. Leukoc. Biol.* 71: 520-530.

86. Okenwa, C., A. Kumar, D. Rego, Y. Konarski, L. Nilchi, K. Wright, and M. Kozlowski. 2013. SHP-1-Pyk2-Src protein complex and p38 MAPK pathways independently regulate IL-10 production in lipopolysaccharide-stimulated macrophages. *J. Immunol.* 191: 2589-2603.

87. Kelly, E. K., L. Wang, and L. B. Ivashkiv. 2010. Calcium-activated pathways and oxidative burst mediate zymosan-induced signaling and IL-10 production in human macrophages. *J. Immunol.* 184: 5545-5552.

88. Nathan, C., S. Srimal, C. Farber, E. Sanchez, L. Kabbash, A. Asch, J. Gailit, and S. D. Wright. 1989. Cytokine-induced respiratory burst of human neutrophils: dependence on extracellular matrix proteins and CD11/CD18 integrins. *J. Cell Biol.* 109: 1341-1349.

89. Kanthasamy, A. G., M. Kitazawa, A. Kanthasamy, and V. Anantharam. 2003. Role of proteolytic activation of protein kinase Cdelta in oxidative stress-induced apoptosis. *Antioxid. Redox. Signal.* 5: 609-620.

90. Gardai, S., B. B. Whitlock, C. Helgason, D. Ambruso, V. Fadok, D. Bratton, and P. M. Henson. 2002. Activation of SHIP by NADPH oxidase-stimulated Lyn leads to enhanced apoptosis in neutrophils. *J. Biol. Chem.* 277: 5236-5246.

91. Chiarugi, P., G. Pani, E. Giannoni, L. Taddei, R. Colavitti, G. Raugei, M. Symons, S. Borrello, T. Galeotti, and G. Ramponi. 2003. Reactive oxygen species as essential mediators of cell adhesion: the oxidative inhibition of a FAK tyrosine phosphatase is required for cell adhesion. *J. Cell Biol.* 161: 933-944.

92. Carman, C. V., and T. A. Springer. 2003. Integrin avidity regulation: are changes in affinity and conformation underemphasized? *Curr. Opin. Cell Biol.* 15: 547-556.

93. Kong, F., A. J. Garcia, A. P. Mould, M. J. Humphries, and C. Zhu. 2009. Demonstration of catch bonds between an integrin and its ligand. *J. Cell Biol.* 185: 1275-1284.

94. Chen, W., J. Lou, and C. Zhu. 2010. Forcing switch from short- to intermediate- and long-lived states of the alphaA domain generates LFA-1/ICAM-1 catch bonds. *J. Biol. Chem.* 285: 35967-35978.

95. Zhu, C., T. Yago, J. Lou, V. I. Zarnitsyna, and R. P. McEver. 2008. Mechanisms for flow-enhanced cell adhesion. *Ann. Biomed. Eng* 36: 604-621.

96. Sokurenko, E. V., V. Vogel, and W. E. Thomas. 2008. Catch-bond mechanism of force-enhanced adhesion: counterintuitive, elusive, but ... widespread? *Cell Host. Microbe* 4: 314-323.

97. Kim, M., C. V. Carman, and T. A. Springer. 2003. Bidirectional transmembrane signaling by cytoplasmic domain separation in integrins. *Science* 301: 1720-1725.

98. Lefort, C. T., Y. M. Hyun, J. B. Schultz, F. Y. Law, R. E. Waugh, P. A. Knauf, and M. Kim. 2009. Outside-in signal transmission by conformational changes in integrin Mac-1. *J. Immunol.* 183: 6460-6468.

99. Springer, T. A., and M. L. Dustin. 2012. Integrin inside-out signaling and the immunological synapse. *Curr. Opin. Cell Biol.* 24: 107-115.

100. Han, S., X. Kim-Howard, H. Deshmukh, Y. Kamatani, P. Viswanathan, J. M. Guthridge, K. Thomas, K. M. Kaufman, J. Ojwang, A. Rojas-Villarraga, V. Baca, L. Orozco, B. Rhodes, C. B. Choi, P. K.

Gregersen, J. T. Merrill, J. A. James, P. M. Gaffney, K. L. Moser, C. O. Jacob, R. P. Kimberly, J. B. Harley, S. C. Bae, J. M. Anaya, M. E. Alarcon-Riquelme, K. Matsuda, T. J. Vyse, and S. K. Nath. 2009. Evaluation of imputation-based association in and around the integrin-alpha-M (ITGAM) gene and replication of robust association between a non-synonymous functional variant within ITGAM and systemic lupus erythematosus (SLE). *Hum. Mol. Genet.* 18: 1171-1180.

101. Rhodes, B., B. G. Furnrohr, A. L. Roberts, G. Tzircotis, G. Schett, T. D. Spector, and T. J. Vyse. 2012. The rs1143679 (R77H) lupus associated variant of ITGAM (CD11b) impairs complement receptor 3 mediated functions in human monocytes. *Ann. Rheum. Dis.* 71: 2028-2034.

102. Fossati-Jimack, L., G. S. Ling, A. Cortini, M. Szajna, T. H. Malik, J. U. McDonald, M. C. Pickering, H. T. Cook, P. R. Taylor, and M. Botto. 2013. Phagocytosis is the main CR3-mediated function affected by the lupus-associated variant of CD11b in human myeloid cells. *PLoS. One.* 8: e57082.

103. Zhou, Y., J. Wu, D. F. Kucik, N. B. White, D. T. Redden, A. J. Szalai, D. C. Bullard, and J. C. Edberg. 2013. Multiple lupus-associated ITGAM variants alter Mac-1 functions on neutrophils. *Arthritis Rheum.* 65: 2907-2916.

104. Reed, J. H., M. Jain, K. Lee, E. R. Kandimalla, M. H. Faridi, J. P. Buyon, V. Gupta, and R. M. Clancy. 2013. Complement receptor 3 influences toll-like receptor 7/8-dependent inflammation: implications for autoimmune diseases characterized by antibody reactivity to ribonucleoproteins. *J. Biol. Chem.* 288: 9077-9083.

105. Diamond, M. S., J. Garcia-Aguilar, J. K. Bickford, A. L. Corbi, and T. A. Springer. 1993. The I domain is a major recognition site on the leukocyte integrin Mac-1 (CD11b/CD18) for four distinct adhesion ligands. *J. Cell Biol.* 120: 1031-1043.

106. Oxvig, C., and T. A. Springer. 1998. Experimental support for a beta-propeller domain in integrin alpha-subunits and a calcium binding site on its lower surface. *Proc. Natl. Acad. Sci. U. S. A* 95: 4870-4875.

107. Luo, B. H., C. V. Carman, and T. A. Springer. 2007. Structural basis of integrin regulation and signaling. *Annu. Rev. Immunol.* 25: 619-647.

108. Hynes, R. O. 2002. Integrins: bidirectional, allosteric signaling machines. *Cell* 110: 673-687.

109. Lu, C., C. Oxvig, and T. A. Springer. 1998. The structure of the beta-propeller domain and C-terminal region of the integrin alphaM subunit. Dependence on beta subunit association and prediction of domains. *J. Biol. Chem.* 273: 15138-15147.

110. Allport, J. R., H. T. Ding, A. Ager, D. A. Steeber, T. F. Tedder, and F. W. Luscinskas. 1997. L-selectin shedding does not regulate human neutrophil attachment, rolling, or transmigration across human vascular endothelium in vitro. *J. Immunol.* 158: 4365-4372.

111. Chen, W., E. A. Evans, R. P. McEver, and C. Zhu. 2008. Monitoring receptor-ligand interactions between surfaces by thermal fluctuations. *Biophys. J.* 94: 694-701.

112. Evans, E., K. Ritchie, and R. Merkel. 1995. Sensitive force technique to probe molecular adhesion and structural linkages at biological interfaces. *Biophys. J.* 68: 2580-2587.

113. Chen, W., V. I. Zarnitsyna, K. K. Sarangapani, J. Huang, and C. Zhu. 2008. Measuring Receptor-Ligand Binding Kinetics on Cell Surfaces: From Adhesion Frequency to Thermal Fluctuation Methods. *Cell Mol. Bioeng.* 1: 276-288.

114. Huang, J., V. I. Zarnitsyna, B. Liu, L. J. Edwards, N. Jiang, B. D. Evavold, and C. Zhu. 2010. The kinetics of two-dimensional TCR and pMHC interactions determine T-cell responsiveness. *Nature* 464: 932-936.

115. Chesla, S. E., P. Selvaraj, and C. Zhu. 1998. Measuring two-dimensional receptor-ligand binding kinetics by micropipette. *Biophys. J.* 75: 1553-1572.

116. Chen, W., J. Lou, E. A. Evans, and C. Zhu. 2012. Observing force-regulated conformational changes and ligand dissociation from a single integrin on cells. *J. Cell Biol.* 199: 497-512.

117. Marshall, B. T., K. K. Sarangapani, J. Wu, M. B. Lawrence, R. P. McEver, and C. Zhu. 2006. Measuring molecular elasticity by atomic force microscope cantilever fluctuations. *Biophys. J.* 90: 681-692.

118. Yu, Y., J. Zhu, L. Z. Mi, T. Walz, H. Sun, J. Chen, and T. A. Springer. 2012. Structural specializations of alpha(4)beta(7), an integrin that mediates rolling adhesion. *J. Cell Biol.* 196: 131-146.

119. Nishida, N., C. Xie, M. Shimaoka, Y. Cheng, T. Walz, and T. A. Springer. 2006. Activation of leukocyte beta2 integrins by conversion from bent to extended conformations. *Immunity.* 25: 583-594.

120. Sen, M., K. Yuki, and T. A. Springer. 2013. An internal ligand-bound, metastable state of a leukocyte integrin, alphaXbeta2. *J. Cell Biol.* 203: 629-642.

121. Chen, X., C. Xie, N. Nishida, Z. Li, T. Walz, and T. A. Springer. 2010. Requirement of open headpiece conformation for activation of leukocyte integrin alphaXbeta2. *Proc. Natl. Acad. Sci. U. S. A* 107: 14727-14732.

122. Faridi, M. H., D. Maiguel, B. T. Brown, E. Suyama, C. J. Barth, M. Hedrick, S. Vasile, E. Sergienko, S. Schurer, and V. Gupta. 2010. High-throughput screening based identification of small molecule antagonists of integrin CD11b/CD18 ligand binding. *Biochem. Biophys. Res. Commun.* 394: 194-199.

123. Faridi, M. H., M. M. Altintas, C. Gomez, J. C. Duque, R. I. Vazquez-Padron, and V. Gupta. 2013. Small molecule agonists of integrin CD11b/CD18 do not induce global conformational changes and are significantly better than activating antibodies in reducing vascular injury. *Biochim. Biophys. Acta* 1830: 3696-3710.

124. Maiguel, D., M. H. Faridi, C. Wei, Y. Kuwano, K. M. Balla, D. Hernandez, C. J. Barth, G. Lugo, M. Donnelly, A. Nayer, L. F. Moita, S. Schurer, D. Traver, P. Ruiz, R. I. Vazquez-Padron, K. Ley, J. Reiser, and V. Gupta. 2011. Small molecule-mediated activation of the integrin CD11b/CD18 reduces inflammatory disease. *Sci. Signal.* 4: ra57.

125. Lu, C. F., and T. A. Springer. 1997. The alpha subunit cytoplasmic domain regulates the assembly and adhesiveness of integrin lymphocyte function-associated antigen-1. *J. Immunol.* 159: 268-278.

126. Lu, C., M. Shimaoka, M. Ferzly, C. Oxvig, J. Takagi, and T. A. Springer. 2001. An isolated, surface-expressed I domain of the integrin alphaLbeta2 is sufficient for strong adhesive function when locked in the open conformation with a disulfide bond. *Proc. Natl. Acad. Sci. U. S. A* 98: 2387-2392.

127. Mayadas, T. N., and X. Cullere. 2005. Neutrophil beta2 integrins: moderators of life or death decisions. *Trends Immunol.* 26: 388-395.

128. Arnaout, M. A. 1990. Structure and function of the leukocyte adhesion molecules CD11/CD18. *Blood* 75: 1037-1050.

129. Pfirsch-Maisonnas, S., M. Aloulou, T. Xu, J. Claver, Y. Kanamaru, M. Tiwari, P. Launay, R. C. Monteiro, and U. Blank. 2011. Inhibitory ITAM signaling traps activating receptors with the phosphatase SHP-1 to form polarized "inhibisome" clusters. *Sci. Signal.* 4: ra24.

130. Aloulou, M., M. S. Ben, M. Biarnes-Pelicot, T. Boussetta, H. Souchet, E. Rossato, M. Benhamou, B. Crestani, Z. Zhu, U. Blank, P. Launay, and R. C. Monteiro. 2012. IgG1 and IVIg induce inhibitory ITAM signaling through FcgammaRIII controlling inflammatory responses. *Blood* 119: 3084-3096.

131. Herter, J., and A. Zarbock. 2013. Integrin Regulation during Leukocyte Recruitment. *J. Immunol.* 190: 4451-4457.

132. Mayadas, T. N., X. Cullere, and C. A. Lowell. 2014. The multifaceted functions of neutrophils. *Annu. Rev. Pathol.* 9: 181-218.

133. Ding, Z. M., J. E. Babensee, S. I. Simon, H. Lu, J. L. Perrard, D. C. Bullard, X. Y. Dai, S. K. Bromley, M. L. Dustin, M. L. Entman, C. W. Smith, and C. M. Ballantyne. 1999. Relative contribution of LFA-1 and Mac-1 to neutrophil adhesion and migration. *J. Immunol.* 163: 5029-5038.

134. Dunne, J. L., R. G. Collins, A. L. Beaudet, C. M. Ballantyne, and K. Ley. 2003. Mac-1, but not LFA-1, uses intercellular adhesion molecule-1 to mediate slow leukocyte rolling in TNF-alpha-induced inflammation. *J. Immunol.* 171: 6105-6111.

Appendix I.

I. Supplemental Figures

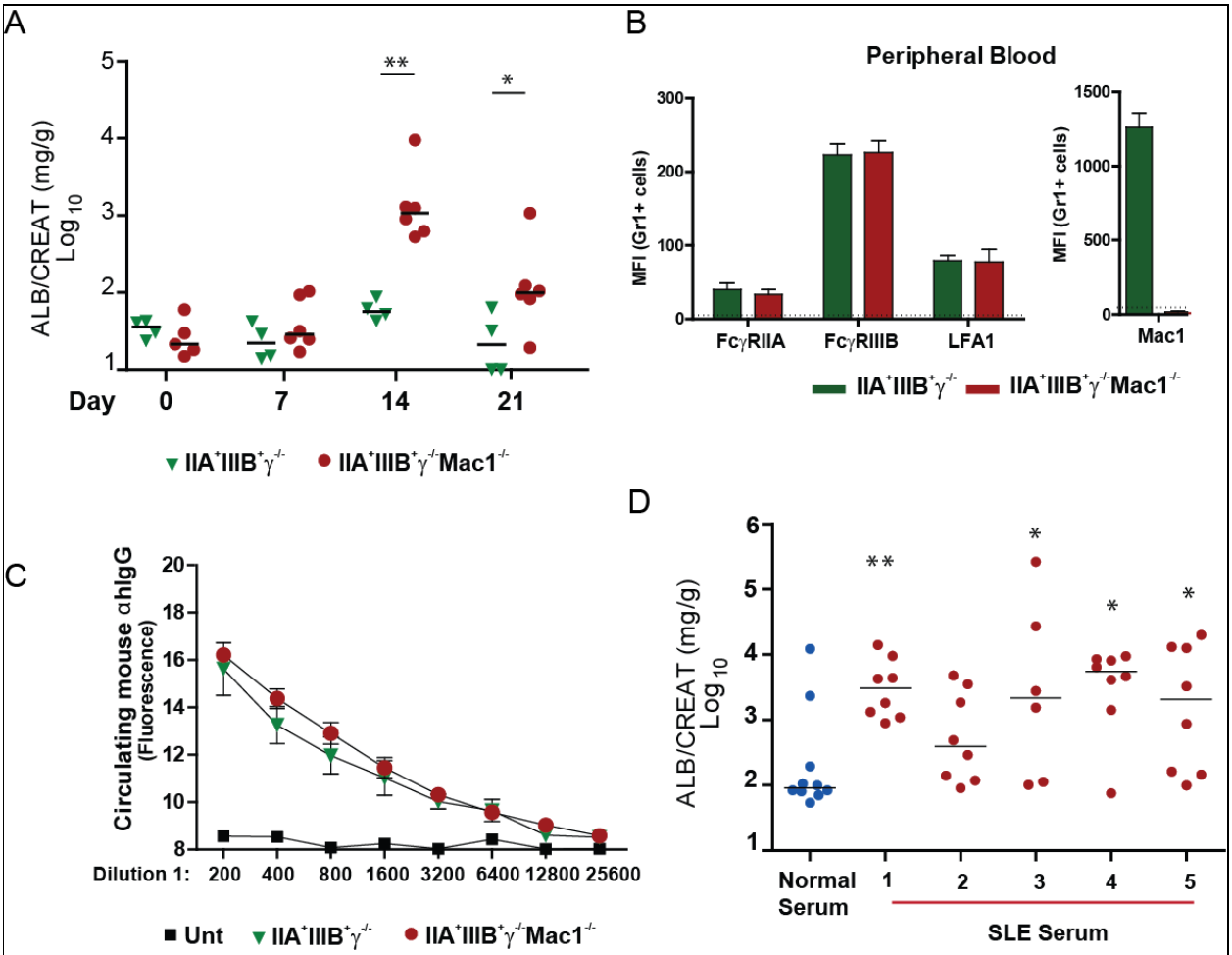

Supplemental 1. (A) Kinetics of albuminuria following transfer of SLE sera. Urinary albumin/creatinine ratio was evaluated after transfer of human SLE serum into IIAIIIBγ$^{-/-}$ and IIAIIIBγ$^{-/-}$Mac-1$^{-/-}$ mice. Each data point represents one animal, the line indicates the median. *p<0.05, **p<0.01. **(B)** Surface levels of FcγRIIA and FcγRIIIB and Mac-1 were evaluated in peripheral blood (Gr1^{+} cells), from IIAIIIBγ$^{-/-}$ and IIAIIIBγ$^{-/-}$Mac-1$^{-/-}$ mice by flow cytometry using respective antibodies. The average of the MFI ± SEM was graphed. **(C)** Analysis of circulating mouse anti-human IgG in indicated mice after SLE sera transfer. Circulating mouse anti-human IgG antibodies were measured by ELISA on serum collected from mice at day 14, using human IgG (100µg/mL) to coat the plate. **(D)** Evaluation of proteinuria at day 14 of IIAIIIBγ$^{-/-}$Mac-1$^{-/-}$ mice that received sera from healthy donors (Normal, data pooled from 3 donors) or 5 SLE patients (1-5) (from Instituto Nacional de Ciencias Medicas y Nutricion, Salvador Zubiran, Mexico). Each data point represents one mouse, and the line indicates the median. *p<0.05, **p<0.01 compared to mice given normal serum.

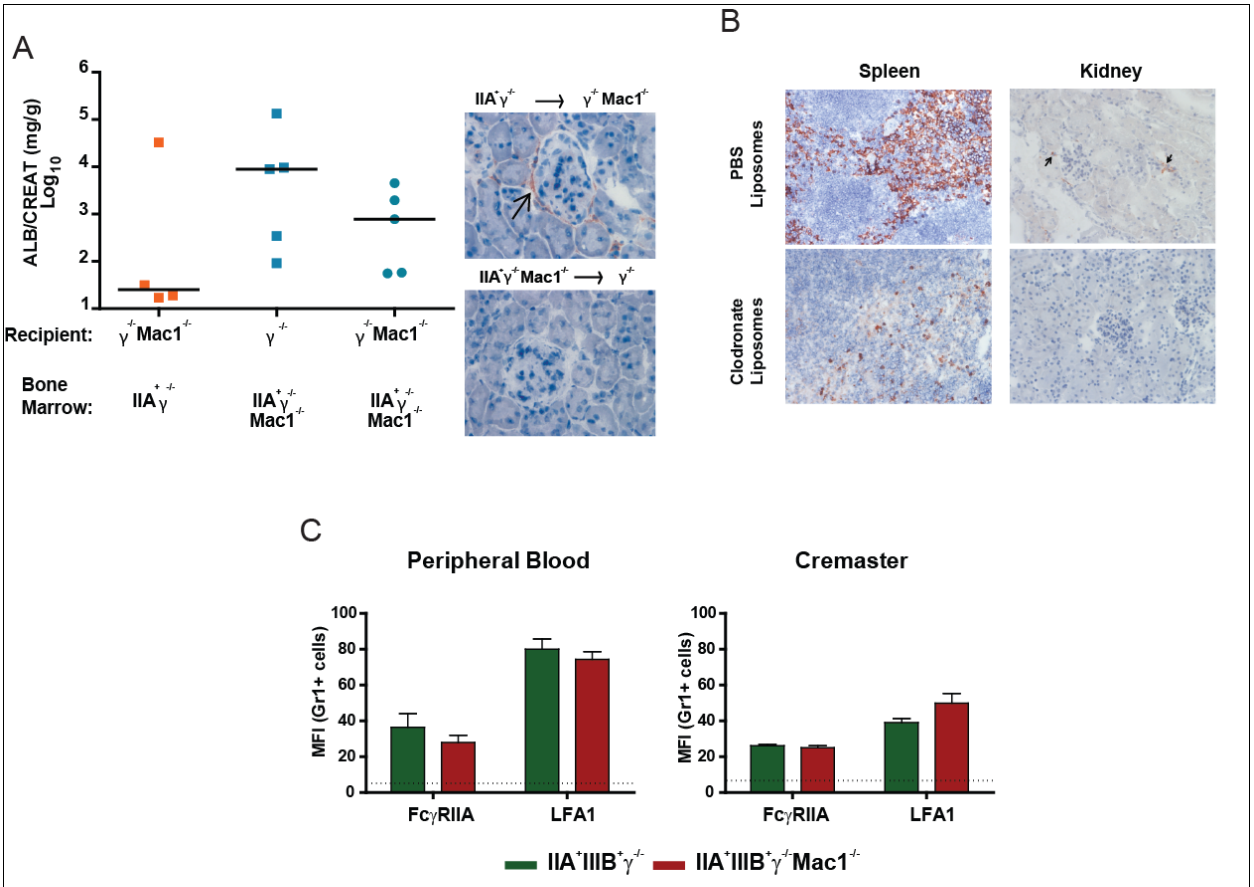

Supplemental 2. **(A)** IIAγ$^{-/-}$Mac-1$^{-/-}$ bone marrow confers susceptibility for the development of SLE-serum induced nephritis. Bone marrow from IIAγ$^{-/-}$ and IIAγ$^{-/-}$Mac-1$^{-/-}$ mice were transferred into lethally irradiated γ$^{-/-}$Mac-1$^{-/-}$ or γ$^{-/-}$ mice, respectively (or IIAγ$^{-/-}$Mac-1γ$^{-/-}$ into γ$^{-/-}$Mac-1$^{-/-}$ as positive control). Three months later, mice received SLE serum intravenously. Left panel: proteinuria at day 14 after SLE serum injection is shown. Right panel: anti-CD11b (BD Pharmingen) immunohistochemistry following SLE-serum injection shows that kidneys are infiltrated by macrophages from the donor bone marrow. **(B)** Immunohistochemistry with anti-F4/80 of spleen and kidney samples taken at day 14 after SLE serum injection from mice that were treated with liposomes containing PBS or clodronate. Macrophage infiltration observed in spleen and kidney (arrow) of PBS liposome treated mice is reduced in clodronate liposome treated animals. (**C**) FcγRIIA and LFA-1 expression in Gr1^{+} neutrophils in the peripheral blood and the cremaster after RPA induction. 3hrs after RPA induction, blood was collected from the retroorbital plexus and the cremaster was digested (Collagenase type I and DNAse) to obtain a single cell suspension. Samples were analyzed by flow cytometry using anti-FcγRIIA and anti-LFA antibody. Average of 3 mice per group ±SEM is shown. Dashed line represent average of MFI of isotype control antibodies.

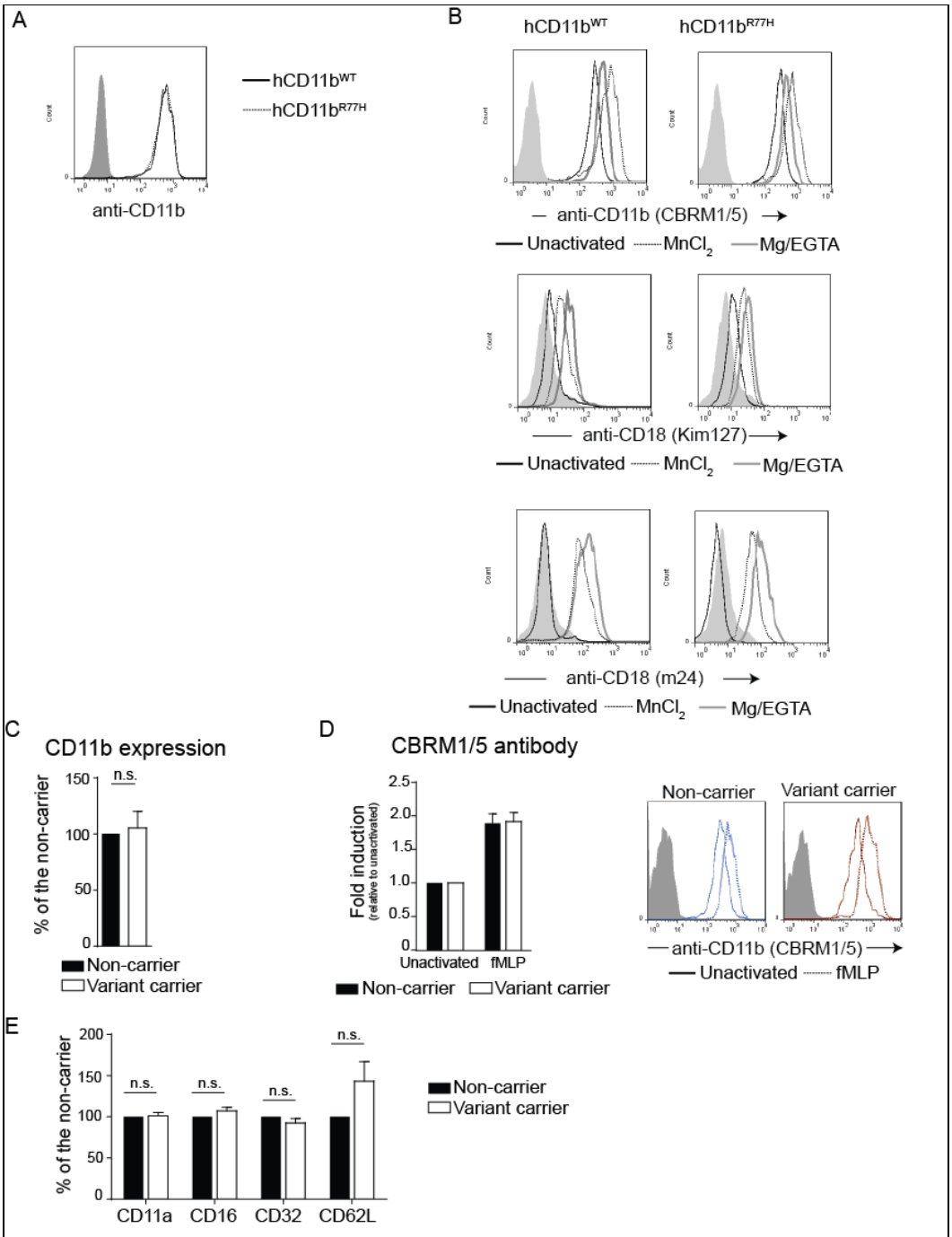

Supplemental 1 (A) Surface expression (flow cytometry) of CD11b in K562 cells bearing the common ($CD11b^{WT}$) or risk-associated ($CD11b^{R77H}$) variants. **(B)** CD11b activation (Mg^{2+}/EGTA and Mn^{2+}) on K562 cells evaluated by flow cytometry using the CD11b-specific reporter antibody CBRM1/5, and the CD18 specific antibodies Kim127 and Monoclonal Ab24 (m24). Representative histograms are shown. **(C)** Similar surface expression of CD11b on neutrophils from non-carrier or variant carrier donors, evaluated by flow cytometry. **(D)** Similar expression of surface activation markers on neutrophils in the two groups. Data is presented as fold induction relative to neutrophils from the non-carrier donors. **(E)** CBRM1/5 antibody binding (CD11b activation) to neutrophils from carriers and non-carriers after fMLP cell activation. Cumulative data is presented as fold induction relative to non-activated neutrophils. Representative histograms are shown.

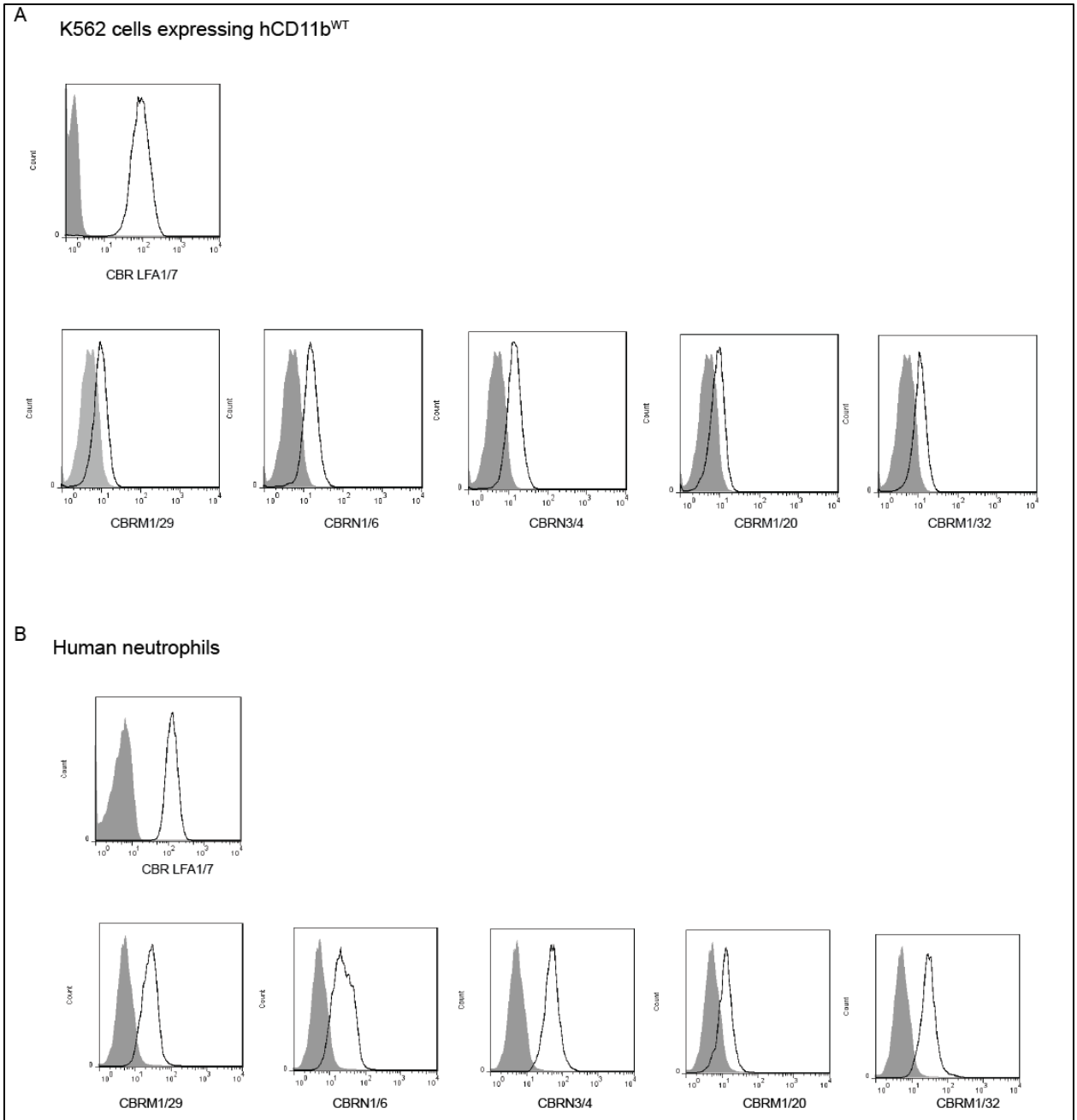

Supplemental 4. Fluorescence intensity histograms of (A) K562 cells expressing hCD11bWT or (B) Human neutrophils with the control antibody CBR LFA1/7, CBRM1/29, CBRN1/6, CBRN3/4, CBRM1/20 and CBRM1/32 antibodies. Goat-anti mouse APC was used as a secondary antibody.

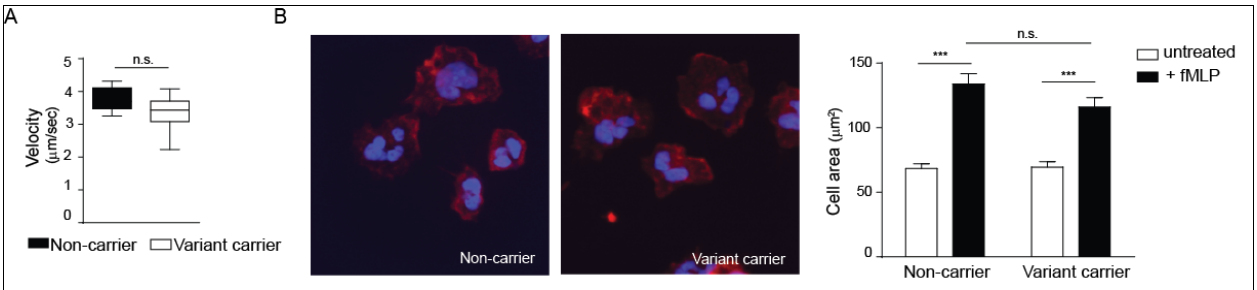

Supplemental 5. (A) Crawling velocity of fMLP-activated neutrophils over a plasma-coated surface. Cumulative data from 8 samples is shown. **(B)** Spreading of fMLP-activated neutrophils on an iC3b coated surface. Quantification of cell area was perfomed, and representative photographs of cells stained with phalloidin (red) and DAPI (blue) are shown. (n.s.= no statistical significance).

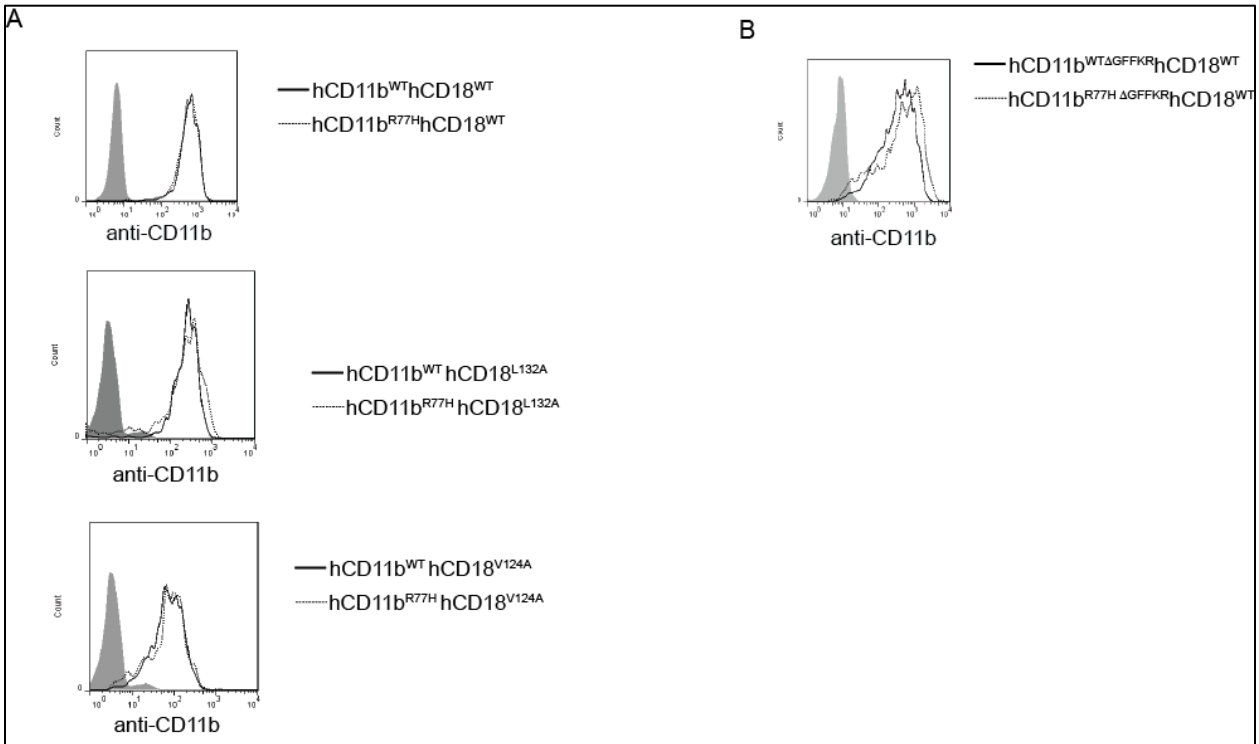

Supplemental 6. Surface expression (flow cytometry) of CD11b in K562 cells bearing (A) the common ($CD11b^{WT}$) or risk-associated ($CD11b^{R77H}$) variants coupled with the $CD18^{WT}$, $CD18^{V124A}$ or $CD18^{L132A}$ β2 chain mutations, or **(B)** the common ($CD11b^{WT\ /GFFKR}$) or risk-associated ($CD11b^{R77H/GFFKR}$) variants lacking the GFFKR regulatory region.

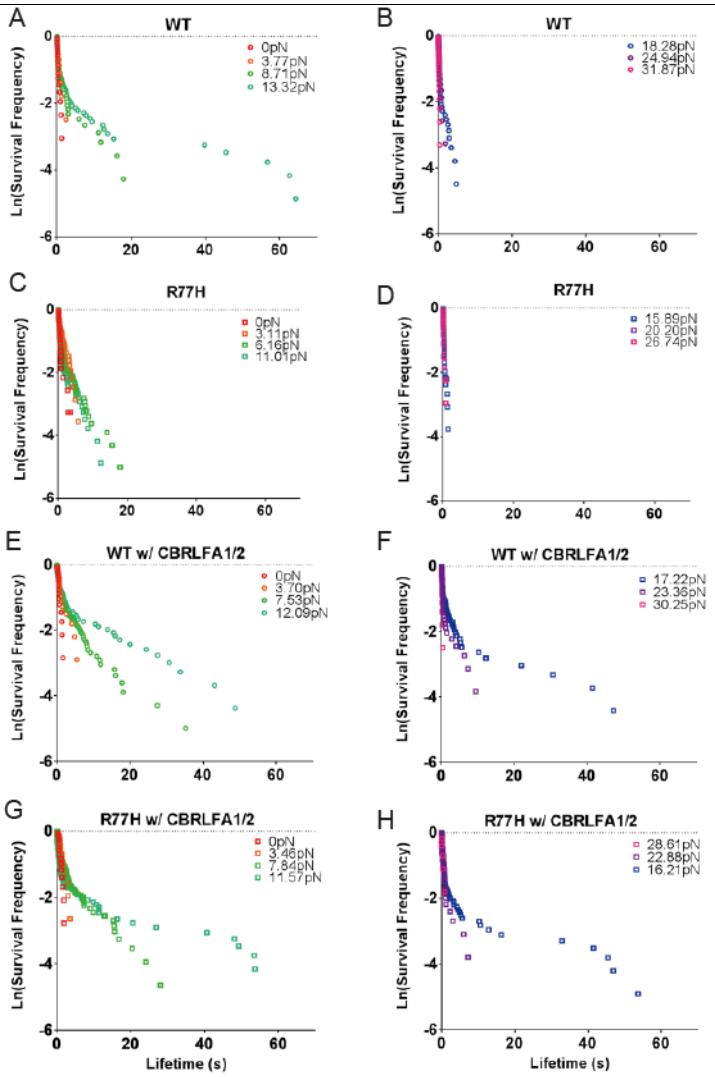

Supplemental 7. Plots of Ln (Survival frequency) *vs* lifetime of $CD11b^{WT}$ **(A, B, E, F)** and $CD11b^{R77H}$ **(C, D, G, H)** Mac-1 binding to ICAM-1 under different forces. Survival frequency, by definition means for each lifetime event, the proportion of the rest lifetime events longer than the current one.

A, B, C, D are without Ab stimulation; E, F, G, H are pre-incubated with CBR LFA1/2.

A, C, E, G are under lower forces and B, D, F, H are under higher forces.

According to Bell's model, Ln (Survival frequency) should follow a linear correlation with lifetime if only one binding state exists, while the addition of more states would be indicated by a change of the slope in the middle of the curve. This slope change was found in all four experimental setups, indicating the existence of at least two binding states between Mac-1 and ICAM-1.

II. Supplemental Tables

A. Immune Complex and IgG levels in human SLE sera

Source	Designation (+= hIgG-IC deposition in kidney, "pathogenic")	ICs (μg Eq/mL)	hIgG (mg/mL)
Control donor	-	ND	16.3
Patient SLE-A	+	5.2	10.5
Patient SLE-B	+	11.7	10.2
Patient SLE-C	+	18.2	5.8
Patient SLE-E	+	5.1	Not determined
Patient SLE-D	-	5.8	14.4
Patient SLE-F	-	7.3	12.8

B. Class of lupus nephritis and autoantibody profile of SLE patients in the study

SLE-Serum	Pathogenic	Lupus nephritis[a]	Autoantibodies: ANA	RNP	Sm	SSA	SSB	dsDNA	Low complement	SLEDAI[b]
A	+	Class IIIA	+	+	+	+	+	+	+	0-20
B	+	Unknown	+	+	+	-	-	+	+	0-36
C	+	Class IV	+	-	-	-	-	+	+	12-16
D	-	Class IV	+	-	-	+	-	+	+	0-12
E	+	-		+	+	+	+	+	+	5-10
F	-	Class IV	+	-	-	-	-	+	+	0

[a]Lupus nephritis according to WHO classification (Weening JJ et al., The classification of glomerulonephritis in systemic lupus erythematosus revisited. *Kidney Int.* 2004; 65:521-30)

[b]Serum samples were obtained form patients at several time points during different periods of disease activity. The pathogenic capacity of the sera was not modified by variations in the autoantibody levels (including dsDNA levels), overall SLE disease activity index (SLEDAI) and renal disease activity (as defined by proteinuria, hematuria and pyuria) at the time of the blood draw.

C. Peripheral blood analysis in mice

	Untreated		SLE serum		
	$IIA^+IIIB^+\gamma^{-/-}$ (n=3)	$IIA^+IIIB^+\gamma^{-/-}Mac\text{-}1^{-/-}$ (n=3)	$IIA^+IIIB^+\gamma^{-/-}$ (n=6)	$IIA^+IIIB^+\gamma^{-/-}Mac\text{-}1^{-/-}$ (n=8)	p-value
Total Leukocytes (K/μL)	2.89 ± 0.40	1.76 ± 0.15	4.99 ± 0.81	4.55 ± 0.83	ns
Neutrophils (K/μL)	0.67 ± 0.14	0.43 ± 0.02	2.42 ± 0.43	1.70 ± 0.34	ns
Lymphocytes (K/μL)	1.29 ± 0.23	1.55 ± 0.11	2.23 ± 0.44	2.59 ± 0.54	ns
Monocytes (K/μL)	0.18 ± 0.01	0.15 ± 0.00	0.24 ± 0.09	0.21 ± 0.54	ns
Red Blood Cells (M/μL)	4.62 ± 0.93	4.52 ± 0.11	7.59 ± 0.73	6.47 ± 0.86	ns
Platelets (K/μL)	706.33 ± 138.80	624 ± 85.73	1156.33 ± 191.17	1298.63 ± 182.95	ns
Hemoglobin (g/dL)	5.33 ± 1.10	5.23 ± 0.33	7.61 ± 0.60	6.60 ± 0.75	ns

Supplemental Table 1 A) Immune complex and IgG levels in human SLE sera. Immune complexes (ICs) and total human IgG were quantified by ELISA in indicated sera. "+" refers to its capacity to deposit in glomeruli and induce nephritis; thus the designation "pathogenic" sera. ND= not detectable. **B)** Class of lupus nephritis and autoantibody profile of SLE patients in the study. **C)** Peripheral blood analysis in mice. Blood collected at day 21 after SLE sera "A" injection, or from untreated mice was analyzed using an automated cell counter (Hemavet). No significant differences (p-value, ns) were observed between $IIAIIIB\gamma^{-/-}$ and $IIAIIIB\gamma^{-/-}Mac\text{-}1^{-/-}$ mice in untreated or SLE serum treated groups.

A

	K562 cells CD11b ^{WT}					
		% Inhibition of IgG control (min 8)			Static	
		Average	± SEM		Average	± SEM
	IgG control	0.0	0.0		0.0	
	CBRM 1/29	74.6	9.1		37.2	23.5
iC3b	CBRM 1/32	96.7	2.2		65.4	20.6
	CBRM 1/20	29.8	9.3		34.9	1.6
	CBRN 1/6	82.7	11.4		20.8	3.8
	CBRN 3/4	52.7	22.8		37.4	12.5
	IgG control	0.0				
	CBRM 1/29	92.5				
ICAM-1	CBRM 1/32	98.4				
	CBRM 1/20	-4.4				
	CBRN 1/6	74.4				
	CBRN 3/4	59.7				

B

Human Neutrophils						
		% Inhibition of IgG control (min 8)			Static	
		Average	± SEM		Average	± SEM
	IgG control	0.0	0.0		0.0	
	CBRM 1/29	35.9	3.2		29.4	5.1
	CBRM 1/32	50.3	10.2		15.7	7.6
iC3b	CBRM 1/20	6.9	4.6		-6.3	14.1
	CBRN 1/6	39.5	3.6		4.4	7.0
	CBRN 3/4	44.7	12.0		-2.6	11.2

Supplemental Table 2. K562 cells expressing CD11b^{WT} (A) or human neutrophils (B) isolated from peripheral blood were activated with Mn^{2+} or fMLP respectively. Binding to indicated ligand-coated surfaces was assessed under shear flow (0.38dynes/cm^2) and static conditions. CBRM1/29 antibody was used to block the I-domain and CBRM1/32, CBRM1/20, CBRN1/6 and CBRN 3/4 to block different areas of the β-propeller.